12-3-2008

Mechanisms for Methylmercury Cell-to-Bath Transport by the Basolateral Membrane of the Rabbit Proximal Tubule

Carol Ann Hoban

MECHANISMS FOR METHYLMERCURY CELL-TO-BATH TRANSPORT BY THE BASOLATERAL MEMBRANE OF THE RABBIT PROXIMAL TUBULE

by

CAROL A. HOBAN

Under the Direction of Delon W. Barfuss

ABSTRACT

The bath-to-cell transport, cytosolic concentration, and tubular content of methylmercury ($Me^{203}Hg^{+}$) and the sulfhydryl-amino acids and sulfhydryl-amino acid derivatives conjugated to $Me^{203}Hg^{+}$ were studied in the non-perfused S_2 segments of the proximal tubule of the rabbit kidney. Active transport of $Me^{203}Hg^{+}$ was established by a temperature dependent (greater than 100% reduction in bath-to-cell transport, 99% decrease in cytosolic concentration, 63% decline in the tubular contents at 12°C when compared to 37°C). Conjugates of $Me^{203}Hg^{+}$ showed mixed results, with *L*-cysteine and *L*-taurine demonstrating the most significant increase in uptake. Transport of $Me^{203}Hg^{+}$-*L*-cysteine was also temperature dependent with a 77% reduction in bath-to-cell transport, 76% decrease in cytosolic concentration, and 86% decline in tubular contents at 12°C when compared to 37°C. A significant decrease in transport was seen with the classic organic anion transport (OAT) inhibitors of PAH (71% and 67%) and probenicid (48% and 38%), as well as, the dicarboxylates, adepate (over 100%) and glutarate (69% and 52%) in

both bath-to-cell and cytosolic concentration respectively. The addition of *L*-methionine to the $Me^{203}Hg^{+}$-*L*-cysteine conjugate significantly reduced the bath-to-cell transport by 64% and the cytosolic contents by 47%. The $Me^{203}Hg^{+}$-*L*-taurine conjugate also demonstrated temperature dependence (99% reduction and 91% decrease in bath-to-cell and cytosolic concentration respectively, at 12°C when compared to 37°C). Inhibition with PAH was also seen (77% reduction) in bath-to-cell transport and 67% decline in cytosolic concentration giving further evidence to the transport of the $Me^{203}Hg^{+}$-*L*-taurine conjugate via OAT. When $Me^{203}Hg^{+}$ was conjugated to *L*-methionine a 55% reduction in bath-to-cell transport was seen which was also temperature dependent (59% decrease at 12°C when compared to 37°), although no significant decrease in transport was noted with the addition of PAH. Analysis of the methylmercury conjugates via mass spectrometry demonstrated that *L*-cysteine, *L*-taurine, and *L*-methionine all are binding with methylmercury in the same unknown common configuration (MW=409). These results indicate the mercuric conjugate is gaining entry into the renal epithelial cells via the OAT and the amino acid transport system in the basolateral membrane of the proximal tubule.

INDEX WORDS: Methylmercury, Basolateral membrane, Transport, Proximal tubule, Kidney, Sulfhydryl-containing amino acids, Non-perfused tubule

MECHANISMS FOR METHYLMERCURY CELL-TO-BATH TRANSPORT BY THE BASOLATERAL MEMBRANE OF THE RABBIT PROXIMAL TUBULE

by

CAROL A. HOBAN

A Dissertation Submitted in Partial Fulfillment of the Requirement for the Degree of

Doctor of Philosophy

in the College of Arts and Sciences

Georgia State University

2008

MECHANISMS FOR METHYLMERCURY CELL-TO-BATH TRANSPORT BY THE BASOLATERAL MEMBRANE OF THE RABBIT PROXIMAL TUBULE

by

CAROL A. HOBAN

Major Professor: Delon W. Barfuss

Committee: Andrew Clancy
Yuan Liu

Electronic Version Approved:

Office of Graduate Studies
College of Arts and Sciences
Georgia State University
December 2008

DEDICATION

I would like to dedicate this dissertation to my parents, for always pushing me to strive to be the best that I can. Without their support, I would not have been able to pursue my education and for that, I am eternally grateful to them.

ACKNOWLEDGEMENTS

I would like to thank Dr. Delon Barfuss for his never-ending support, guidance, patience, and mentoring throughout the completion of this degree. Dr. Barfuss is undoubtedly the best teacher I have ever had during my academic career and I feel honored to have been his last PhD student. I would also like to thank my doctoral committee, Dr. Andrew Clancy and Dr. Yuan Liu for their support, comments, and feedback throughout this entire process. I would also like to thank Brandon Smith for his technical support.

TABLE OF CONTENTS

LIST OF TABLES

LIST OF FIGURES

LIST OF ABBREVIATIONS

amu	Atomic mass unit
Ca^{2+}	Calcium ion
Cd^{2+}	Cadmium ion
Cl^{-}	Chloride ion
Co^{2+}	Cobalt ion
CPM	Counts per minute
Cu^{2+}	Copper 2 ion
Cys	Cysteine
DCM	Dichloromethane
DMPS	2,3 Dimercaptopropane-1-sulfonate
DMSA	Meso-2,3-dimercaptosuccinic acid
DMT1	Divalent metal transporter 1
EDTA	ethylenediaminetetraacetic acid
FEP	Flourinated Ethylene Propylene
fmol	Femtamolar
γ-GT	γ-glutamyltransferase
GI	Gastrointestinal
GSH	Glutathione
HCl	Hydrochloric acid

HCO_3^-	Bicarbonate ion
Hcys	Homocysteine
Hg°	Mercury metal
Hg^{2+}	Inorganic mercury
Hg^+-C	Organic mercury
HgO	Mercury oxide
K^+	Potassium ion
KCl	Potassium chloride
$Me^{203}Hg^+$	Radioactive methylmercury
Na^+	Sodium ion
NAC	*N*-Acetylcysteine
NaCl	Sodium chloride
NaH_2PO_4	Anhydrous monosodium dihydrogen phosphate
Na_2HPO_4	Anhydrous disodium monohydrogen phosphate
Na^+,K^+ATPase	Sodium-potassium pump
NaOH	Sodium hydroxide
Ni^{2+}	Nickel ion
OAT	Organic anion transporter
OC	Organic cation
OCT	Organic cation transporter
PAH	Para-aminohippurate

Pb^{2+}	Lead ion
PO_4^{3-}	Phosphate ion
PT	Proximal tubule
Pt^{2+}	Platinum ion
RPM	Revolutions per minute
TCA	Tricholoroacetic acid
TEA	Tetraethylammonium
Zn^{2+}	Zinc ion

CHAPTER I: INTRODUCTION

Methylmercury ($Me^{203}Hg^{+}$), an organic form of mercury is a highly toxic heavy metal, a common environmental pollutant and continues to pose appreciable health risks to humans even today. The inorganic form of mercury, Hg, enters the environment from such natural processes as emissions from the earth's crust and through man-made sources, mostly industrial pollution (Figure 1). In the United States, coal-burning power plants account for the largest source of unregulated mercury emissions (Management, 2003). The elemental form of mercury can then be methylated by algae and bacteria in water and soil which can then move up through the food chain via bioaccumulation, especially in aquatic species of fish (Figure 1). Methylmercury is of particular concern as a pollutant in seafood as fish and other seafood products are the main source of $Me^{203}Hg^{+}$ in the human diet (Aschner and Syversen, 2005). Consumption of contaminated seafood accounts for the majority of the exposure to humans. Methylmercury is considered to be the most toxic and most frequently encountered form of the metal, found in not only fish, but also poultry that have been fed a diet including fishmeal, pesticides, fungicides, and insecticides (Patrick, 2002). Other forms of $Me^{203}Hg^{+}$ poisoning that pose a public health threat are from the adverse effects of thimerosal, a vaccine preservative that is metabolized to ethylmercury (EtHg) in the body (Aschner and Syversen, 2005).

Mercury toxicity has been recognized as a health threat since the 19th century and is a serious clinical problem with over 2,000 exposures to mercury or mercury containing

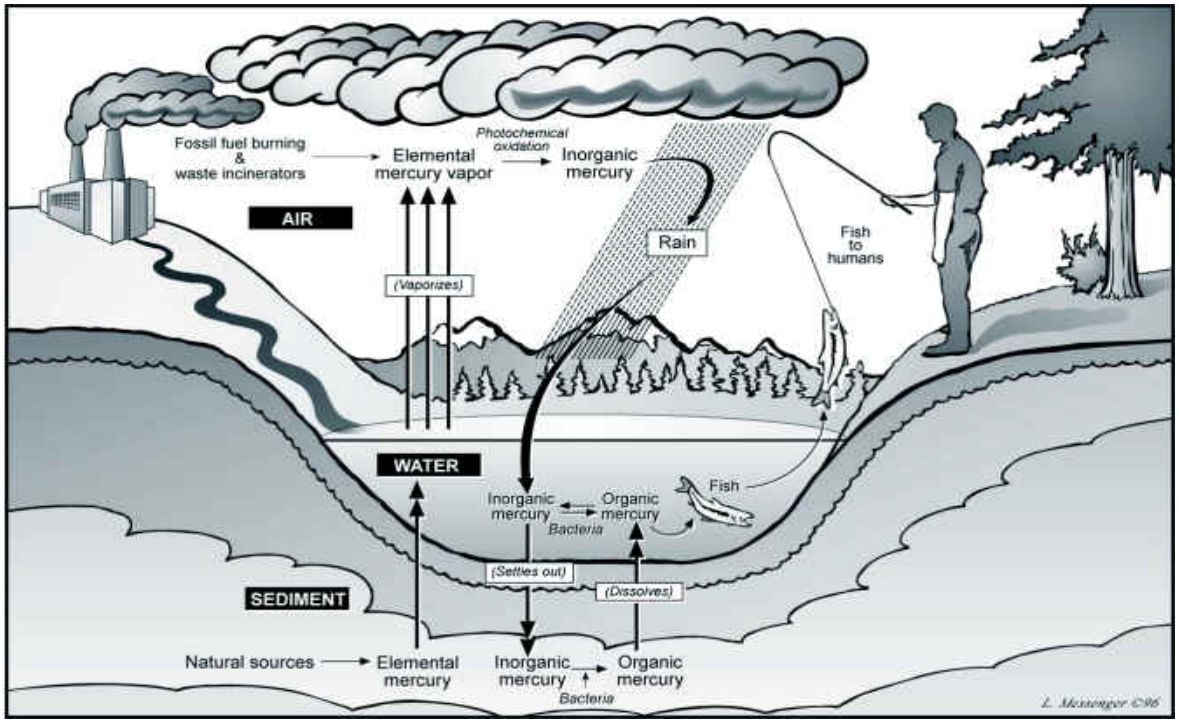

Figure 1: Atmospheric transport of mercury.
(http://www.mercury.utah.gov/atmospheric_transport.htm)

compounds each year (Watson, 2003). Furthermore, mercury toxicity is considered to be the second-most common cause of acute heavy metal poisoning (Patrick, 2002). Exposure to mercury in any form is toxic, but the severity of the response depends upon the route of absorption in the body and the patient's response to treatment. Mercury poisoning can result from digestion, inhalation, injection, or absorption through the skin and is distributed to all body tissues including the brain. In the body, $Me^{203}Hg^{+}$ is present as a water-soluble complex, mostly attached to thiol-containing ligands. Fetuses are particularly vulnerable to $Me^{203}Hg^{+}$ because of their rapid brain development. Once ingested it is rapidly distributed to all tissues, causing toxicity (Koh et al, 2002). The physiological mechanism for removing ingested $Me^{203}Hg^{+}$ is by filtration or secretion (Figure 2), the latter requiring basolateral transport of the heavy metal. While the former process will prevent $Me^{203}Hg^{+}$ from entering the renal epithelial cells and

inducing toxicity, the latter (secretion) will promote renal epithelial cell accumulation and toxicity.

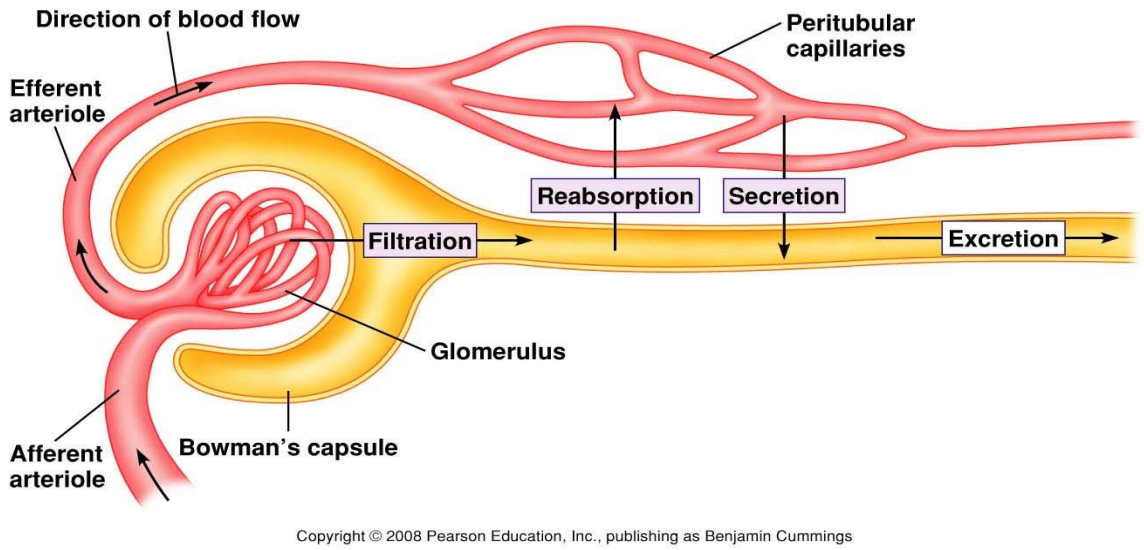

Figure 2: The three exchange processes in the renal tubules. (Principles of Human Physiology, Third Edition, Figure 18.7, The Urinary System: Renal Function @ 2008 Pearson Education, Inc. Benjamin Cummings, Co.)

Relatively little is known about the mechanisms involved in the transport of $Me^{203}Hg^{+}$ by the epithelial cells lining the renal proximal tubule (PT). Previous studies have identified a divalent metal transporter 1 (DMT1) that is located not only in the gastrointestinal (GI) tract, but also highly expressed in the kidney. DMT1 transports trace elements, as well as toxic cations such as Cd^{2+}, Pb^{2+}, Co^{2+}, Ni^{2+} and Pt^{2+}. Other studies have indicated that Zn^{2+} may be transported in the PT complexed to other amino acids such as, *L*-cysteine or *L*-histidine via a sodium-amino acid transporter (Barbier et al, 2005). Toxic metal poisoning may create competition for these transporters, especially for those heavy metals that form *L*-cysteine conjugates such as mercury and cadmium. Heavy metal exposure can cause both acute and

chronic intoxications with varying levels of severity. The nature of damage that occurs depends upon the dose, route and duration of exposure (Zalups, 2000). Once mercury is ingested, elimination from the body must be adequate to prevent toxicity.

Current clinical strategies for removing $Me^{203}Hg^{+}$ include hemodialysis, chelation therapy (a type of treatment that uses ethylenediaminetetraacetic acid [EDTA] to bind mercury and clear it from the body), and exchange transfusion (Koh et al, 2002). Heavy metals such as, mercury, have a high affinity and bind readily with free sulfhydryl groups (Aschner and Syversen, 2005). The sulfhydryl-containing anionic compound dimercaptopropanesulfonate (DMPS) has been successfully used as a chelation agent in mercury toxicity and is itself excreted in the urine in high concentrations, but the pathway for this remains unknown (Koh et al, 2002). Furthermore, the mechanisms of $Me^{203}Hg^{+}$ uptake, accumulation and excretion all along the nephron remain largely unknown. Therefore, the current study will focus on the transport of $Me^{203}Hg^{+}$ by the kidney.

To fully understand the mechanism of transport of $Me^{203}Hg^{+}$ by the kidney it is first necessary to describe the functional anatomy of the kidney and elucidate to the transport processes present within the nephron. The kidneys function to both absorb nutrients (endogenous compounds such as glucose, amino acids and vitamins) from the filtrate and return them to the blood and also to excrete waste substances (xenobiotics and exogenous toxic substances) into the lumen for elimination from the body. Secretion of toxic compounds by the kidney is important in maintaining plasma concentrations and in clearing the body of potentially harmful products. Divalent cations such as Zn^{2+}, Fe^{2+} and Cu^{2+} are essential to homeostasis in the body. These cations are normally found within the body at very low concentrations that are tightly regulated as excess or a deficiency in these metals may cause illness or even death

(Barbier, et al, 2005). Divalent cations of heavy metals such as mercury (Hg), do not however, have a beneficial significance in the human body.

The kidney consists of two distinct regions, both an outer cortex and an inner medulla (Figure 3). Within the cortex and medullary regions, is the functional unit of the kidney known as the nephron (Figure 3). Humans contain approximately 0.8 X 10^6 to 1.2 X 10^6 nephrons, which consist of the renal corpuscle and the tubule segments. The renal corpuscle contains the glomerular capillaries and Bowman's capsule. The glomerulus produces a protein-free ultrafiltrate from the plasma.

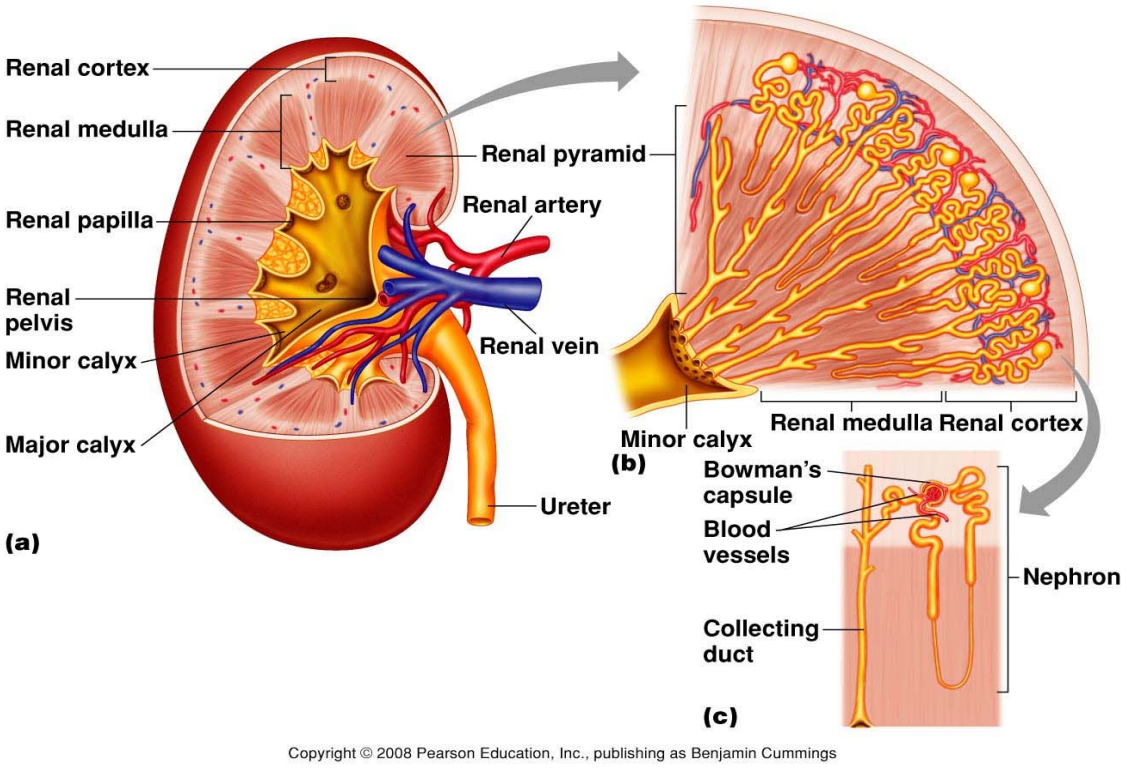

Figure 3: Macroscopic anatomy of the kidney (Principles of Human Physiology, Third Edition, Figure 18.2, The Urinary System: Renal Function @ 2008 Pearson Education, Inc. Benjamin Cummings, Co.)

The tubule consists of: (1) the PT, (2) the loop of Henle including the descending thin limb, ascending thin limb and ascending thick limb, (3) the distal convoluted tubule, and (4) the collecting duct (Figure 4). The fluid entering the tubular portion of the nephron absorbs the remaining endogenous substances and ultimately forms urine.

Within the kidney, two types of nephrons can be distinguished: superficial (or cortical) and juxtamedullary based on the length of the loop of Henle and the position of the glomerulus in the cortex (Figure 5).

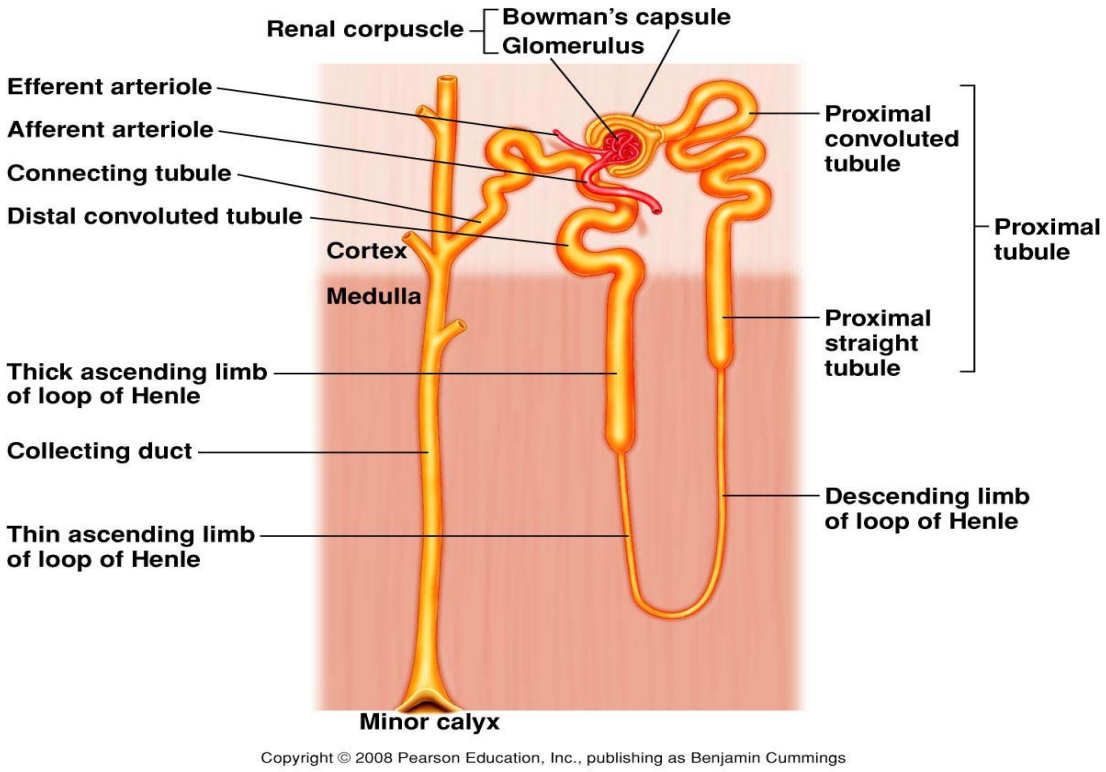

Figure 4: Anatomy of the nephron (Principles of Human Physiology, Third Edition, Figure 18.3, The Urinary System: Renal Function @ 2008 Pearson Education, Inc. Benjamin Cummings, Co.)

Superficial nephrons generally have short loops of Henle with midcortical glomeruli, while juxtamedullary nephrons generally have longer loops of Henle and are located in the corticomedullary boundary. Humans have approximately 80-85% superficial nephrons and 15-20% juxtamedullary nephrons.

The PT begins at the glomerulus and consists of an initial convoluted portion, the pars convoluta, which is a continuation of the parietal epithelium of Bowman's capsule and continues on to a straight segment, the pars recta (Figure 4). The length of the PT in humans is approximately 14 mm and in the rabbit, the length is about 10 mm. Three distinct segments

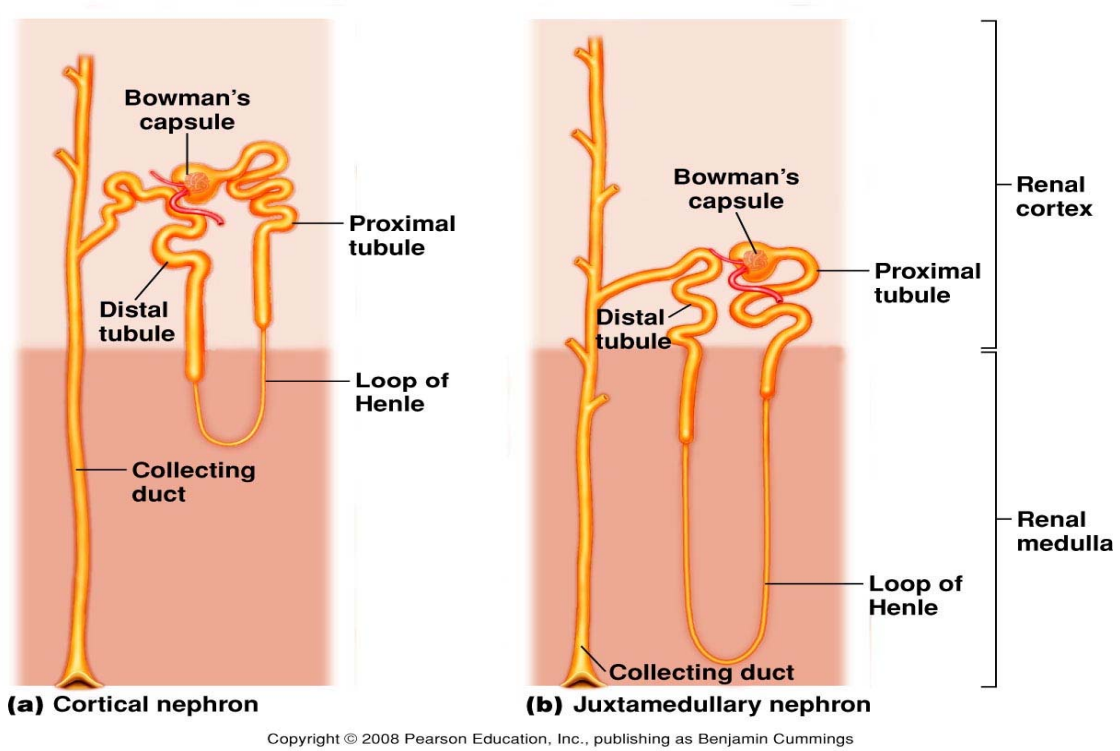

Figure 5: Locations of cortical and juxtamedullary nephron (Principles of Human Physiology, Third Edition, Figure 18.4, The Urinary System: Renal Function @ 2008 Pearson Education, Inc. Benjamin Cummings, Co.)

of the PT can be distinguished, S_1, S_2, and S_3 based upon their histology. The initial portion of the proximal tubule, the S_1 segment begins at the glomerulus and constitutes approximately two thirds of the pars convoluta. The S_2 segment consists of the remainder of the pars convoluta and the initial portion of the pars recta. The S_3 segment represents the remainder of the pars recta and is located in the deep inner cortex and the outer stripe of the outer medulla.

The morphology of the PT epithelial cells exhibit polarity of structure and function which aid in the transport and absorption of many substances, such as Na^+, HCO_3-, Cl^-, K^+, Ca^{2+}, PO_4^{3-}, water, and organic solutes such as glucose and amino acids from the blood into the lumen of the cell. As noted in Figure 6, the epithelial cells of the PT, the basolateral (blood side of the cell) and the luminal or apical membrane (urine side of the cell) begin and end at the tight junctions, which segregate the transport proteins of the basolateral and luminal membranes thereby coordinating paracellular transport movement. However, the tight junctions found in the PT are quite leaky making them permeable to water and most ions, which is in direct contrast to the tight junctions located in the distal tubules and collecting ducts. The basolateral plasma membrane forms numerous lateral invaginations and lateral cell processes which extend from the apical to the basal surface. These lateral cell processes and invaginations also serve to increase the intercellular space of the basolateral membrane which is also where the Na^+,K^+ATPase or Na^+ pump is located. Housed within the lateral cell processes elongated mitochondria can be found and are in close proximity to the plasma membrane, which is characteristic of active transport mechanisms. The apical or luminal surface of the PT, contains extensive microvilli forming the brush border membrane and thereby greatly increasing the surface area of apical membrane. The polarity of the PT epithelium is further evidenced by the unequal distribution of

enzymes, receptors and membrane-bound transporters between the apical and basolateral membranes.

As previously mentioned, the PT has three morphologically distinct segments, S_1, S_2, and S_3. The S_1 segment has a tall brush border and a well-defined vacuolar-lysosomal system. The plasma membrane on the basolateral side of the S_1 segment has numerous lateral invaginations and lateral cell processes containing mitochondria, which is indicative of many active transport processes. The S_2 segment is quite similar to that of the S_1 segment; however, the brush border is shorter, fewer basolateral invaginations are found, and mitochondria are smaller. Within the S_3 segment, virtually no lateral cell processes or invaginations are noted and very few, small mitochondria are randomly distributed within the cell.

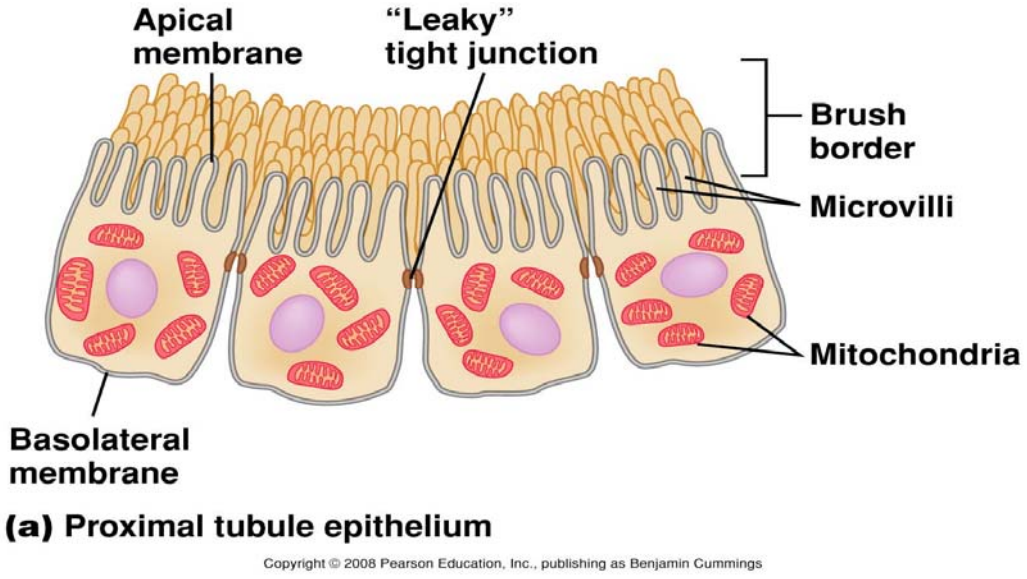

Figure 6: Epithelial cells in selected portions of a renal tubule (Principles of Human Physiology, Third Edition, Figure 18.17a, The Urinary System: Renal Function @ 2008 Pearson Education, Inc. Benjamin Cummings, Co.)

As aforementioned, the proximal tubule is responsible for the uptake of amino acids which occur via several amino acid transporters both on the luminal and basolateral membranes. These amino acid transporters may be ion dependent (e.g., Na^+), or utilize a H^+ gradient and are mostly located on the luminal membrane within the pars convoluta of the proximal tubule to facilitate absorption of amino acids from the filtrate. Furthermore, these transport systems are classified based upon their ability to transport neutral, acidic or basic amino acids. On the luminal membrane, system $B^{0,+}$ has been shown to transport neutral and dibasic amino acids and previous studies have shown that methylmercury thiol-conjugates were transported from lumen-to-cell by system $B^{0,+}$ (Bridges and Zalups, 2006). The basolateral membrane contains at least two amino acid transporters, *A* and *ASC*, which are responsible for the uptake of Na^+-dependent or neutral amino acids. Cysteine or homologs of *L*-cysteine with an additional carbon would be candidates for these amino acid transport systems on the basolateral membrane.

The epithelial cells lining the renal PT have been shown to be the primary cellular targets where mercuric ions gain entry, accumulate, and induce toxic effects *in vivo* (Zalups and Barfuss, 1993). Previous studies with other divalent cations, such as Zn^{2+}, have implicated that these metals may be transported in the kidney bound to amino acids using a Na^+-dependent co-transporter (Barbier et al, 2005). Other studies have implicated at least one of the organic anion transport systems as the method of mercury uptake in the kidney (Koh et al, 2002). However, the mechanism of $Me^{203}Hg^+$ transport, the major form of mercury found in the environment, has yet to be fully understood. Since free $Me^{203}Hg^+$ is very lipid soluble it is important to examine the amount of transport that is occurring via simple diffusion in the basolateral membrane versus actual transport. This will allow for determination of any non-specific binding of $Me^{203}Hg^+$ to surface membrane proteins. Based on the size of the $Me^{203}Hg^+$ molecule (215 amu) and the

toxicity it induces in the PT cells, transport in the renal tubule is most likely occurring via transport with another molecule. $Me^{203}Hg^{+}$ may be combining with an amino acid to act as a molecular homolog and be transported along with these amino acids in the proximal membrane. The most likely candidates for amino acid conjugates are the sulfur containing amino acids such as, *L*-cysteine, *N*-acetylcysteine (NAC), and *L*-homocstyeine since $Me^{203}Hg^{+}$ readily forms bonds with sulfhydryl groups. Furthermore, inorganic mercury is transported as an amino acid conjugate (e.g., Cys-Hg-Cys) using the organic anion transporter (OAT), which is found in the basolateral surface of proximal tubule cells (Zalups et al, 2004). However, it is unknown how the organic form of mercury, $Me^{203}Hg^{+}$, is transported in the basolateral membrane of the PT.

This current research project using the non-perfused tubule technique, will investigate the mechanisms for $Me^{203}Hg^{+}$ transport across the basolateral membrane of the proximal tubule of the rabbit kidney. Basolateral transport will be examined using non-perfused tubules with a volume marker ([^{3}H] *L*-glucose), which will allow for the calculation of the amount of $Me^{203}Hg^{+}$ that contaminates the sample, measuring the cell-to-bath ratios, cytosolic concentrations, and tubular contents. Competitive inhibitors of $Me^{203}Hg^{+}$ conjugates was studied by adding various amino acids or analogs that are transported by the same amino acid transporters as *L*-cystine, such as *L*-cysteine, *N*- acetylcysteine (NAC), and *L*-homocstyeine to the bathing solution. Molecular characterization of the mechanism of renal transport of $Me^{203}Hg^{+}$ will enhance our knowledge of mercury clearance and augment our ability to clinically treat chronic or acute toxic ingestion of $Me^{203}Hg^{+}$ by the addition of competitive inhibitors preventing the uptake of methylmercury in the basolateral membrane of the proximal tubule thus eliminating the induction of the toxic effects.

First Hypothesis: $Me^{203}Hg^{+}$ conjugated to a sulfhydryl-containing amino acid will be transported across the basolateral membrane into the tubular epithelial cells via an amino acid transporter. This mechanism of transport will occur via molecular homology or "mimicry" as the molecular structure of the methylmercury-sulfhydryl conjugate of *L*-cysteine (Cys-S-MeHg-S-Cys) is similar to the amino acid *L*-cystine (Cys-S-S-Cys).

Second Hypothesis: $Me^{203}Hg^{+}$ conjugated to sulfhydryl-containing amino acids will be transported across the basolateral membrane into the tubular epithelial cells by the organic anion transport (OAT) system.

Third Hypothesis: $Me^{203}Hg^{+}$ will be bound to a sulfhydryl-containing amino acid when presented to the basolateral membrane via the blood which will account for the basolateral membrane uptake of $Me^{203}Hg^{+}$ in the PT. The rationale for this hypothesis is that the affinity of $Me^{203}Hg^{+}$ for sulfhydryl groups is quite high, but the molecular form of $Me^{203}Hg^{+}$ is presented for processing in the kidney remains unknown.

CHAPTER II: REVIEW OF THE LITERATURE

Methylmercury's history and toxicity

Methylmercury is just one of the many forms of the heavy metal, mercury (Hg). Mercury has been around for many years and in fact dates back in history to 1100 BC when the Chinese first mined a compound called cinnabar, vermillion, or Chinese red which was in fact mercury sulfide. Some argue that humans have been exposed to the methylated form of the metal dating back to before *Homo sapiens* evolved (Clarkson, 2002). Around 1500 BC, mercury was also found in Egyptian tombs. During the 1800s, mercury was used in hat making by the felters, who were subject to chronic exposures, giving rise to the term "mad as a hatter" as they appeared insane. Methylmercury first appeared during the 1860s when it was synthesized in a laboratory in London and subsequently killed two of the laboratory technicians.

The cycling of mercury begins with the evaporation of mercury vapor from the earth's surfaces, particularly volcanoes. Coal plants, fossil fuel combustion, and waste incineration are also all significant sources of mercury in the environment. Globally, most of the mercury supply is found in Almaden, Spain which has the largest mercury mine in the world and in Idria, Slovenia. Mercury has been used in the treatment of burns, chronic skin disorders, leprosy and syphilis. Dentists have used mercury amalgams since 1833 in New York City (Ozuah, 2000). Throughout history, mercury was found in a number of medicinal products such as diuretics, antibacterial agents, antiseptics, and laxatives. The more recent history of mercury includes the epidemics of $Me^{203}Hg^{+}$ poisoning that have been documented in Japan and Iraq. The Minamata Bay, Japan outbreak of the organic form of the metal occurred in 1953 by the release of Hg^{+}

compounds from a vinyl chloride factory into the bay subsequently poisoning the fish which was later consumed by the local community. Fifty-two people died in this outbreak, while many others suffered brain damage, paralysis, and vision impairment. The outbreak in Iraq occurred from the consumption of homemade bread that was made from seeds treated with ethyl mercury fungicides (Ozuah, 2000). During this outbreak, the warning labels on the packaging were not in the native language, so the local community was unaware that the grains were treated with EthylHg. This was one of the largest outbreaks ever known to occur with over 500 deaths, 6,000 cases admitted to hospitals and as many as, 40,000 individuals poisoned (Clarkson, 2002). The 2006 annual report of the American Association of Poison Control Centers' Toxic Exposure Surveillance System documented 2,477 exposures to mercury or mercury containing compounds. Of these, 274 were in children younger than 6 years of age and 961 were in persons older than 19 years. Overall, 23 individuals were reported to have moderate effects, 1 had major effects, and none died as a result of mercury exposure.

Mercury can exist in three basic forms: elemental mercury, Hg°, liquid or mercury vapor; inorganic mercury; and organic mercury (ethyl-, methyl-, alkyl-, or phenylmercury). The toxic effects of the metal depend upon the type of mercury involved, the method of entry, the exposure dose, and the duration of exposure. The ability of $Me^{203}Hg^{+}$ to accumulate within the body results from its binding properties. Therefore, activity of mercury within humans or other species must consider the different bonding properties of the ions. Mercury ions have a greater propensity for bonding to sulfur atoms (affinity constants ranging from $10^{15} – 10^{20}$), especially on thiol-containing molecules, forming –S-Hg-R. Endogenous thiol-containing compounds include *L*-glutathione, *L*-cysteine, *L*-homocysteine, *N*-acetylcysteine, metallothionein, and albumin. Mercury may also bind with oxygen or nitrogen containing compounds, but the affinity

constants for these groups is about 10 orders of magnitude lower. Although, methylmercury has a high affinity for sulfhydryl compounds, it may also rapidly redistribute to other sulfhydryl groups when available, indicating that the complex may be easily dissociated.

Elemental mercury is the pure metallic form of the metal and is most commonly found in barometers, batteries, calibration instruments, chlor-alki production, dental amalgams, electroplating, fingerprinting products, fluorescent and mercury lamps, infrared detectors, the jewelry industry, latex paint, manometers, neon lamps, paper pulp production, photography, silver and gold production, semiconductor cells, thermometers, and thermostats. Elemental mercury may also be methylated by microorganisms in soil, water, and the GI tract (Patrick, 2002). The toxic effects of elemental mercury transpire after the metal becomes oxidized to the mercuric ion (Hg^{2+}) which may then inhibit cellular function by acting as an enzyme inhibitor, a protein denaturant, may interfere with membrane transport, and neurotransmitter release and uptake. Acute exposure to elemental mercury in significant quantities may produce damage to the lungs, skin, eyes, and gingival (turns green). Lower dose chronic exposures involve the central and peripheral nervous systems (Ozuah, 2000). Manifestations of chronic exposure commonly include excitability, irritability, tremors and gingivitis (Patrick, 2002).

Inorganic mercury (Hg^{2+}), or mercury salts, consists of elemental mercury bound to any other atom except carbon and is formed from the metabolism of elemental mercury vapor or methylmercury. Inorganic mercury is found in antiseptics, antisyphilitic agents, acetaldehyde production, chemical laboratory work, cosmetics, disinfectants, diuretics, explosives, embalming fluid, fur hat processing materials, ink manufacturing, laxatives, mercury vapor lamps, mirror silvering, perfume processing, photography materials, spermicidal jellies, tattooing inks, taxidermy production, teething powders, vinyl chloride production, and wood preservation.

Within the body, inorganic mercury will complex with glutathione in the liver and be secreted in bile as a cysteine-mercury or glutathione-mercury complex (Patrick, 2002). Acute inorganic mercury toxicity primarily affects the kidneys and GI tract. Chronic exposure primarily affects the kidney possibly causing renal failure and the GI tract manifesting as colitis, stomatitis, gingivitis, and extreme salivation (Patrick, 2002).

Organic mercury consists of a mercury atom bonded to at least one carbon, and primarily consists of methylmercury (CH_3HgX) and phenyl mercury (C_6H_5HgX). The organic form of the metal is also the most toxic and frequently encountered form of exposure. Organic mercury toxicity may result from exposure to antiseptics, bactericidals, embalming agents, the farming industry, fungicides, germicidal agents, insecticidal products, laundry products, diaper products, paper manufacturing, pathology products, histology products, seed preservation, and vaccine and wood preservatives. Acute exposure to $MeHg^+$ involves the central nervous system, cardiovascular disease, and the kidney. Nearly all of the $MeHg^+$ (~ 95 %) ingested will be absorbed in the GI tract, although where is still unknown, and subsequently distributed to body tissues (Clarkson, 2002). The remaining 5 % will be found in the blood, mostly bound to red blood cells, but some still remains in the plasma. The half-life of $MeHg^+$ in the body is quite long, approximating 70 days.

In patients suspected of mercury poisoning, it is important to review the patient's occupation, hobbies and consumption of seafood in order to determine the level of exposure. However, both acute and chronic toxicity involve multiple organ systems leading to further diagnostic complications and may even be suggestive of other diseases. Mercury poisoning may present in many ways depending on the form of mercury involved. Elemental mercury usually results in acute toxicity and can lead to pulmonary distress. Symptoms such as shortness of

breath, fever, chills, chest pain, metallic taste, lethargy, confusion, and vomiting may occur. Exposures to inorganic mercury mainly occur through the oral cavity and GI tract with initial symptoms of vomiting, severe abdominal pain, shock, and discoloration of the mucous membranes. Within hours of exposure symptoms may escalate to include loosening of the teeth, metallic taste, and inflammation of the mucosal membranes in the mouth, gingivitis, and necrosis of the renal tubules. Chronic exposures most often result from the organic form of the metal via ingestion of contaminated food, but may also involve acute exposures. The onset of symptoms are usually delayed for days to weeks following exposure and will manifest as neurological, hearing loss, mental deterioration, muscle tremors, paralysis, and possibly death. Thus, a better understanding of $MeHg^{+}$ transport in the kidney will enhance our ability to clinically treat patients exposed to this toxic substance (by facilitating excretion) and preventing entry into the epithelial cells of the kidney.

Methylmercury's induced nephrotoxicity

The kidneys are the primary organs where all forms of mercury are absorbed, accumulated, and will ultimately express toxicity (Zalups, 2000). As aforementioned, the extent of renal damage will depend upon the nature of exposure. Heavy metal uptake in the kidneys can occur via different pathways depending upon the form of the element and segment of the nephron where absorption occurs. Divalent cations in the body may exist as either a non-diffusible (bound to a protein) or diffusible (ionized) form. Heavy metal ions in the blood bind rapidly to albumin, the most abundant protein in the plasma. However, the albumin-metal conjugate formed will not be present in the ultrafiltrate of the nephron as the size of the molecule is too large to pass through the glomerular filtration membrane. Since the majority of mercury

does not exist in the free ionic form in blood, but rather bound to some protein, identification of the mercury conjugate will give further insight into how this metal enters the epithelial cells via the basolateral and luminal membrane of the kidney and induces its toxic effects.

Both the inorganic and organic forms of the heavy metal have been shown to accumulate primarily in the renal cortex and the outer stripe of the medullary region (Zalups, 2000). In a review by Zalups, it was noted that studies have shown that the predominant form of mercury within the kidney of animals exposed to $MeHg^{+}$ is of the inorganic form, suggesting that $MeHg^{+}$ is oxidized to inorganic mercury before or after entering the renal tubule epithelial cells but the mechanism for this transformation remains unknown (Zalups, 2000). Although the renal disposition of divalent cations, such as $MeHg^{+}$ have not been fully elucidated, research studies indicate that the proximal tubule is the primary site of absorption with nearly 70% of the transport occurring within this segment of the nephron (Barbier, 2005). When considering the nephrotoxicity of $MeHg^{+}$, the excretion of the heavy metal must also be considered. Several pathways have been described for the elimination of the metal from the body, including acetylation and conjugation with *L*-cysteine and *L*-glutathione by the liver. Most (~90%) of the $MeHg^{+}$ will exist via fecal excretion, leaving only a small portion of $MeHg^{+}$ to exit via the urine after acetylation in the liver (Ozuah, 2000). The *N*-acetyl-homocysteine methylmercury complex will be excreted along with bile for presentation at the kidneys. This complex may then be absorbed within the renal tubules allowing for the toxic effects of the metal to be induced. However, the location and mechanism of uptake have not been elucidated to date.

Transport of methylmercury across the basolateral membrane in the proximal tubule

The proximal tubule functions as a major transport site for solutes within the nephron, both on the basolateral (blood) and apical (urine of filtrate) membranes. A previous study by Zalups and Barfuss in 1993 examined the luminal transport and toxicity of unbound $Me^{203}Hg^{+}$ in the isolated perfused tubule of the rabbit kidney and noted that the S_1 segment of the proximal tubule was most vulnerable to the toxic effects of free $MeHg^{+}$ as seen by the extent of cellular injury and degeneration that occurred during perfusion with free $Me^{203}Hg^{+}$ at very low concentrations. This study also demonstrated that free or unbound inorganic mercury (Hg^{2+}) does not appear to produce the same level of toxicity to the proximal tubule. Other research has shown that the luminal uptake of inorganic and to some extent, organic mercury within the kidney is linked to the activity of γ-glutamyltransferase (γ-GT), an enzyme predominantly found in the luminal membrane of the proximal tubule (Zalups, 2000).

The proximal tubular cells contain two major organic transport mechanisms, the organic anion transporter (OAT) and the organic cation transporter (OCT) and amino acids transport systems. The organic anion transporter is located on both the basolateral (OAT1, OAT2, OAT3) and luminal (OAT4) side of the PT and functions to carry anions across the membrane. Several molecular species of organic anion transport have been cloned, two of which (OAT1and OAT3) are expressed in the basolateral membrane of the proximal tubule. OAT1 is predominantly found in the S_2 segment of the proximal tubule, and to a lesser extent it is also found in the S_1 and S_3 segments and OAT3 is expressed in all segments of PT ($S_1 > S_2 = S_3$). Evidence implicating the basolateral uptake of mercuric ions via the organic anion transporter comes from studies showing pre-treatment with *para*-aminohippurate (PAH), a competitive substrate for OAT, caused significant reductions in the transport of inorganic mercury (Zalups, 2000). Other

data have also shown that probenicid, another specific substrate for OAT, significantly reduced the renal uptake and accumulation of organic mercury compounds on the basolateral membrane of the proximal tubule (Zalups, 2000).

The organic anion transporters (OATS) within the proximal tubule are driven by a dicarboxylate gradient which is produced by a dicarboxylic acid exchanger mechanism at the basolateral membrane and via intracellular metabolism. Normal metabolic processes with the renal epithelial cells generate α-ketoglutarate, resulting in a gradient favoring the movement of this compound out of the cell. If the gradient becomes large enough, α-ketoglutarate is exchanged with organic anions via OAT. Furthermore, α-ketoglutarate along with other dicarboxylic acids, may all re-enter via the basolateral membrane by the Na^+-dicarboxylic acid cotransporter driven by the Na^+ or sodium ion gradient, which is produced by the Na^+, K^+-ATPase mechanism. It is plausible to then ascertain that other dicarboxylates may create competition for the sodium dependent uptake of α-ketoglutarate at the dicarboxylic acid cotransporter thereby reducing the basolateral mechanism promoting the update of α-ketoglutarate. This will in turn, decrease the concentration of α-ketoglutarate and further reduce its movement out of the proximal tubular cells in exchange for the uptake of an organic anion. Furthermore, excessive dicarboxylates may also present competition for organic anion transport at OAT and hence, decrease mercuric conjugates presented at the basolateral membrane as well. Other studies have suggested that conjugated Hg^{2+} is taken up by the proximal tubule cells of the kidney via an organic anion exchanger, but the mechanism of this transporter has not been well characterized (Zalups et al, 2004).

Several possible ligands have been suggested to be bound to mercury when presented at the organic anion transporter of the basolateral membrane of the proximal tubule. Two ligands

that have been examined are *L*-glutathione and *L*-cysteine. Glutathione transport by OAT was demonstrated by studies of Lash and Jones in 1983, who showed that transport of this tri- amino acid, was blocked by probenicid. Other data has demonstrated that *L*-cysteine conjugates were also OAT dependent and transport was inhibited by PAH and probenicid. These data implicate that mercuric conjugates of *L*-glutathione and *L*-cysteine, as well as, any other thiol containing amino acid or amino acid derivative such as *DL*-homocysteine, *N*-acetylcysteine, *L*-taurine or *L*-methionine could also be taken up at the basolateral membrane of the proximal tubule by the organic anion transport system.

The organic cation transporters (OCT) are also located on the basolateral (OCT1, OCT2, OCT3) and luminal (OCT2) membrane and transport cations, as well as, weak organic bases. Two transporters have been identified known as OCT1 and OCT2. This class of compounds includes molecules that are not only physiologically important, but may also include molecules that have a toxicological effect in the body. Organic cation entry into the cell via the basolateral membrane occurs because of the inside negative membrane potential, whereas organic cation exit follows a transmembrane electrochemical gradient for H^+. In the kidney, the proximal tubule is the primary site of active organic cation secretion (Wright, 2004).

As previously stated, very little is known about the transport of $MeHg^+$ in the proximal tubule. Other heavy metals, such as zinc, have been shown to be transported attached to an amino acid via a sodium ion or Na^+-dependent amino acid exchanger, therefore; maybe $MeHg^+$ is conjugated to an amino acid in the same way during transport. Previous studies have established that the proximal tubule contains amino acid transport systems present in both the basolateral and the luminal membranes (Cannon et al, 2001; Kanai and Endou, 2003). Luminal transport studies of $Me^{203}Hg^+$ were done in 1993 by Barfuss and Zalups which demonstrated

differential toxicity of $Me^{203}Hg^{+}$ among the three segments of the proximal tubule. That study found that the S_1 segment of the proximal tubule was most vulnerable to the toxic effects of $Me^{203}Hg^{+}$ as seen by the extent of cellular injury and degeneration that occurred during perfusion with $Me^{203}Hg^{+}$ at very low concentrations of free $Me^{203}Hg^{+}$ and that free inorganic mercury (Hg^{2+}) does not appear to produce the same level of toxicity to the proximal tubule. However, the transport of $MeHg^{+}$ has yet to be fully characterized for the luminal or the basolateral membranes of the proximal tubule. A better understanding of the renal mechanisms of $MeHg^{+}$ transport within the body and ultimately blocking those transport mechanisms thereby allowing the metal to be excreted in the urine will enhance the clinical treatment of mercury poisoning. This is the first study designed to address the transport of $MeHg^{+}$ at the basolateral membrane.

Possible measures that protect against $Me^{203}Hg^{+}$ toxicity

Accelerating $MeHg^{+}$ clearance from the body can reduce or eliminate its toxicity. However, the mechanisms of $MeHg^{+}$ clearance from the body remains unknown. As mentioned above, divalent cation transporters (DCT) in the proximal convoluted tubule cells of the kidney are important for the regulation of plasma concentrations of endogenous and exogenous compounds including those that are toxic. One of the current mechanisms of accelerating $MeHg^{+}$ clearance involves the use of chelating agents. The more commonly used chelators consist of non-sulfur conjugates such as, ethylenediaminetetraacetate, triethylenetetramine, deferoxamine, and deferiprone or sulfur containing compounds such as, meso-2,3-dimercaptosuccinic acid (DMSA), DMPS, and diethyldithiocarbonate, both of which can be toxic to the human body. The sulfur containing chelators make use of the bonding properties of $MeHg^{+}$, encouraging the metal to move from one sulfhydryl-containing compound to another.

Another chelating agent, *N*-acetylcysteine, which is not toxic to the body and rapidly eliminated in the urine has been investigated as a possible use in the treatment of $MeHg^{+}$ poisoning (Ballatori et al, 1998). These chelating agents could be used to treat acute and chronic exposures to methylmercury by facilitating the secretion of the metal into the urine and ultimately out of the body

CHAPTER III: MATERIALS AND METHODS

Animals

Female New Zealand White rabbits (1-2 kg) were used in the current study. Rabbits were adapted to housing for at least two days prior to any experimentation. Water and a commercial laboratory diet for rabbits were provided *ad libitum* during all phases of the study.

Composition of buffer solution

The buffer solution for all experiments consisted of a simple electrolyte solution. Tissue was placed in a sucrose/phosphate buffer containing 125 mM sucrose, 13.3 mM anhydrous monosodium dihydrogen phosphate (NaH_2PO_4), and 56 mM anhydrous disodium monohydrogen phosphate (Na_2HPO_4). The pH was adjusted to 7.4 by the addition of either 1 N NaOH (sodium hydroxide) or HCl (hydrochloric acid). The osmolality was adjusted to 290 mOsm/Kg of water by the addition of either water or NaCl (sodium chloride).

Composition of bathing and tubular dissection solution

In all experiments performed the solution used for tubular dissection and bathing of the non-perfused tubules consisted of 140 mM Na^+, 140 mM Cl^-, 5 mM K^+, 2.5 mM Ca^{2+}, 1.2 mM Mg^{2+}, 1.2 mM SO_4^{2-}, 2 mM $HPO_4^{2-}/H_2PO_4^-$, 1 mM *D*-glucose, and 0.5 mM *L*-glutamate. The pH was adjusted to 7.4 by the addition of either 1 N NaOH or HCl. The osmolality was adjusted to 290 mOsm/Kg of water by the addition of either water or NaCl. To evaluate the transport of

$Me^{203}Hg^{+}$ or conjugates thereof, $Me^{203}Hg^{+}$ was added to the bathing solution. [^{3}H]-*L*-glucose (14.6 Ci/mmol; American Radiolabeled) was added to the bathing solution as a volume marker. [^{3}H]-*L*-glucose is used as a volume marker because it does not adhere to cell membrane, is not transported, is only slightly able to penetrate tight junctions or cell membranes and is water soluble.

Preparation of $^{203}Hg^{+}$

The preparation of $^{203}Hg^{+}$ begins with 3 mg of pure HgO (mercury oxide) sealed in a pure quartz (silicone oxide) ampule which is heated to seal closed. The sealed ampule is sent to the University of Missouri Research Reactor Center (MURR) in Columbia, Missouri to be irradiated. During irradiation, the 3 mg of HgO becomes ^{203}HgO. The 3 mg of ^{203}HgO is converted to $^{203}HgCl_2$ by crushing the ampule in a 2 ml plastic vial and adding 1 ml of 1 N HCl. This process occurs within a radioactive hood, behind a lead shield with lead bricks protecting both the right and left sides and using all necessary radiation safety precautions. This solution is allowed to incubate for approximately 24 hours to complete the conversion of ^{203}HgO to $^{203}HgCl_2$. Following incubation, the solution is separated from the crushed quartz by transferring to a new vial and the specific activity is measured using an Ion Chamber (1mCi=0.52mR/hr at 0.5M (19.6”) or 1mCi=0.16mR/hr at 1.0M (39.36”)).

Preparation of $Me^{203}Hg^{+}$

The method used for preparation of $Me^{203}Hg^{+}$ was adapted from Rouleau and Block. A 2 M acetate buffer solution was prepared by adding 11.8 ml of glacial acetic acid to 50 ml of Millipore water (de-ionized tap water that has been further filtered using the Millipore filter

system) in a 125 ml FEP (a specific polymer of plastic that minimizes binding) bottle. Then 27.2 g sodium acetate was added and the solution was diluted to 100 ml. This acetate buffer solution was stored in the freezer between experiments. Next, 25 mg of methylcobalamin (the methyl donor) was dissolved in 12 ml of the acetate buffer which turned the solution red. This solution was also stored in the freezer between experiments. The final solution was a 30% KCl in 4% HCl which was prepared by dissolving 37.5 g of potassium chloride in 100 ml of Millipore water in a 125 ml FEP bottle and then adding 5 ml of HCl diluted to 125 ml. Heat was added to the solution to facilitate dissolving and then stored at room temperature between experiments. The $^{203}HgCl_2$ was prepared by adding ^{203}Hg from the original recovery stock solution in 1N HCl with a minimum volume of 40 µl to 1 ml of Millipore water. This solution was then placed in a dried trace metal acid washed 20 ml glass scintillation vial. The pH of this solution was measured to ensure a range of 1-2 which is crucial because if the pH is too high the conversion efficiency to $Me^{203}Hg^{+}$ will be compromised. Alternatively, if the pH is too low, dimethyl-Hg will be formed instead of $Me^{203}Hg^{+}$.

The reaction solution was then prepared by adding 0.67 ml of the 2M acetate buffer solution to the 20 ml scintillation vial containing the 1 ml dilute ^{203}Hg. Next, 2 ml of the methylcobalamin solution was added and then placed in the lead pig to react for approximately 24 hours. The final volume of the reaction solution was 3.67 ml. The total activity was measured using an Ion Chamber (1mCi=0.52mR/hr at 0.5M (19.6") or 1mCi=0.16mR/hr at 1.0M (39.36")).

The extraction of the $Me^{203}Hg^{+}$ was performed by adding 16.7 ml of the potassium chloride solution, 16.7 ml Millipore water and the 3.67 ml reaction mixture to a 125 ml Nalgene separatory funnel (giving a total volume of 37.07). The $Me^{203}Hg^{+}$ was then extracted with five

washes of 8.3 ml of dichloromethane (DCM). The sequence of washes to extract the $Me^{203}Hg^{+}$ was as follows. The pipet was first conditioned by flushing with DCM to prevent dripping. After each addition of 8.3 ml DCM to the solution in the funnel, the separation funnel cap was tightened and then inverted several times to facilitate mixing. Following mixing, the solution was vented by unscrewing the top of the funnel and then the cap was re-tightened. The separator funnel was then place in a foil covered beaker on a benchtop shaker set at approximately 10 rpm and mixed gently for 5 minutes keeping the funnel covered with foil to prevent any light from entering. Following mixing, the funnel was then secured to a stand, the funnel cap was opened and a clean FEP (250 ml) bottle that was wrapped in foil was placed beneath with the valve open. The DCM was then drained from the bottom layer into the FEP bottle. The extraction washes were repeated five times giving a final volume of 41.5 ml of the DCM- $Me^{203}Hg^{+}$ solution. The waste solution (red) was drained out of the funnel into the 125 ml FEP bottle. Next, the DCM- $Me^{203}Hg^{+}$ solution was poured back into the separation funnel and washed twice with 8.3 ml of Millipore water. The top, clear, pink layer formed the aqueous layer and the bottom, clear, colorless layer contained the $Me^{203}Hg^{+}$ in DCM which was saved into the same 250 ml FEP and stored behind the lead shields. The aqueous layer was drained into the waste bottle containing the red solution.

The final extraction of $Me^{203}Hg^{+}$ was performed by adding 8.3 ml of Millipore water to the DCM layer. Nitrogen (N_2) gas was then bubbled through the water layer into the DCM-$Me^{203}Hg^{+}$ solution by using a hypodermic needle on one end of the tubing. The N_2 gas was released at about 5 bubbles per second to ensure that freezing of the solution did not occur. This final extraction step occurred in the dark, covering the FEP bottle aluminum foil and shielded with lead. All of the DCM solution was allowed to evaporate until only 8.3 ml of the water

remained containing the $Me^{203}Hg^{+}$. This final solution was placed in a pre-weighed trace metal acid washed glass 20 ml scintillation vial and weighed to determine the final volume. Pure HCl was added resulting in a final 8.3 ml of $Me^{203}Hg^{+}$ solution in 1% HCl by volume.

Samples of 20 μM $Me^{203}Hg^{+}$ and 5 μM [^{3}H]-*L*-Glucose were dried down to remove the HCl solution. Dried samples were then reconstituted in the standard bathing solution using various amino acids or amino acids plus inhibitors for individual experiments.

Procedure for obtaining segments of proximal tubules

Rabbits were anesthetized with a combination of 33 mg/kg ketamine (FORT DODGE) and 33 mg/kg xylazine (LLOYD). When the rabbit reached a state of deep anesthesia (determined by the absence of a corneal reflex) the abdominal wall was cut and the kidneys were immediately removed. The kidneys were then immediately sliced into 1-2mm thick coronal sections using a single-edge razor blade and placed in a cold (4°C) aqueous sucrose-phosphate buffer solution on ice to be stored for up to 8 hours for dissection. Individual tubule segments were obtained by manual dissection while in the dissection solution. The S_1, S_2 and S_3 segments of the proximal convoluted tubule (PCT) were individually dissected from the coronal sections. The S_1 segments were identified as convoluted tubules dissected from the outer cortical region of the kidney section. The S_2 segments were identified as the straight portion of the proximal tubule spanning the entire thickness of the cortex (Figure 7) and the S_3 segments were identified as the terminal 1 mm portion of the proximal tubule located in the outer stripe of the outer medulla. The S_2 were chosen for study because it makes up the major portion of the pars recta of the

proximal tubule and it not only accumulates the inorganic form of mercury, but is also involved in the nephrotoxicity induced by inorganic mercury, indicating these same effects may be involved with the transport of $Me^{203}Hg^{+}$.

Figure 7: S_2 segment of the rabbit proximal tubule.

Method for non-perfused segments of the proximal tubule

Individual dissected tubules were gathered together in the dissection dish by groups of 10-15 tubules. Transfer to the bathing solution occurred by sucking the group of tubules into a glass pipet via a tuberculin syringe connected by tubing. Dissected tubule segments were then transferred to a Lucite bathing chamber (Figure 8) connected to either a warm bath (for experiments performed at 37°C) or a cooling bath (for experiments performed at 12°C). The Lucite chamber contained 120 µl of bathing solution containing $Me^{203}Hg^{+}$ alone or $Me^{203}Hg^{+}$ conjugated to an amino acid, an amino acid derivative, or the conjugate plus an inhibitor.

Approximately 3 ml of mineral oil was placed on top of the bathing solution to prevent evaporation of the bathing solution water. The bathing solution was continuously stirred with a reciprocating piston pump while the tubule segments were incubated for twenty minutes. Cellular changes were observed during this time for indications of $Me^{203}Hg^{+}$ toxicity by either visual conformation of swelling in the tubules or by the use of a vital stain dye [FD&C green number 3] which will rapidly adhere to cytoplasmic contents, thus indicating that the cellular membrane has been compromised which is indicative of toxicity to the cells. Individual tubule segments lengths were measured during the twenty minute incubation period using an ocular micrometer.

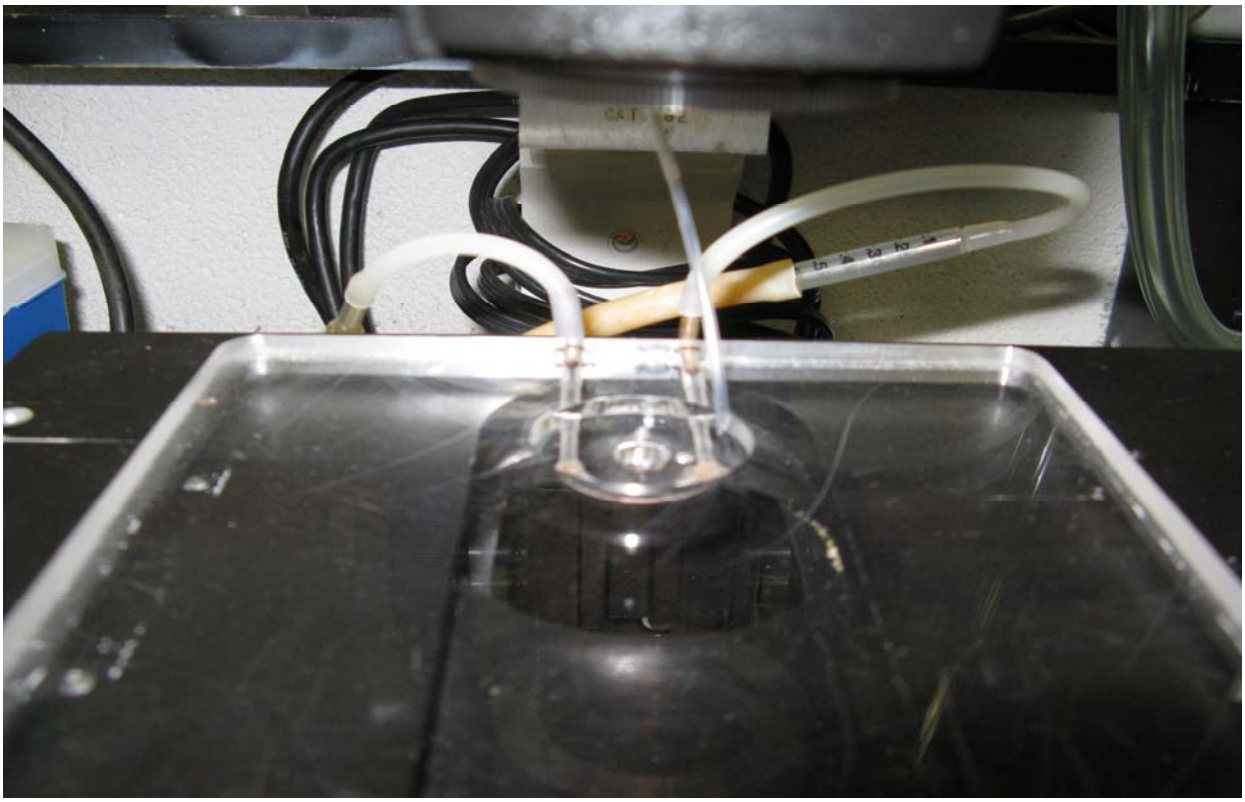

Figure 8: Lucite bathing chamber.

Harvesting of non-perfused segments of the proximal tubule

After the incubation period, single tubule segments were removed from the bathing solution via glass pipets that had been manually made using a Microforge to extend the tips of the pipets. To calculate the cellular content of $Me^{203}Hg^{+}$ in the non-perfused segments of the proximal tubule, the tubule was removed from the bathing solution and placed in 10 µl of 3% (W/V) TCA (trichloroacetic acid). The TCA precipitated the larger proteins leaving the tubule opaque-white and rigid while releasing the cytosolic contents into the TCA solution. The reaction is nearly instantaneous so the tubule segment (TCA-precipitable fraction) was removed after a few seconds of washing from the TCA solution and placed in a vial containing 4 ml of scintillation fluid. The scintillation vials were later counted using standard isotopic methods for the contents of $^{203}Hg^{+}$ and the volume marker, [^{3}H]-*L*-glucose. The TCA solution (TCA-soluble fraction, presumably the cytosolic contents) was also collected, placed in a scintillation vial containing 4 ml of scintillation fluid and later counted using standard isotopic methods. The TCA-soluble fraction allowed for the approximate calculation of the cellular content of $Me^{203}Hg+$ (µM).

Calculations

In bath-to-cell transport experiments, transport of $Me^{203}Hg^{+}$ calculations were based on estimated volumetric cellular concentration taken by the diameter and length of the tubule. Counts per minute (CPM) were used to determine the concentration of $Me^{203}Hg^{+}$ or $Me^{203}Hg^{+}$ conjugates in a given tubule. Pre- and post-bath measurements were counted to estimate any volume dilution of the bathing solution that may have occurred during tubule transfer. Bath

concentrations were determined from the isotope concentration (μM) and the pre/post bathing solution measurements taken.

Cell-to-bath ratio. Cell-to-bath concentration ratio of ^{203}Hg was calculated by dividing the cytoplasmic concentration (μM) of the tubule by the bathing solution concentration (μM).

Cytosolic concentration. Cytosolic concentration (fmol/mm) of ^{203}Hg was calculated by multiplying the cytoplasmic concentration (μM) of the tubule by the cell volume (nL) and dividing by the length (mm) of the tubule segment.

Tubular content. Tubule content (fmol/mm) of ^{203}Hg was calculated by subtracting the amount of ^{203}Hg (fmol) present in the bathing solution collected along with the tubule (extracellular ^{203}Hg) from the total tubular ^{203}Hg and dividing by the tubular length. The amount of extracellular ^{203}Hg was calculated by multiplying the volume of the bathing solution (nl) with the bathing solution ^{203}Hg concentration (fmol/nl). The volume of the bathing solution collected with the tubule was measured by multiplying the total tubule ^{3}H-glucose (CPM) by the concentration of ^{3}H-glucose (nl/CPM) in the bathing solution.

Statistical analysis

A minimum of five tubules were used for each experimental condition. In addition, data for each parameter was assessed by obtaining tubular segments isolated from at least two animals. For each non-perfused tubule, the cell-to-bath, cytosolic and tubular concentrations were averaged. These averaged values were used to compute the overall mean and standard error for each experimental condition. The mean values of the various groups were tested for differences using the student's t-test. Values were assumed to be significantly different when $P<0.05$.

Protocol for plasma samples with $Me^{203}Hg^{+}$

The initial estimate of the amount of $Me^{203}Hg^{+}$ bound within the components of the blood was performed by collecting samples rabbits prior to the removal of the kidneys for the non-perfused experiments described above. Blood was obtained from the renal vein in Na-Citrate collection vials. Aliquots of 1 ml samples of blood were transferred to micro-centrifuge tubes (six total) and 5 µl of $Me^{203}Hg^{+}$ stock solution were added. Three of the six specimens were vortexed lightly to ensure proper mixing of the solutions. Samples were then centrifuged at ~10,000 RPM for 1-2 minutes to separate the cellular fraction of blood from the plasma. The three microcentrifuge tubes containing the $Me^{203}Hg^{+}$ were then placed in a Gamma Counter to estimate the amount of isotope. Plasma from the remaining three vials was then transferred to new vials and 5µl of $Me^{203}Hg^{+}$ was added. These samples were then vortexed lightly and placed in the Gamma Counter as well. To separate the proteins from the plasma solution, 100 µl of 20% TCA was added and the samples were then centrifuged at ~14,000 RPM for 3-5 minutes. The plasma was then transferred to new microcentrifuge vials and all vials were placed in the Gamma Counter for isotopic determination.

Further analysis of the amount of $Me^{203}Hg^{+}$ bound within the components of the blood consisted of only examining the plasma fraction. Blood was again obtained from the renal vein of rabbits in Na-Citrate and Heparin collection vials. Aliquots of 1.5 ml samples of blood were transferred to micro-centrifuge tubes (six total) and centrifuged at ~10,000 RPM for 1-2 minutes to separate the cellular fraction of blood from the plasma. Two of the samples (one from the Heparin collection vial and one from the Na-citrate collection vial) were used as controls. A 100 µl aliquot was removed from each microcentrifuge tube for analysis by mass spectrometry. The control samples were then mixed with a 20 % TCA solution, centrifuged again at ~10,000 RPM

for 1-2 minutes to separate the cellular fraction and another 100 µl aliquot was removed from each microcentrifuge tube for analysis by mass spectrometry.

The remaining four microcentrifuge tubes (two containing the plasma supernatant from the Heparin collection vial and two containing the plasma supernatant from the Na-Citrate collection vial) were mixed with a 20 % TCA solution and centrifuged again at ~10,000 RPM for 1-2 minutes to separate the cellular fraction. The supernatant from each of these tubes was then pipetted into a new microcentrifuge tube and 100 µl of a 20 µM $MeHgCl^+$ solution was added. These samples were then analyzed by mass spectrometry.

Mass spectrometry

An electrospray-quadrupole/time-of-flight spectrometer (Waters Micromass Q-TOF^{TM} micro, Waters Corporation, Milford, Massachustts, USA) was used to carry out the mass spectrometric experiments in a positive or negative mode. The instrument was calibrated with a sodium formate solution. Nitrogen supplied by a nitrogen generator (Model 75-72, Parker Balston, Haverhill, MA, USA) was used as the cone gas at 50 L/hr and as the drying gas heated to 150°C at a flow-rate of 450L/min to evaporate solvents in the spray chamber. Argon was used as the collision gas. The source temperature was at 80^{o}C and the desolvation temperature was at 150^{o}C. The samples were prepared by mixing with MeOH containing 0.1% HCOOH for positive mode analysis or MeOH containing 0.5%NH3 for negative mode at a 1:1 ratio. All solutions were continuously infused by means of a syringe pump at a typical flow-rate of 5 µl min^{-1} into the electrospray probe. MassLynx (version 4.0) software was used for instrument control, data acquisition and processing. Mass spectrometry analysis was performed on $MeHgCl^+$ and $MeHgCl^+$-amino acid conjugates to identify the binding properties of the molecule

with the sulfhydryl containing amino acids (*L*-cysteine, *L*-methionine, *L*-taurine, *L*-glutathione, *DL*-homocysteine, *N*-acetylcysteine). Individual amino acids were examined alone for confirmation of molecular weight and in combination with $MeHg^{+}$. Mass spectrometry analysis was also performed on the supernatant from the plasma samples described above.

CHAPTER IV: RESULTS

Basolateral transport of $Me^{203}Hg^{+}$

To characterize the basolateral uptake of $Me^{203}Hg^{+}$, 20 μM $Me^{203}Hg^{+}$ was added to the bathing solution. The average cell-to-bath ratio and cytosolic contents of $Me^{203}Hg^{+}$ at 12°C and 37°C are noted in Figure 9. Methylmercury uptake (126 ± 13.4) was significantly greater (P = 0.0001) at 37°C when compared to temperature conditions of 12°C (2.5 ± 2.2). The average cytosolic concentration of $Me^{203}Hg^{+}$ at 12°C and 37°C are 59 μM ± 51 and 4,360 μM ± 1090.7 (P = 0.0185) demonstrating again increased cellular contents of $Me^{203}Hg^{+}$ at normal physiological temperatures. To investigate the amount of $Me^{203}Hg^{+}$ bound to the basolateral epithelium the tubular contents (fmol mm^{-1}) and percentage of tubular contents of $Me^{203}Hg^{+}$ at 12°C and 37°C were examined and are noted in Figure 10. The bound $Me^{203}Hg^{+}$ at 12°C was 7,418.9 ± 584.5 fmol mm^{-1} was significantly less than the amount bound at 37°C 20,142.3 ± 2,023.3 fmol mm^{-1} (P = 0.0005). The percentage of bound $Me^{203}Hg^{+}$ when compared to the total contents of $Me^{203}Hg^{+}$ present in the bathing solution was 99 % and 84 % for 12°C and 37°C (P = 0.01), respectively.

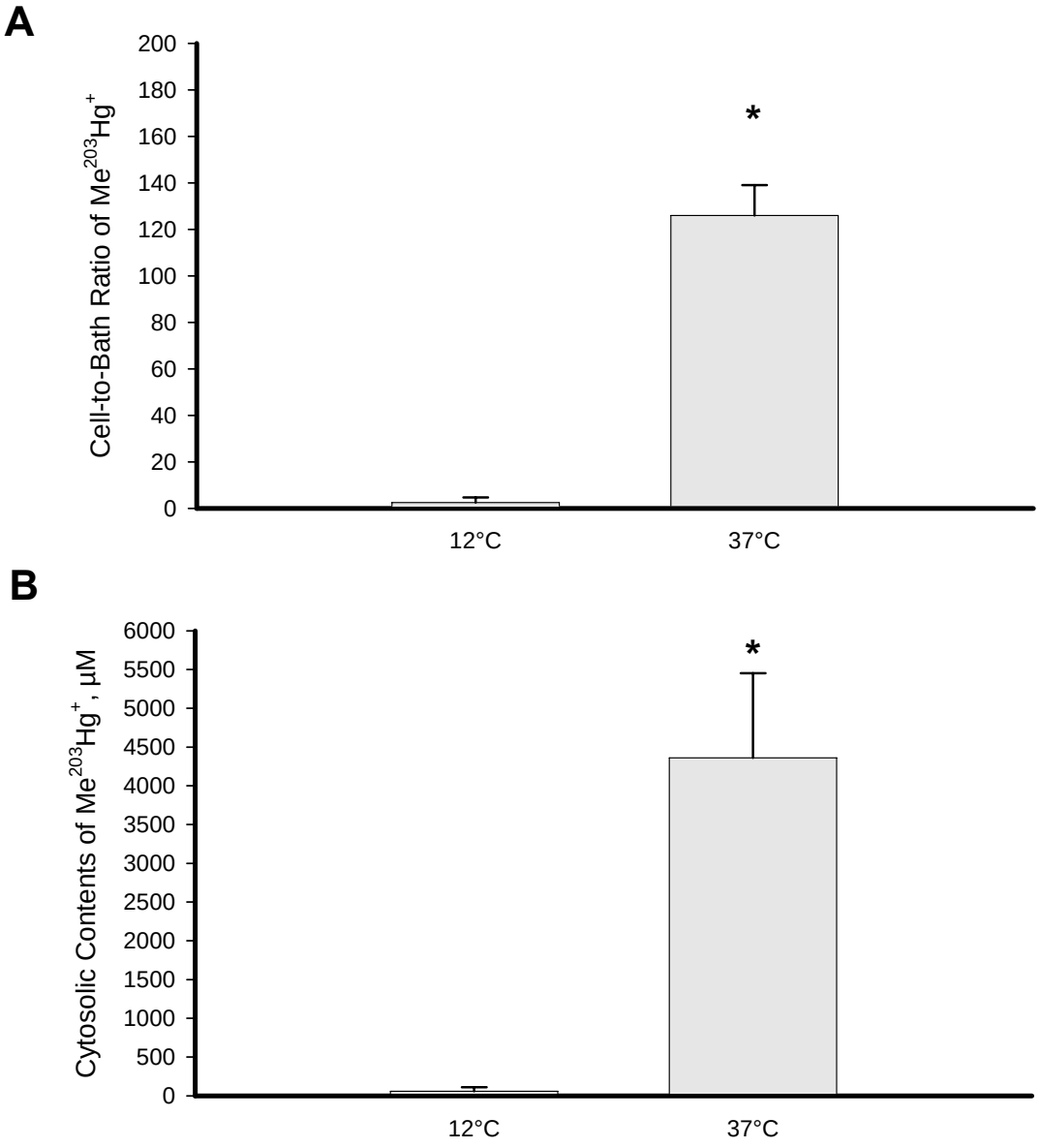

Figure 9: $Me^{203}Hg^{+}$ transport in the basolateral membrane of the S_2 segments of rabbit proximal tubules (A) cell-to-bath ratio and (B) cytosolic contents, µM. Each value represents the mean ± SE with a minimum sample size of 5 tubules. The "*" indicates a significant statistical difference, $P \leq 0.05$.

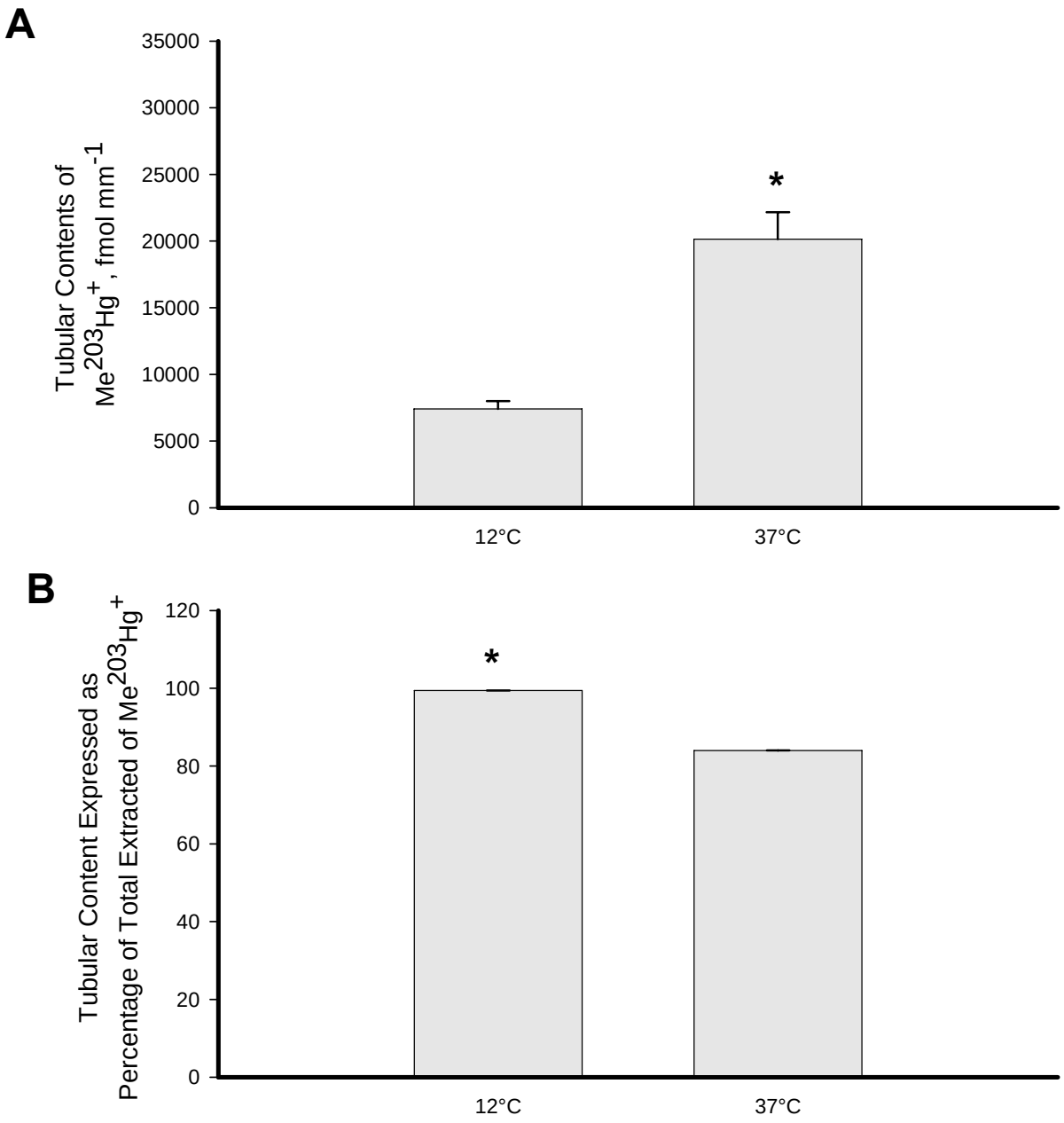

Figure 10: $Me^{203}Hg^{+}$ transport in the basolateral membrane of the S_2 segments of rabbit proximal tubules (A) tubular contents and (B) tubular content expressed as percentage of total extracted. Each value represents the mean ± SE with a minimum sample size of 5 tubules. The "*" indicates a significant statistical difference, $P \leq 0.05$.

The effect of TEA on basolateral transport of $Me^{203}Hg^{+}$

To characterize the effect of TEA on the basolateral uptake of $Me^{203}Hg^{+}$, 20 μM $Me^{203}Hg^{+}$ along with 22 μM TEA was added to the bathing solution. The average cell-to-bath ratio and cytosolic contents of $Me^{203}Hg^{+}$-TEA at 37°C are noted in Figure 11. Bath-to-cell uptake of $Me^{203}Hg^{+}$-TEA (162.5 ± 34) was not significantly increased (P = 0.2380) at 37°C when compared to uptake of $Me^{203}Hg^{+}$ alone (126 ± 13.4). The average cytosolic concentration of $Me^{203}Hg^{+}$ and $Me^{203}Hg^{+}$-TEA are 4,360 μM ± 1090.7 and 2,282.5 μM ± 500 (P = 0.202) demonstrating no significant increase in the cellular contents of $Me^{203}Hg^{+}$ versus $Me^{203}Hg^{+}$-TEA at normal physiological temperatures. The amount of $Me^{203}Hg^{+}$ versus $Me^{203}Hg^{+}$-TEA bound to the basolateral epithelium the tubular contents (fmol mm^{-1}) and percentage of tubular contents are noted in Figure 12. The bound $Me^{203}Hg^{+}$-TEA complex (22,388 ± 2,820.5 fmol mm^{-1}) was not significantly greater than the bound $Me^{203}Hg^{+}$ (20,142.3 ± 2,023.3 fmol mm^{-1}) (P = 0.525). The percentage of bound $Me^{203}Hg^{+}$-TEA complex compared to the percentage of $Me^{203}Hg^{+}$ bound was 92.1 % and 84 % (P = 0.097), respectively.

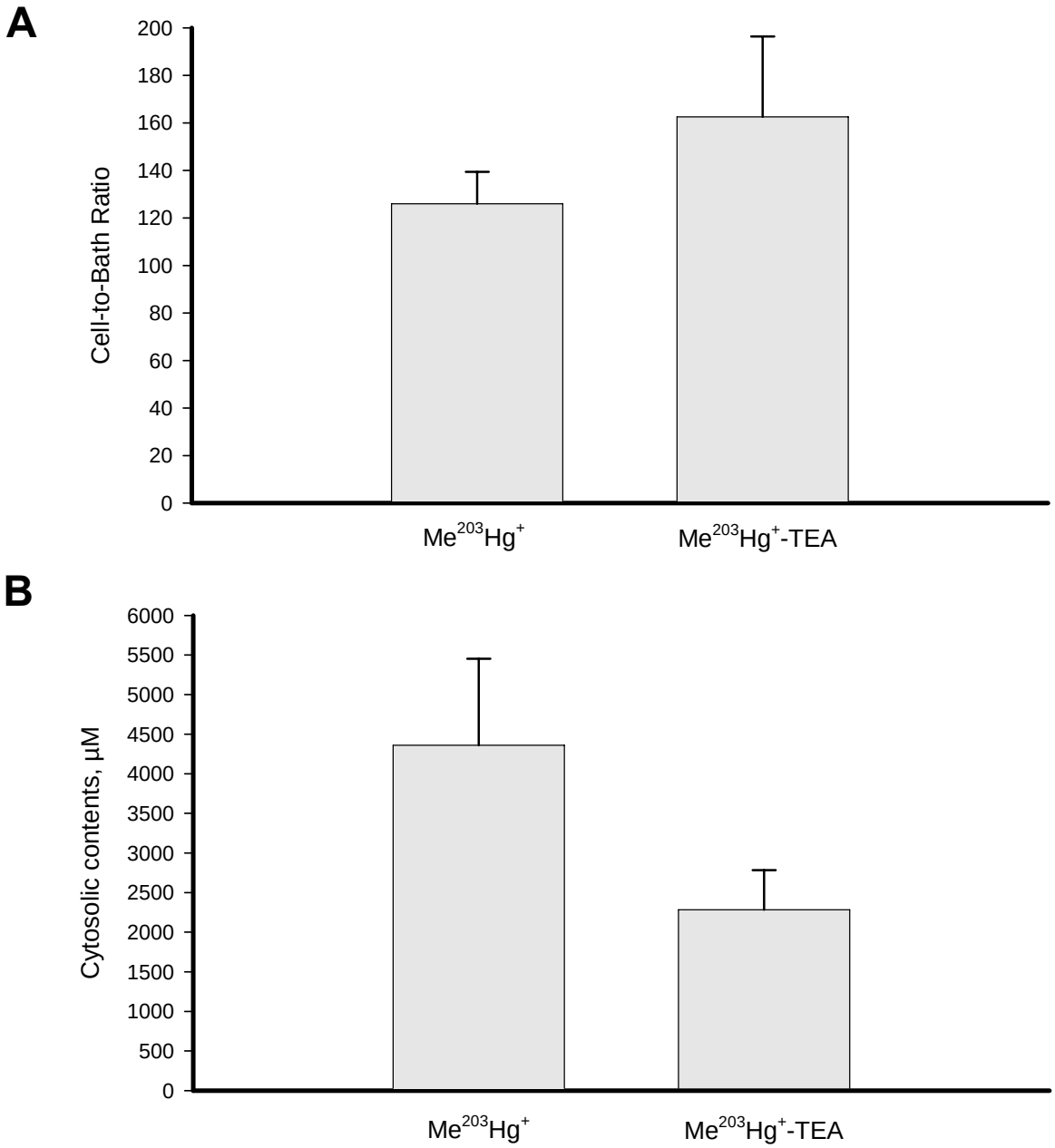

Figure 11: The effect of TEA on $Me^{203}Hg^{+}$ transport in the basolateral membrane of the S_2 segments of rabbit proximal tubules (A) cell-to-bath ratio and (B) cytosolic contents, µM. Each value represents the mean ± SE with a minimum sample size of 5 tubules.

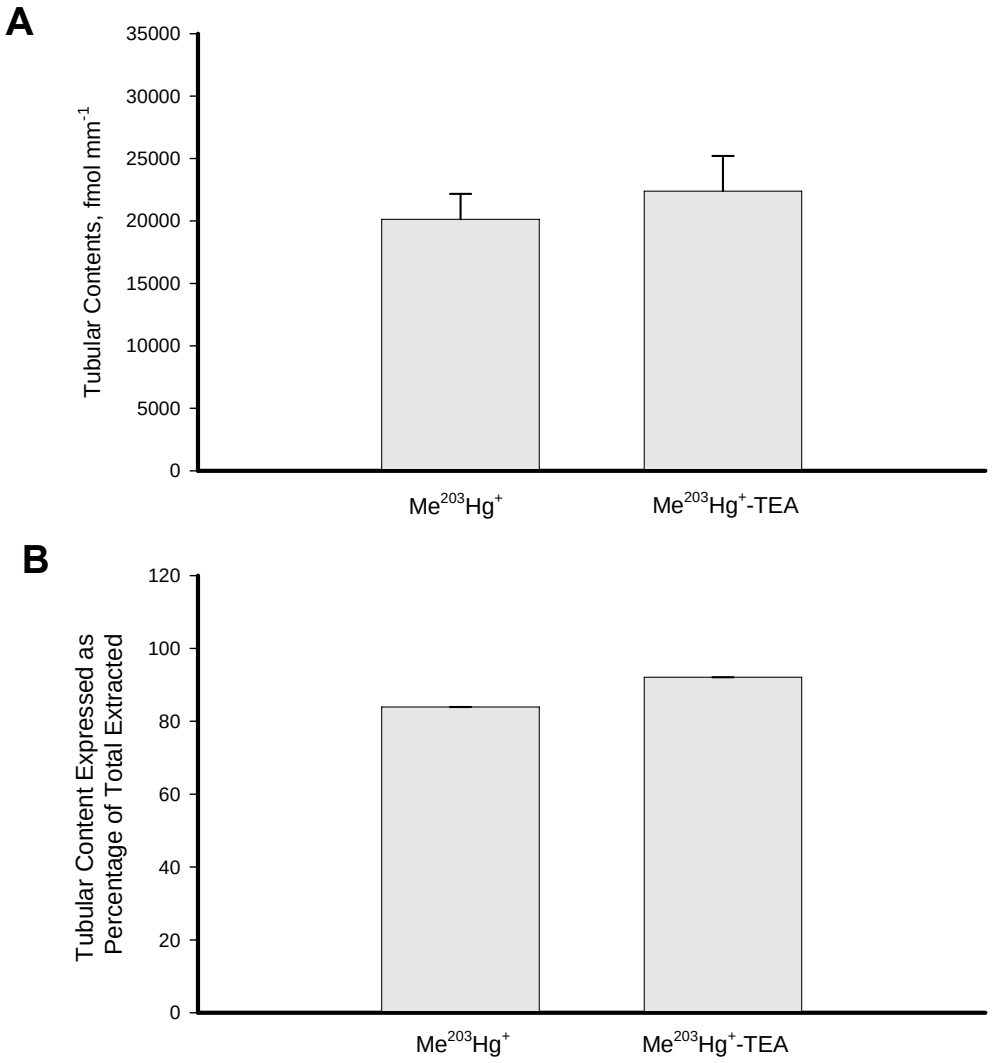

Figure 12: The effect of TEA on $Me^{203}Hg^{+}$ transport in the basolateral membrane of the S_2 segments of rabbit proximal tubules (A) tubular contents and (B) tubular content expressed as percentage of total extracted. Each value represents the mean ± SE with a minimum sample size of 5 tubules.

The effect of *L*-cysteine on the basolateral transport of $Me^{203}Hg^{+}$

To characterize the effect of *L*-cysteine on the basolateral uptake of $Me^{203}Hg^{+}$, 20 μM of $Me^{203}Hg^{+}$ along with 22 μM of *L*-cysteine was added to the bathing solution. The average cell-to-bath ratio and cytosolic contents of $Me^{203}Hg^{+}$-*L*-cysteine at 12°C and 37°C are noted in Figure 13. Bath-to-cell uptake of $Me^{203}Hg^{+}$-*L*-cysteine (32.1 ± 5.2) was significantly increased (P = 0.0023) at 37°C when compared to uptake of $Me^{203}Hg^{+}$-*L*-cysteine at 12°C (7.3 ± 2.3). The average cytosolic concentration of $Me^{203}Hg^{+}$-*L*-cysteine at 12°C and 37°C was 119.2 μM ± 37 and 496.8 μM ± 71.2 respectively, demonstrating significantly (P = 0.001) increased cellular contents of $Me^{203}Hg^{+}$-*L*-cysteine at normal physiological temperatures. The amount of $Me^{203}Hg^{+}$-*L*-cysteine at 12°C and 37°C bound to the basolateral epithelium of the tubule (fmol mm^{-1}) and percentage of tubular contents are noted in Figure 14. The amount of bound $Me^{203}Hg^{+}$-*L*-cysteine complex at 37°C was 11,107.8 ± 1,822.6 fmol mm^{-1} which is significantly (P = 0.0008) greater than the bound $Me^{203}Hg^{+}$-*L*-cysteine at 12°C was 1,533.4 ± 233.9 fmol mm^{-1}. The percentage of bound $Me^{203}Hg^{+}$-*L*-cysteine complex at 12°C compared to the percentage of $Me^{203}Hg^{+}$-*L*-cysteine bound at 37°C was 93.5 % and 89.6 % (P = 0.3120), respectively.

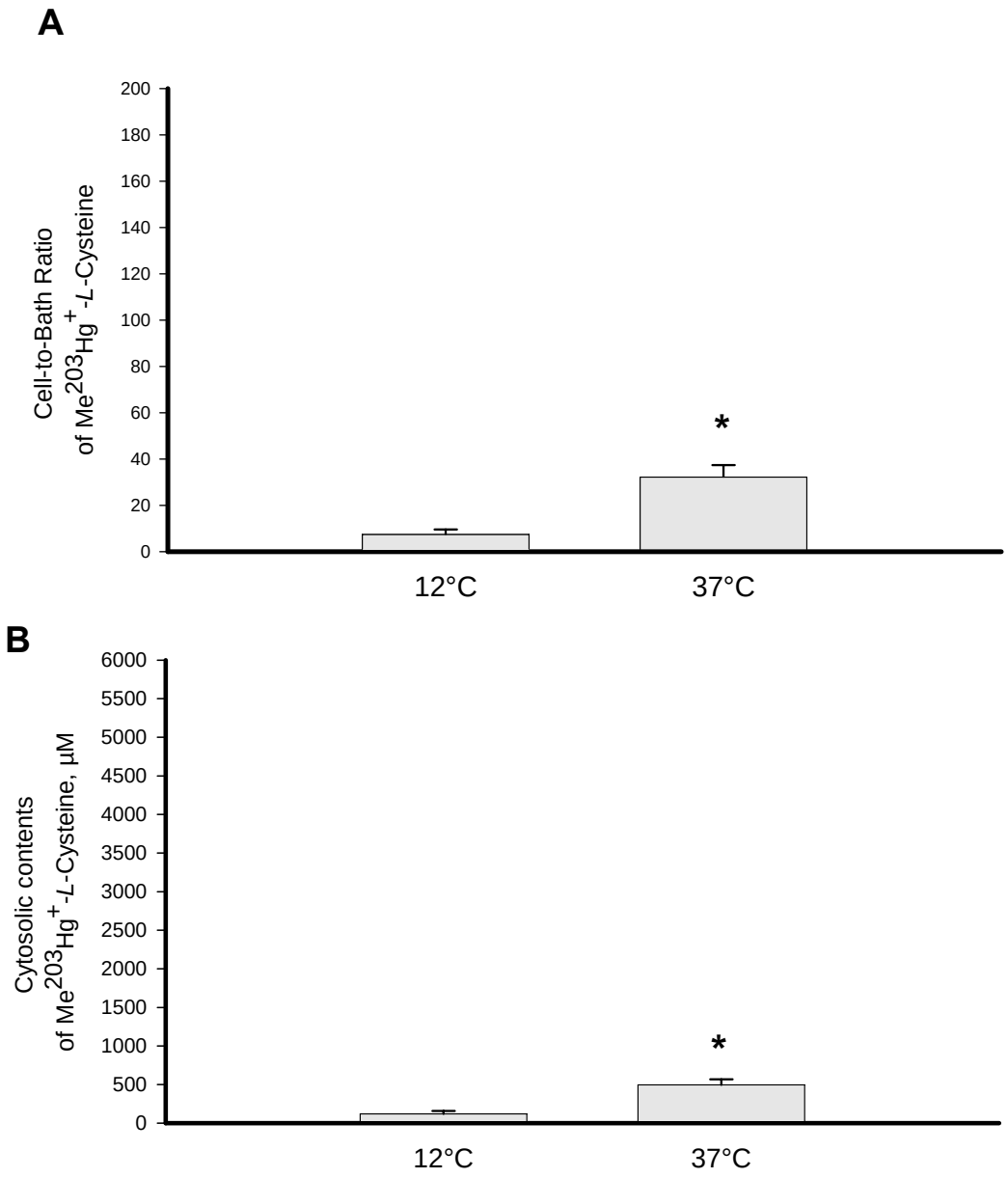

Figure 13: $Me^{203}Hg^{+}$-*L*-cysteine transport in the basolateral membrane of the S_2 segments of rabbit proximal tubules (A) cell-to-bath ratio and (B) cytosolic contents, µM. Each value represents the mean ± SE with a minimum sample size of 5 tubules. The "*" indicates a significant statistical difference, $P \leq 0.05$.

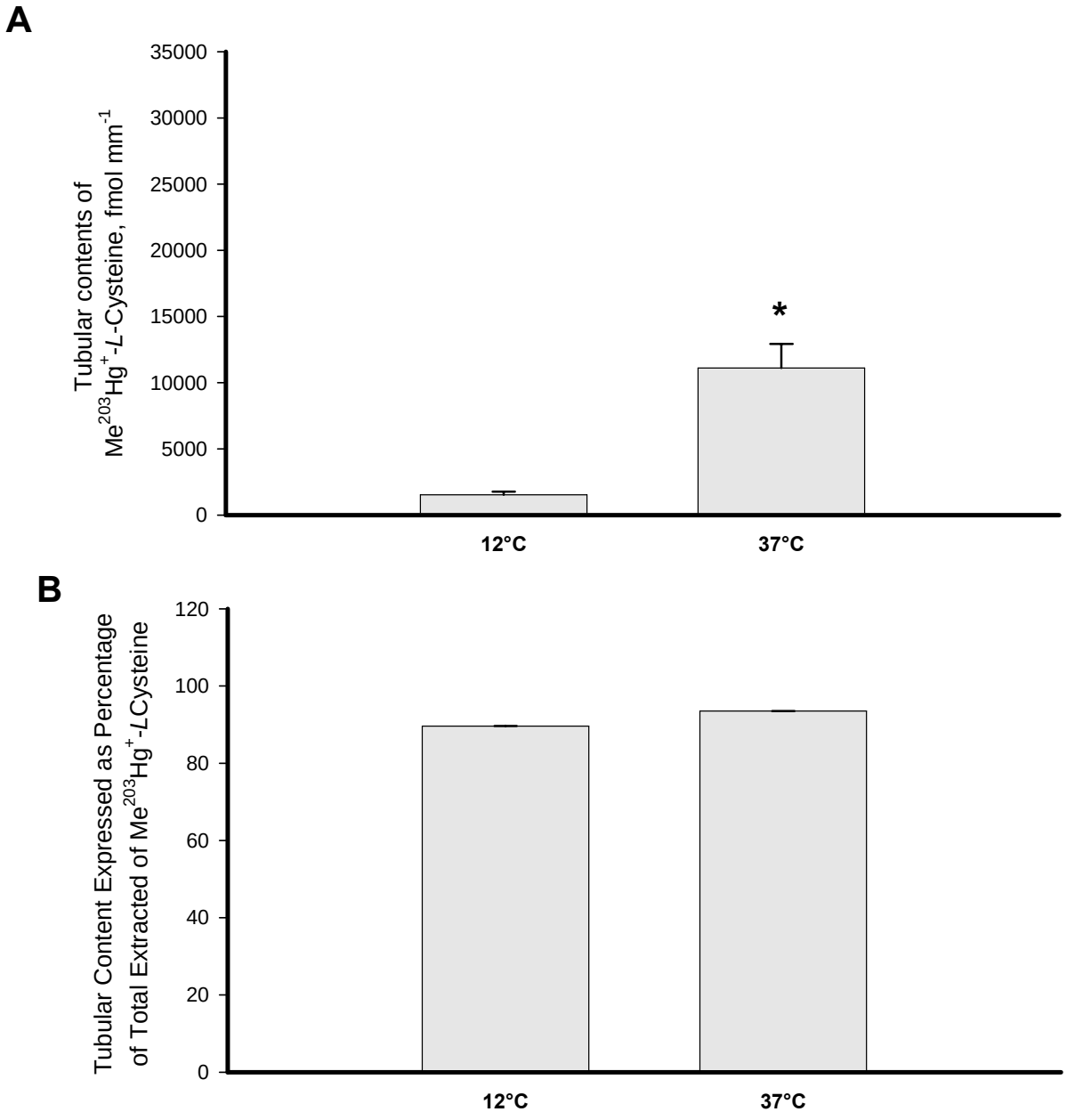

Figure 14: $Me^{203}Hg^{+}$-*L*-cysteine transport in the basolateral membrane of the S_2 segments of rabbit proximal tubules (A) tubular contents and (B) tubular content expressed as percentage of total extracted. Each value represents the mean ± SE with a minimum sample size of 5 tubules. The "*" indicates a significant statistical difference, $P \leq 0.05$.

The effect of PAH on the basolateral transport of $Me^{203}Hg^{+}$-*L*-cysteine

To determine if the conjugate, $Me^{203}Hg^{+}$-*L*-cysteine, is being carried through one of the OAT transporters 200 μM of PAH was added to the bathing solution along with 20 μM of $Me^{203}Hg^{+}$ and 22 μM of *L*-cysteine. The average cell-to-bath ratio and cytosolic contents of $Me^{203}Hg^{+}$-*L*-cysteine versus $Me^{203}Hg^{+}$-*L*-cysteine+PAH is shown in Figure 15. The addition of PAH to the bathing solution significantly reduced the amount of $Me^{203}Hg^{+}$-*L*-cysteine being transported from the bath-to-cell (9.2 ± 2.6, P = 0.0053) and the amount of cytosolic contents within the cell (162.6 μM ± 46.6, P = 0.0067). Figure 16 shows the amount of bound $Me^{203}Hg^{+}$-*L*-cysteine at the tubular epithelium was significantly increased in the presence of PAH, (29,262.2 fmol mm^{-1} ± 2,501.3, P = 0.0001). This also represented a statistically significant increase in the overall percentage of bound tubular contents of $Me^{203}Hg^{+}$-*L*-cysteine in the presence of PAH, (99.3 %, P = 0.018).

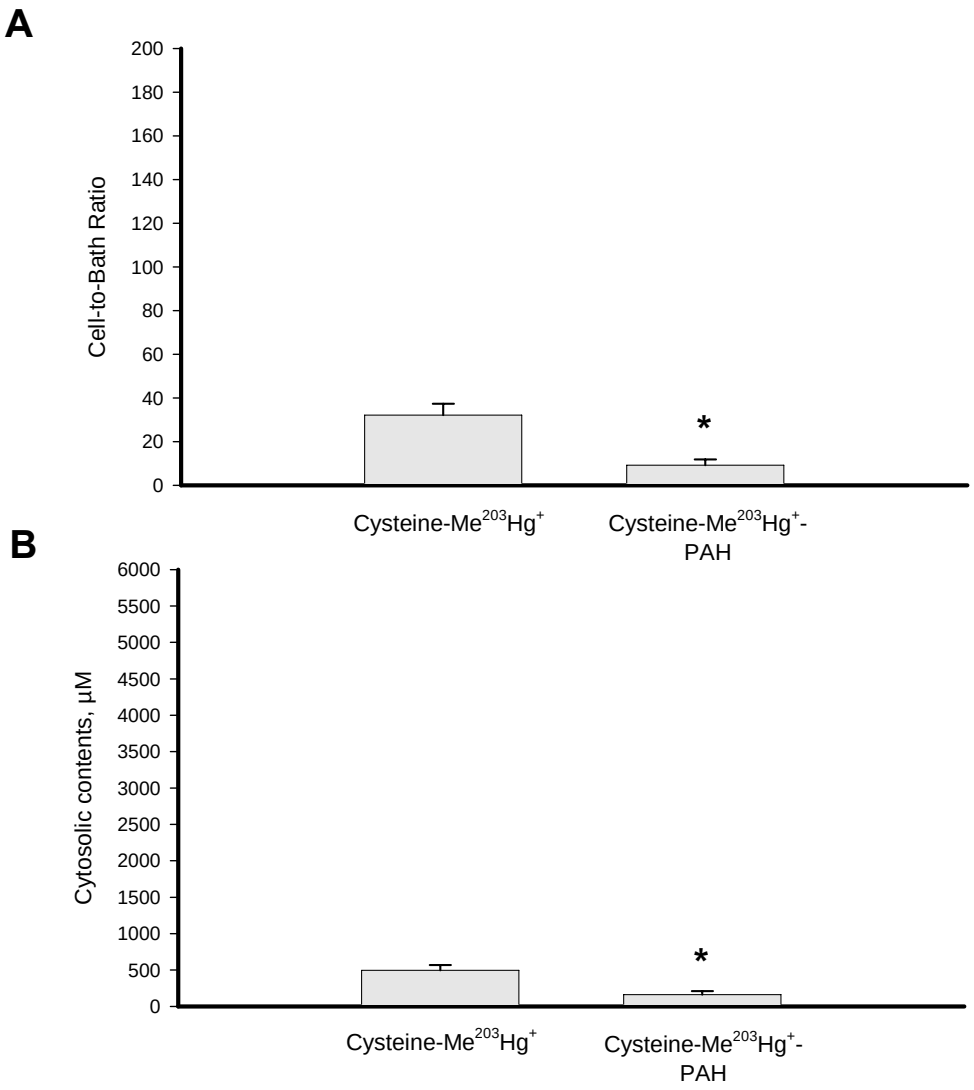

Figure 15: The effect of PAH on $Me^{203}Hg^{+}$-*L*-cysteine transport in the basolateral membrane of the S_2 segments of rabbit proximal tubules (A) cell-to-bath ratio and (B) cytosolic contents, µM. Each value represents the mean ± SE with a minimum sample size of 5 tubules. The "*" indicates a significant statistical difference, $P \leq 0.05$.

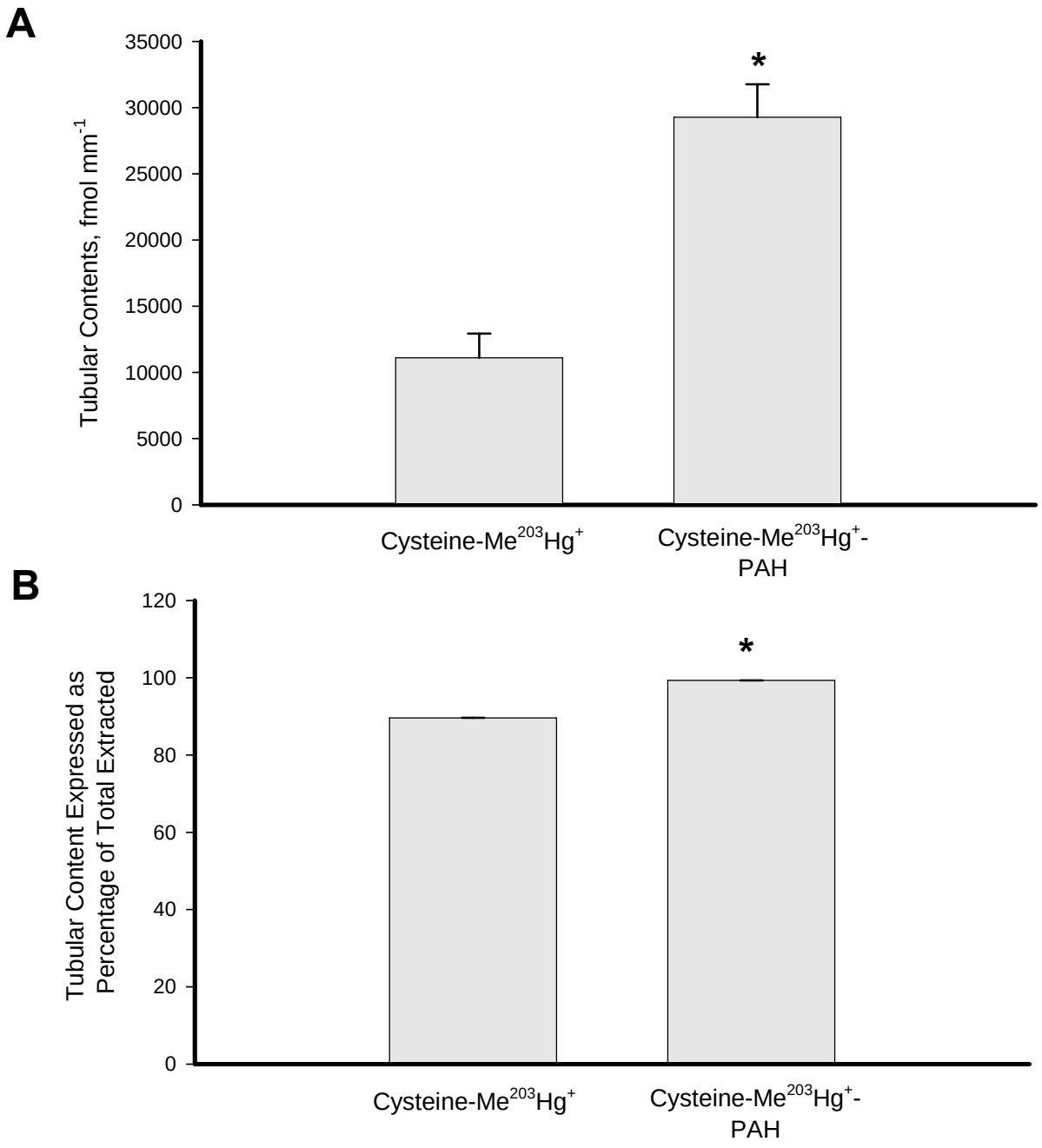

Figure 16: The effect of PAH on $Me^{203}Hg^{+}$-*L*-cysteine transport in the basolateral membrane of the S_2 segments of rabbit proximal tubules (A) tubular contents and (B) tubular content expressed as percentage of total extracted. Each value represents the mean ± SE with a minimum sample size of 5 tubules. The "*" indicates a significant statistical difference, $P \leq 0.05$.

The effect of probenicid on the basolateral transport of $Me^{203}Hg^{+}$-*L*-cysteine

Further classification of whether the conjugate, $Me^{203}Hg^{+}$-*L*-cysteine, is being carried through one of the OAT transporters was determined by the addition of 200 μM probenicid to the bathing solution along with 20 μM of $Me^{203}Hg^{+}$ and 22 μM of *L*-cysteine. The average cell-to-bath ratio and cytosolic contents of $Me^{203}Hg^{+}$-*L*-cysteine versus $Me^{203}Hg^{+}$-*L*-cysteine+probenicid is shown in Figure 17. The addition of probenicid to the bathing solution reduced the amount of $Me^{203}Hg^{+}$-*L*-cysteine being transported from the bath-to-cell (16.8 ± 3.4) although the results were not statistically significant (P = 0.1545). The amount of cytosolic contents within the cell were also reduced in the presence of probenicid (310.2 μM ± 62), but were also not statistically significant (P = 0.2122). Figure 18 shows the amount of bound $Me^{203}Hg^{+}$-*L*-cysteine at the tubular epithelium was significantly increased in the presence of probenicid (21,107 fmol mm^{-1} ± 3,152.1, P = 0.0181). This did not represent a statistically significant increase in the overall percentage of bound tubular contents of $Me^{203}Hg^{+}$-*L*-cysteine in the presence of probenicid, (98.7 %, P = 0.0934).

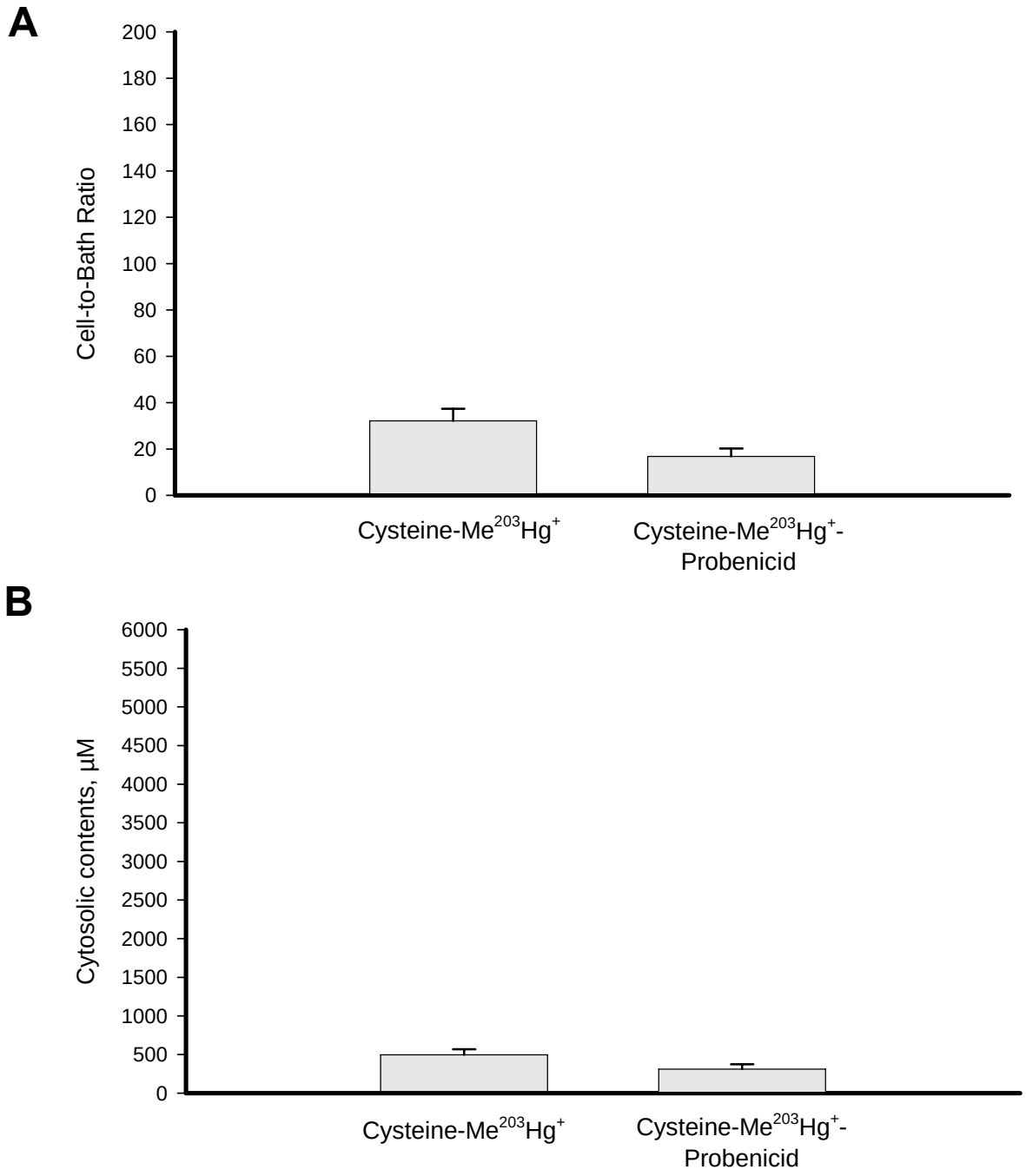

Figure 17: The effect of probenicid on $Me^{203}Hg^{+}$-*L*-cysteine transport in the basolateral membrane of the S_2 segments of rabbit proximal tubules (A) cell-to-bath ratio and (B) cytosolic contents, µM. Each value represents the mean ± SE with a minimum sample size of 5 tubules.

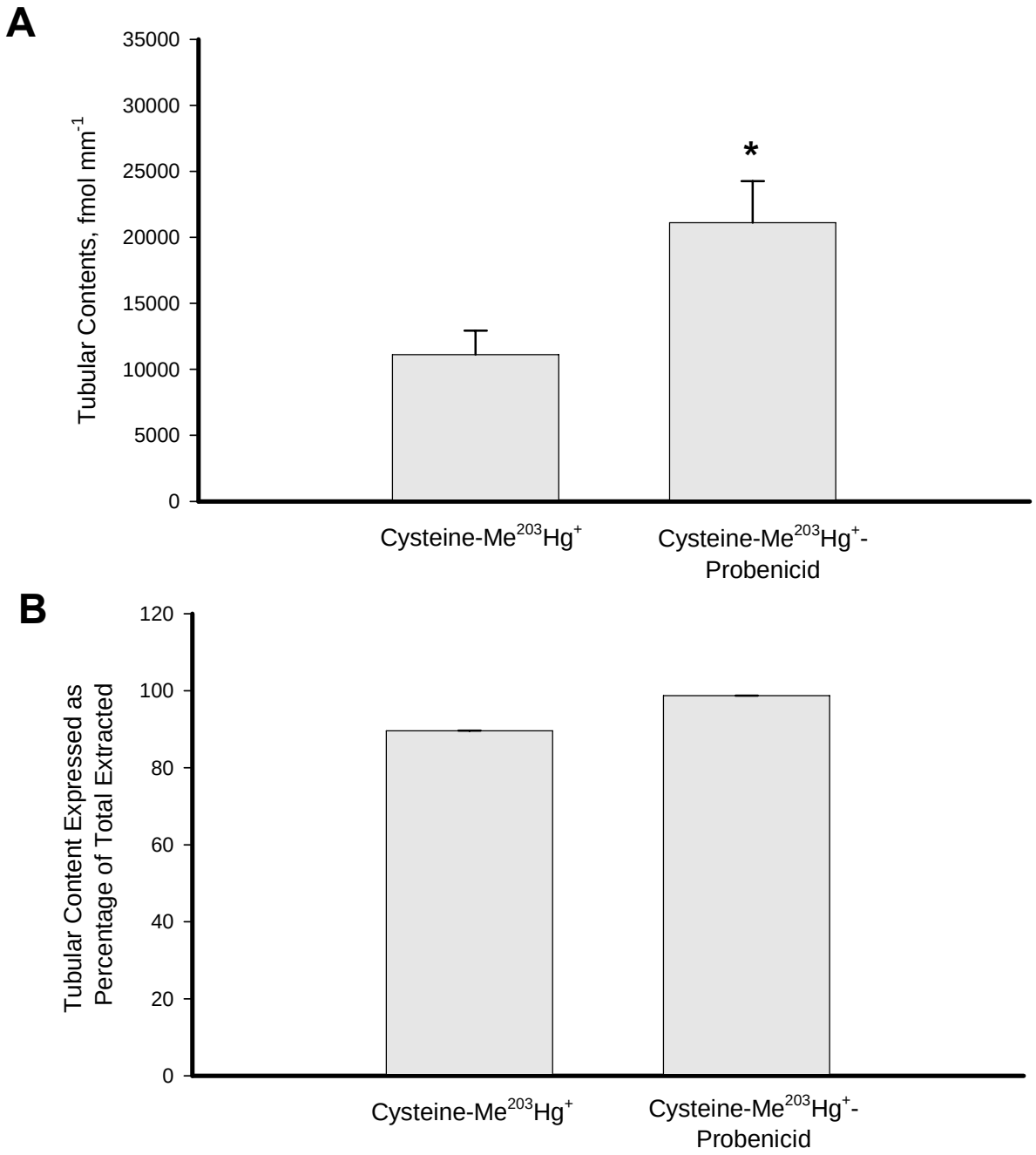

Figure 18: The effect of probenicid on $Me^{203}Hg^{+}$-*L*-cysteine transport in the basolateral membrane of the S_2 segments of rabbit proximal tubules (A) tubular contents and (B) tubular content expressed as percentage of total extracted. Each value represents the mean ± SE with a minimum sample size of 5 tubules. The "*" indicates a significant statistical difference, $P \leq 0.05$.

The effect of *L*-adepate on the basolateral transport of $Me^{203}Hg^{+}$-*L*-cysteine

Figure 19 shows the inhibition of the addition of 200 μM *L*-adepate to the bathing solution along with 20 μM of $Me^{203}Hg^{+}$ and 22 μM of *L*-cysteine on the cell-to-bath ratios and the cytosolic concentrations. The addition of *L*-adepate significantly reduced the cell-to-bath uptake of $Me^{203}Hg^{+}$-*L*-cysteine by a factor of nine-fold (-4.5 ± 3.9, P = 0.0002). The contents of the cytoplasm were -98.2 μM ± 84.7 in the presence of *L*-adepate, a significant reduction in transport (P = 0.0001). The amount of $Me^{203}Hg^{+}$-*L*-cysteine bound to the tubule was also significantly reduced by approximately 71 %, P = 0.0105 [Fig. 20]. Comparison of the percentage of $Me^{203}Hg^{+}$-*L*-cysteine bound versus $Me^{203}Hg^{+}$-*L*-cysteine+adepate did not demonstrate a statistically significant difference, P = 0.2060.

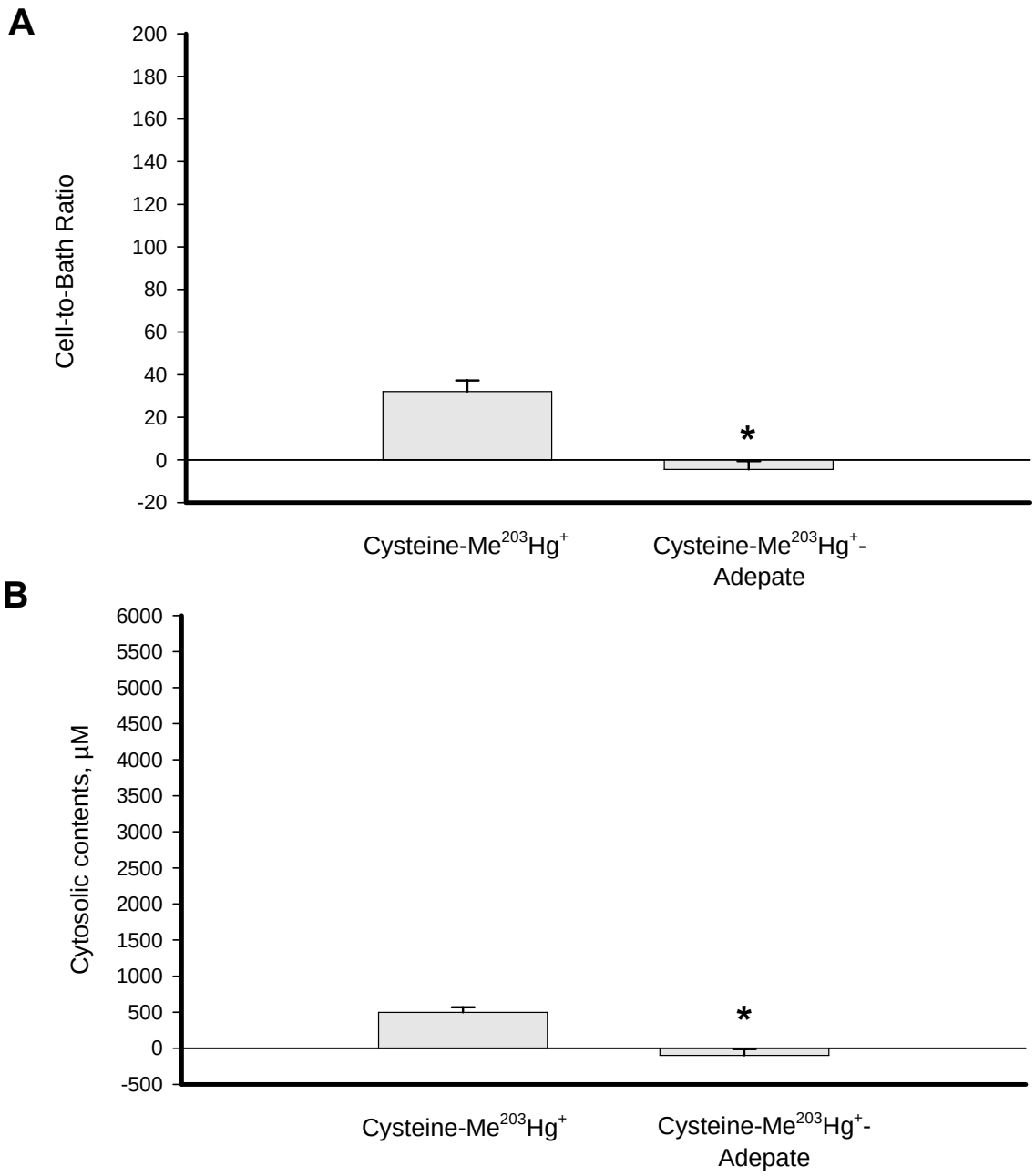

Figure 19: The effect of *L*-adepate on $Me^{203}Hg^{+}$-*L*-cysteine transport in the basolateral membrane of the S_2 segments of rabbit proximal tubules (A) cell-to-bath ratio and (B) cytosolic contents, µM. Each value represents the mean ± SE with a minimum sample size of 5 tubules. The "*" indicates a significant statistical difference, $P \leq 0.05$.

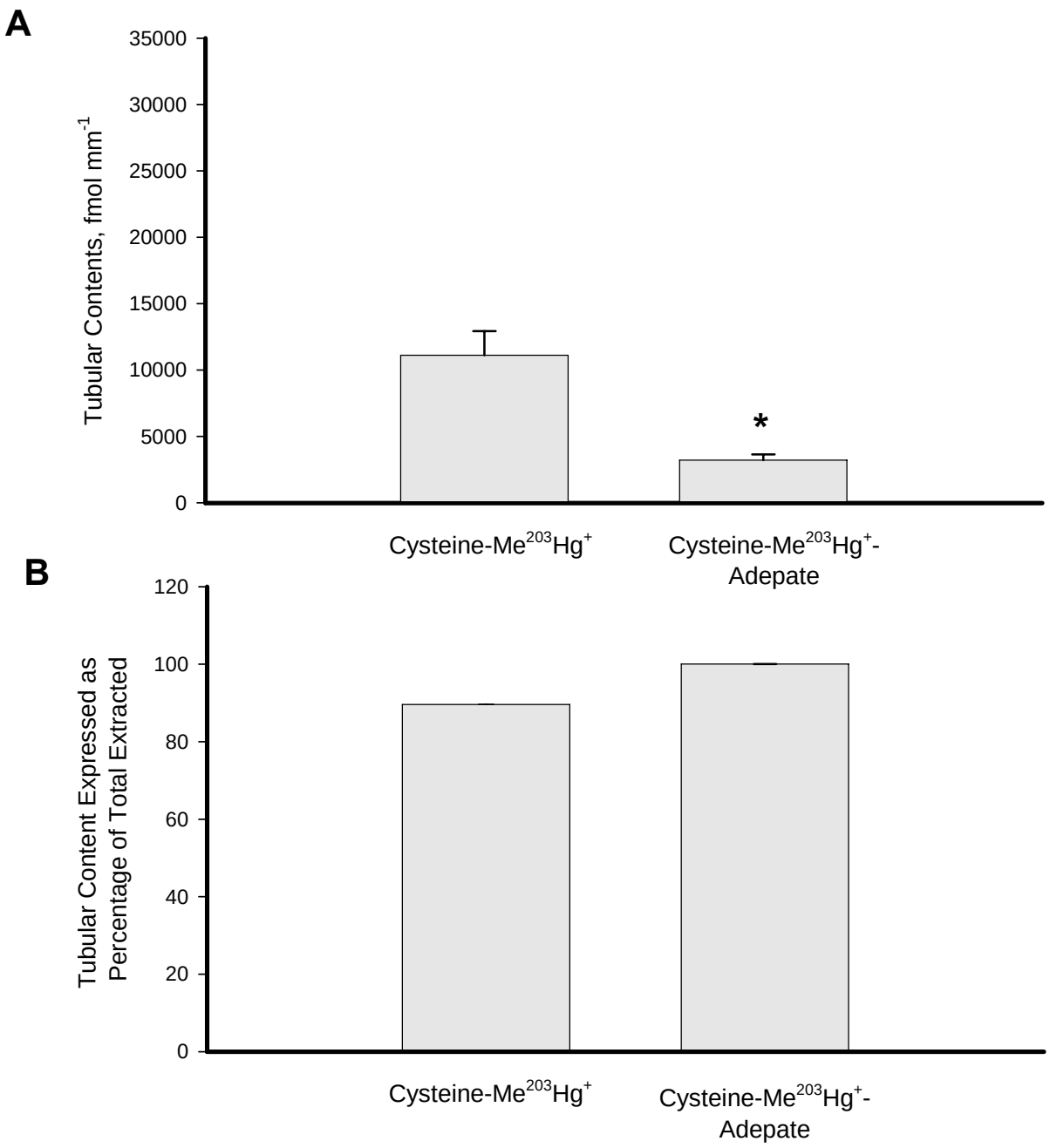

Figure 20: The effect of *L*-adepate on $Me^{203}Hg^{+}$-*L*-cysteine transport in the basolateral membrane of the S_2 segments of rabbit proximal tubules (A) tubular contents and (B) tubular content expressed as percentage of total extracted. Each value represents the mean ± SE with a minimum sample size of 5 tubules. The "*" indicates a significant statistical difference, $P \leq 0.05$.

The effect of *L*-glutarate on the basolateral transport of $Me^{203}Hg^{+}$-*L*-cysteine

Addition of 200 μM *L*-glutarate to the bathing solution significantly reduced the transport of $Me^{203}Hg^{+}$-*L*-cysteine at the basolateral membrane as noted in Figure 21 below showing the cell-to-bath ratio (A) and the cytosolic contents (B). A three-fold reduction in cell-to-bath ratio was noted (10.1 ± 2.4 versus 32.1 ± 5.2, P = 0.0023) and a 52 % reduction in the cytosolic contents (237 μM ± 56.5 versus 496.8 μM ± 71.7, P = 0.0133). As noted in Figure 22, the amount of bound $Me^{203}Hg^{+}$-*L*-cysteine at the tubular epithelium was reduced over two-fold (4,925.4 fmol mm^{-1} ± 522.8 versus 11,107.8 fmol mm^{-1} ± 1,822.6, P = 0.0102). Comparing the percentage of bound $Me^{203}Hg^{+}$-*L*-cysteine versus the percentage of bound $Me^{203}Hg^{+}$-*L*-cysteine did not show a statistically significant difference (95 % versus 89.6 %, P = 0.1255).

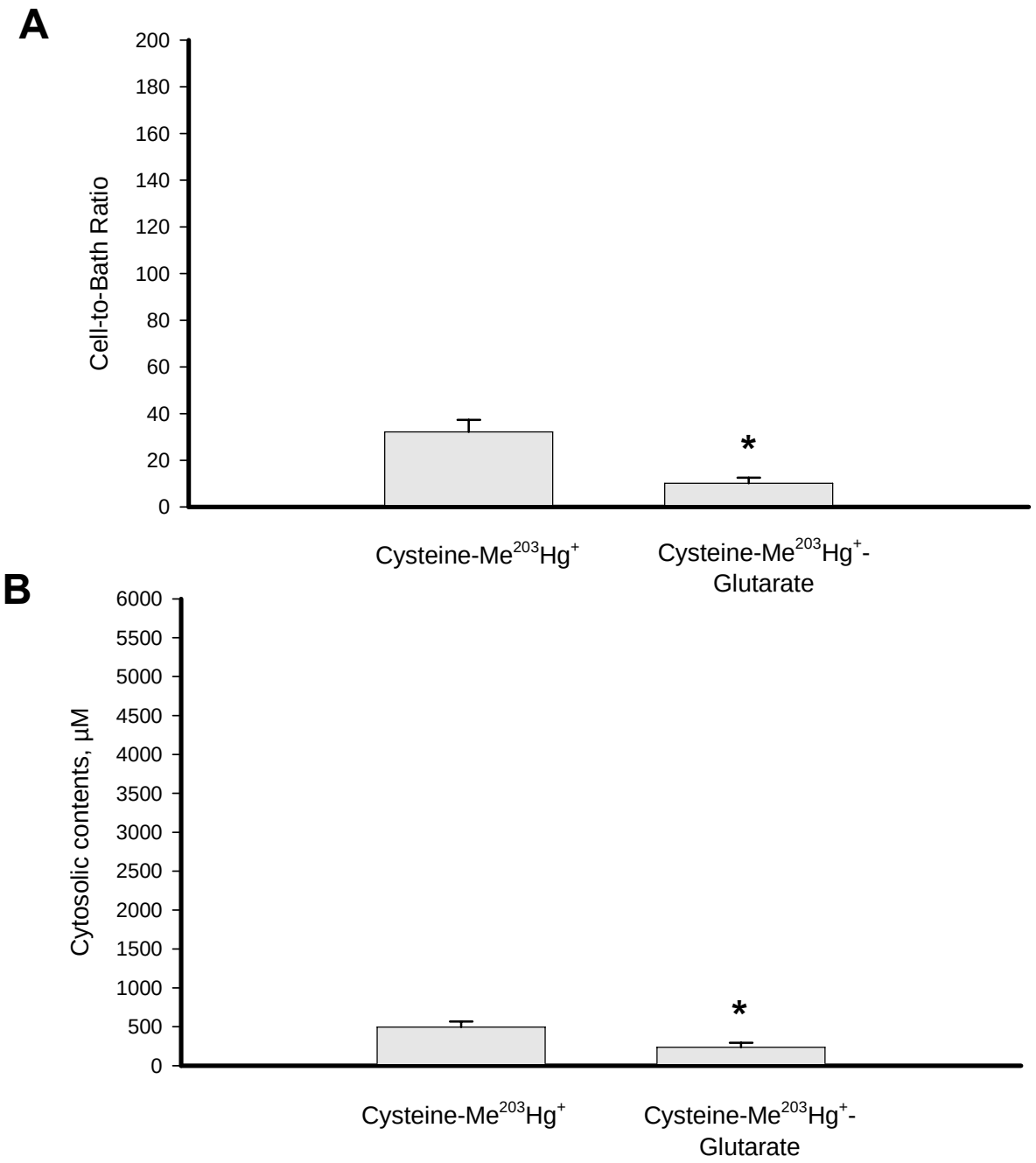

Figure 21: The effect of *L*-glutarate on $Me^{203}Hg^{+}$-*L*-cysteine transport in the basolateral membrane of the S_2 segments of rabbit proximal tubules (A) cell-to-bath ratio and (B) cytosolic contents, µM. Each value represents the mean ± SE with a minimum sample size of 5 tubules. The "*" indicates a significant statistical difference, $P \leq 0.05$.

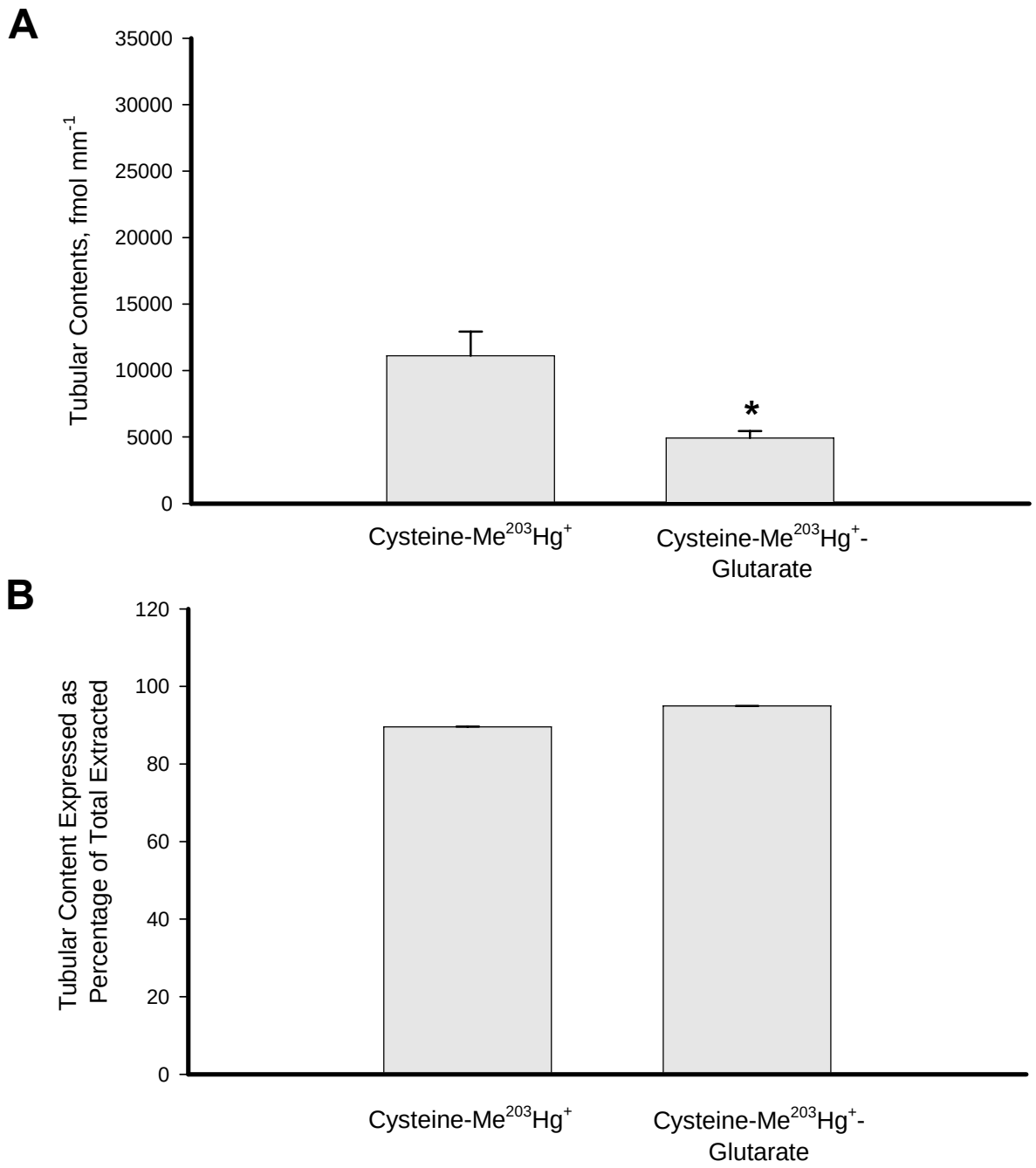

Figure 22: The effect of *L*-glutarate on $Me^{203}Hg^{+}$-*L*-cysteine transport in the basolateral membrane of the S_2 segments of rabbit proximal tubules (A) tubular contents and (B) tubular content expressed as percentage of total extracted. Each value represents the mean ± SE with a minimum sample size of 5 tubules. The "*" indicates a significant statistical difference, $P \leq 0.05$.

The effect of *L*-methionine on the basolateral transport of $Me^{203}Hg^{+}$-*L*-cysteine

To determine whether *L*-methionine had an effect on the transport of the $Me^{203}Hg^{+}$-*L*-cysteine 200 μM was added to the bathing solution containing 20 μM $Me^{203}Hg^{+}$ and 22 μM *L*-cysteine. As seen in Figure 23 (A), the addition of *L*-methionine significantly reduced the cell-to-bath ratio of $Me^{203}Hg^{+}$-*L*-cysteine when compared to $Me^{203}Hg^{+}$-*L*-cysteine transport alone (14.3 ± 3.3 versus 32.1 ± 5.2, P = 0.0265). The concentration of the cytosol was also significantly (265.7 μM ± 65.5, P = 0.0454) reduced in the presence of *L*-methionine as seen in Figure 23 (B). The addition of *L*-methionine did not significantly increase the contents of the tubule (12,572.4 fmol mm^{-1} ± 2,937.3, P = 0.6596). When comparing the percentage of tubular contents between $Me^{203}Hg^{+}$-*L*-cysteine and $Me^{203}Hg^{+}$-*L*-cysteine+*L*-methionine a significant increase was noted, 89.6 % and 98.7 % respectively (P = 0.0197) [Fig. 24].

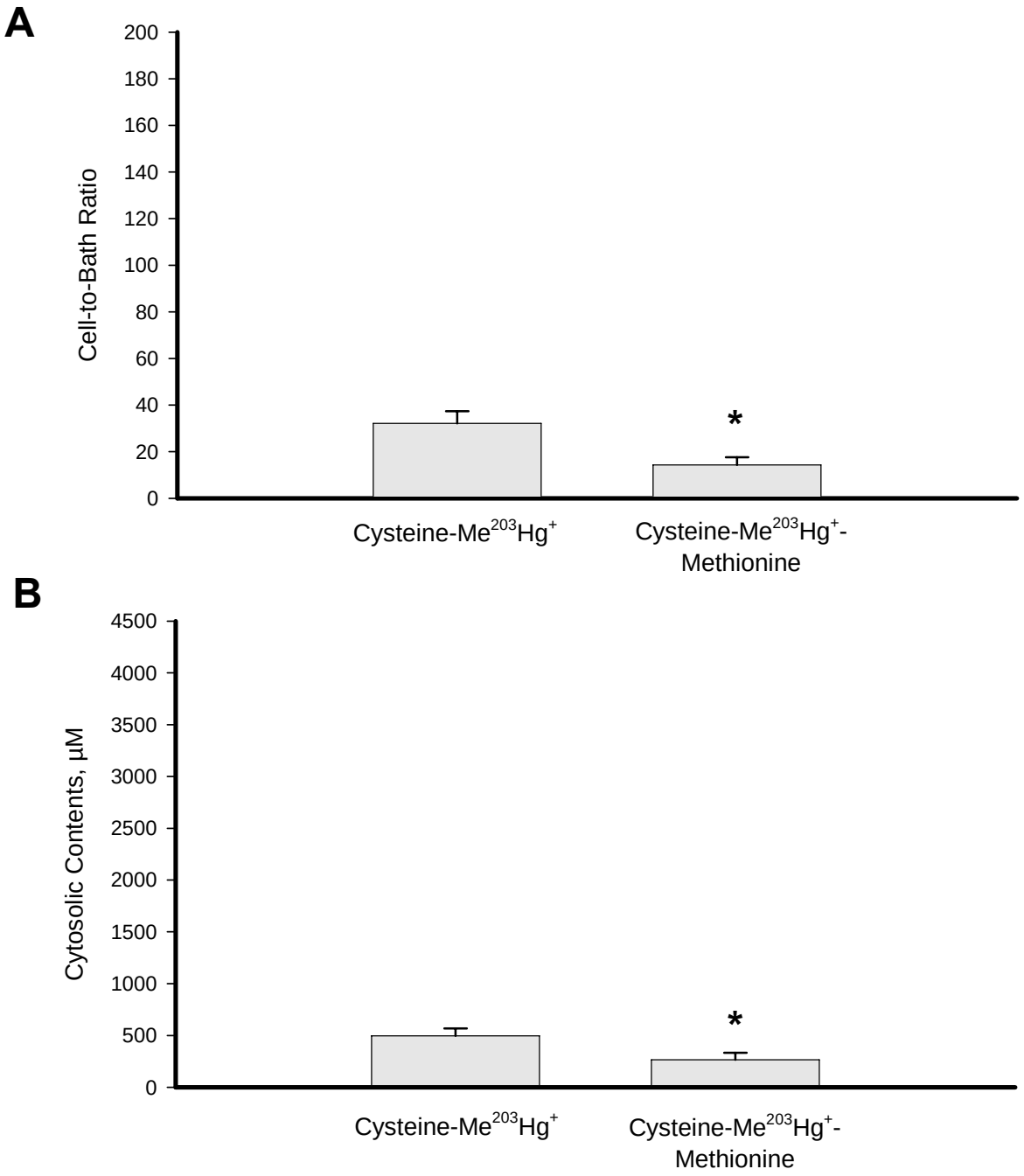

Figure 23: The effect of *L*-methionine on $Me^{203}Hg^{+}$-*L*-cysteine transport in the basolateral membrane of the S_2 segments of rabbit proximal tubules (A) cell-to-bath ratio and (B) cytosolic contents, µM. Each value represents the mean ± SE with a minimum sample size of 5 tubules. The "*" indicates a significant statistical difference, $P \leq 0.05$.

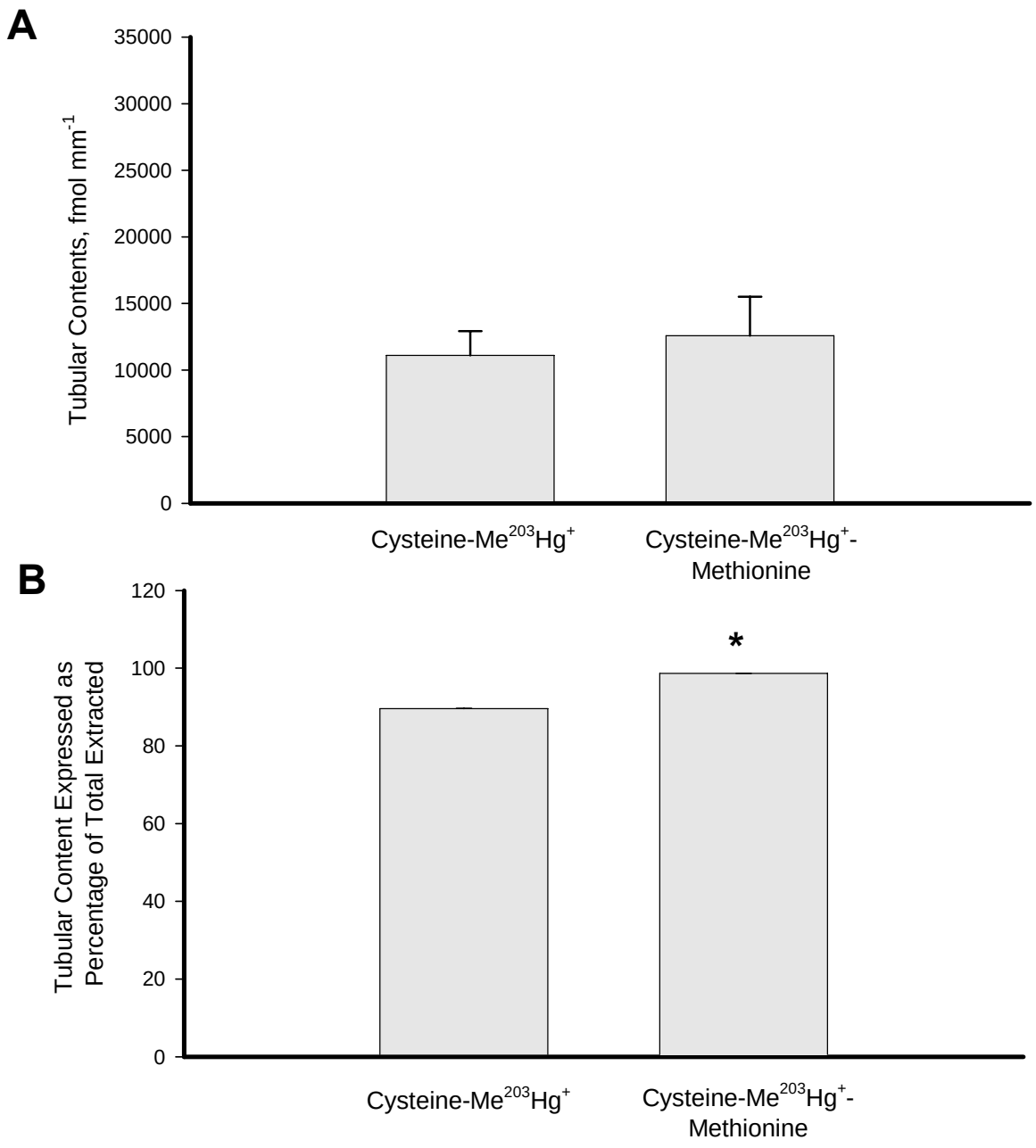

Figure 24: The effect of *L*-methionine on $Me^{203}Hg^{+}$-*L*-cysteine transport in the basolateral membrane of the S_2 segments of rabbit proximal tubules (A) tubular contents and (B) tubular content expressed as percentage of total extracted. Each value represents the mean ± SE with a minimum sample size of 5 tubules. The "*" indicates a significant statistical difference, $P \leq 0.05$.

The effect of *L*-methionine on the basolateral transport of $Me^{203}Hg^{+}$

To characterize the effect of *L*-methionine on the basolateral uptake of $Me^{203}Hg^{+}$, 20 μM of $Me^{203}Hg^{+}$ along with 22 μM of *L*-methionine was added to the bathing solution. The average cell-to-bath ratio and cytosolic contents of $Me^{203}Hg^{+}$-*L*-methionine at 12°C and 37°C are noted in Figure 25. Bath-to-cell uptake of $Me^{203}Hg^{+}$-*L*-methionine (65.4 ± 12.7) was significantly increased (P = 0.0201) at 37°C when compared to uptake of $Me^{203}Hg^{+}$-*L*-methionine at 12°C (26.5 ± 4.0). The average cytosolic concentration of $Me^{203}Hg^{+}$-*L*-methionine at 12°C and 37°C was 467.1 μM ± 64.6 and 890.2 μM ± 202.2 respectively, which was not a significant (P = 0.101) increase in the cellular contents. The amount of $Me^{203}Hg^{+}$-*L*-methionine at 12°C and 37°C bound to the basolateral epithelium of the tubule (fmol mm^{-1}) and percentage of tubular contents are noted in Figure 26. The amount of bound $Me^{203}Hg^{+}$-*L*-methionine complex at 37°C was 11,794.6 ± 1,691.6 fmol mm^{-1} which is significantly (P = 0.0295) greater than the bound $Me^{203}Hg^{+}$-*L*-methionine at 12°C was 6,852.4 ± 801.7 fmol mm^{-1}. The percentage of bound $Me^{203}Hg^{+}$-*L*-methionine complex at 12°C compared to the percentage of $Me^{203}Hg^{+}$-*L*-methionine bound at 37°C was 94.3 % and 91.6 % (P = 0.3237), respectively.

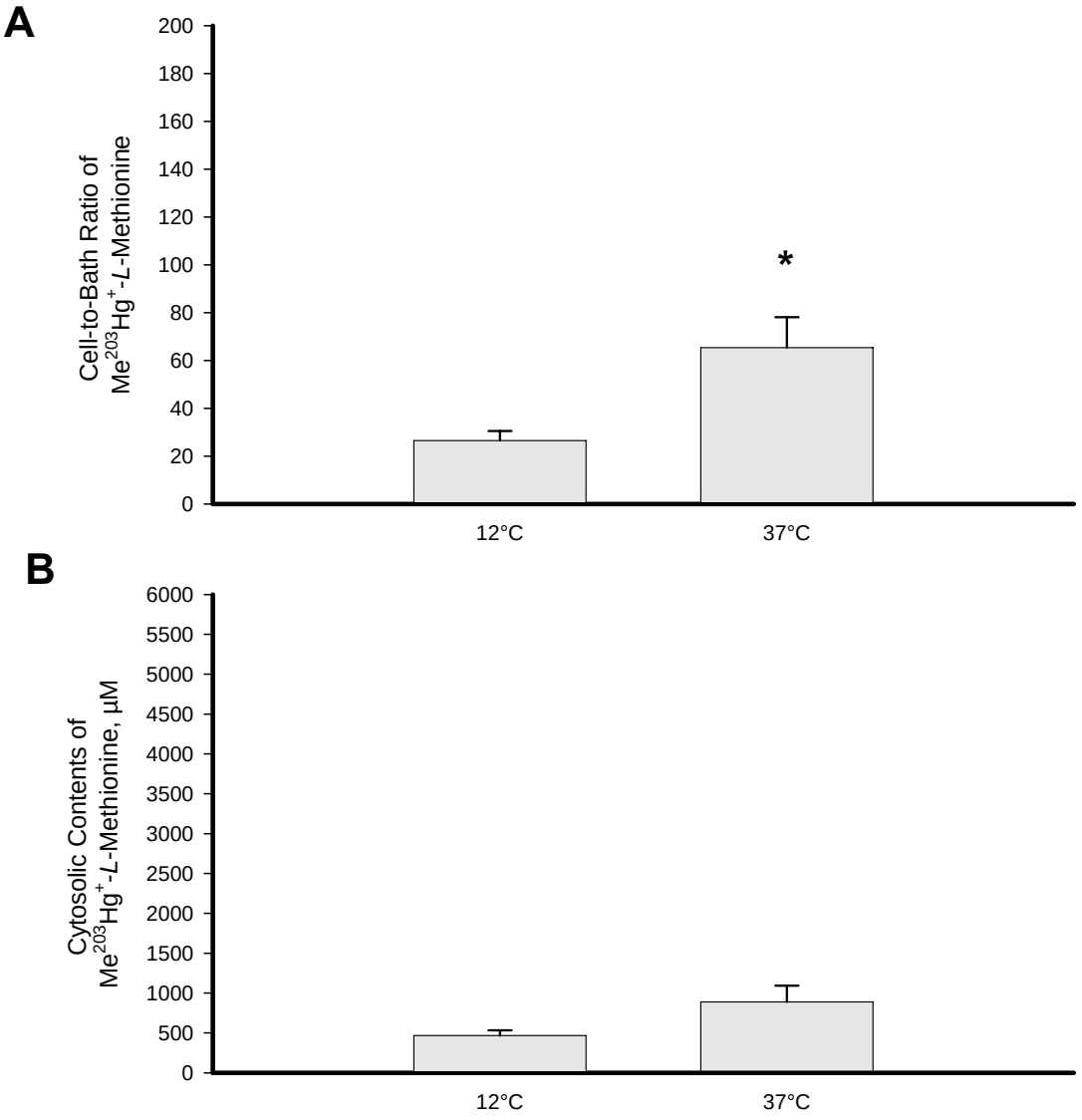

Figure 25: $Me^{203}Hg^{+}$-*L*-methionine transport in the basolateral membrane of the S_2 segments of rabbit proximal tubules (A) cell-to-bath ratio and (B) cytosolic contents, µM. Each value represents the mean ± SE with a minimum sample size of 5 tubules. The "*" indicates a significant statistical difference, $P \leq 0.05$.

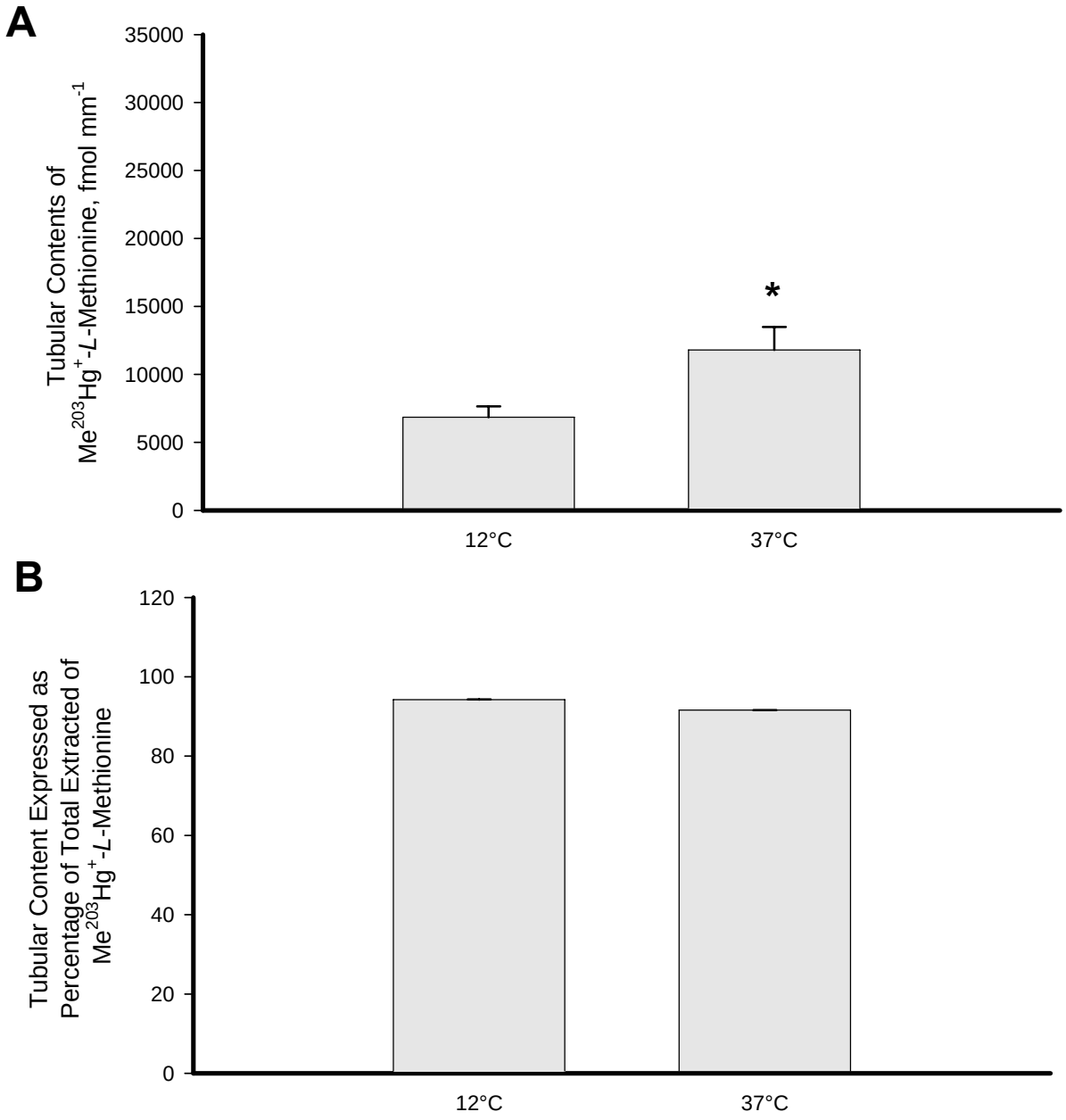

Figure 26: $Me^{203}Hg^{+}$-*L*-methionine transport in the basolateral membrane of the S_2 segments of rabbit proximal tubules (A) tubular contents and (B) tubular content expressed as percentage of total extracted. Each value represents the mean ± SE with a minimum sample size of 5 tubules. The "*" indicates a significant statistical difference, $P \leq 0.05$.

The effect of PAH on the basolateral transport of $Me^{203}Hg^{+}$-*L*-methionine

Examination of the cell-to-bath ratios and cytosolic contents of the conjugate, $Me^{203}Hg^{+}$-*L*-methionine (20 μM of $Me^{203}Hg^{+}$ and 22 μM of *L*-methionine), in the presence of 200 μM PAH is shown in Figure 27. The addition of PAH to the bathing solution did not significantly reduce the amount of $Me^{203}Hg^{+}$-*L*-methionine being transported from the bath-to-cell (31.6 ± 15.1, P = 0.3831) or the amount of cytosolic contents within the cell (543.3 μM ± 259.4, P = 0.4626). Figure 28 shows the amount of bound $Me^{203}Hg^{+}$-*L*-methionine at the tubular epithelium was also not significantly altered in the presence of PAH, (21,334.1 fmol mm^{-1} ± 12,630.9, P = 0.1517). This also did not represent a statistically significant decrease in the overall percentage of bound tubular contents of $Me^{203}Hg^{+}$-*L*-methionine in the presence of PAH, (90.9 %, P = 0.9056).

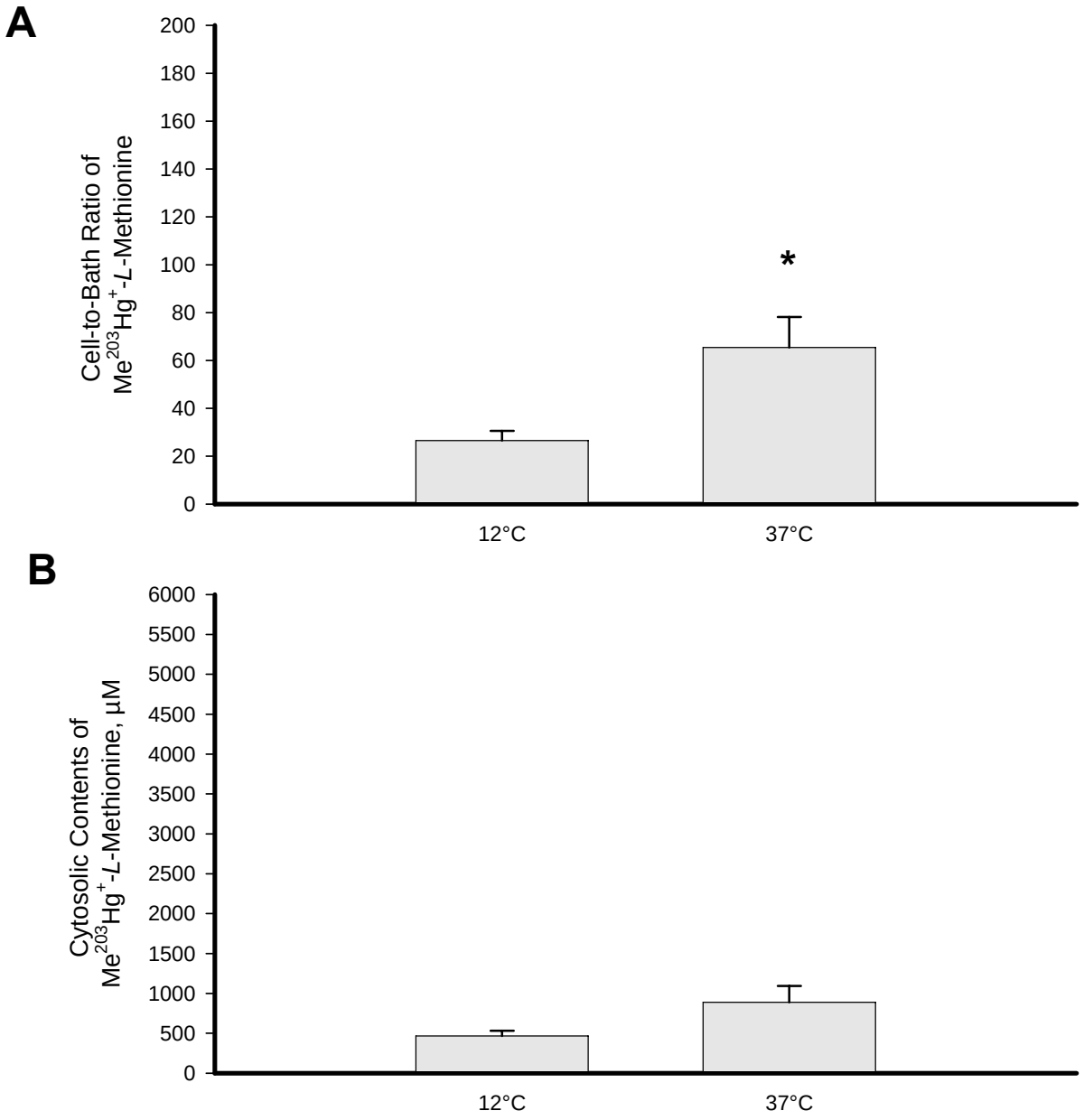

Figure 27: The effect of PAH on $Me^{203}Hg^{+}$-*L*-methionine transport in the basolateral membrane of the S_2 segments of rabbit proximal tubules (A) cell-to-bath ratio and (B) cytosolic contents, µM. Each value represents the mean ± SE with a minimum sample size of 5 tubules.

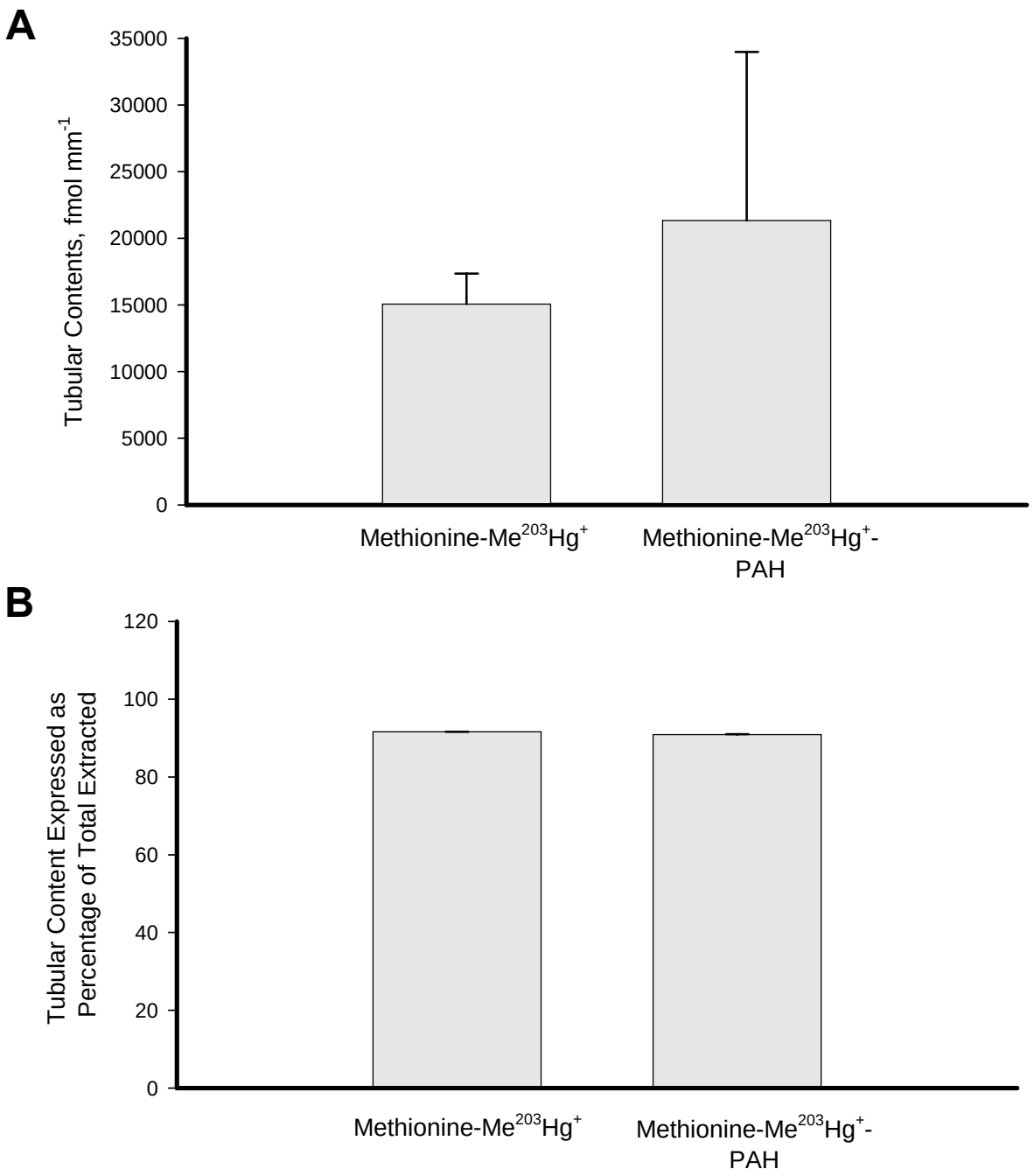

Figure 28: The effect of PAH on $Me^{203}Hg^{+}$-*L*-methionine transport in the basolateral membrane of the S_2 segments of rabbit proximal tubules (A) tubular contents and (B) tubular content expressed as percentage of total extracted. Each value represents the mean ± SE with a minimum sample size of 5 tubules.

The effect of *L*-taurine on the basolateral transport of $Me^{203}Hg^{+}$

To analyze the effect of *L*-taurine on the basolateral uptake of $Me^{203}Hg^{+}$, 20 μM of $Me^{203}Hg^{+}$ along with 22 μM of *L*-taurine was added to the bathing solution. The average cell-to-bath ratio and cytosolic contents of $Me^{203}Hg^{+}$-*L*-taurine at 12°C and 37°C are noted in Figure 29. Bath-to-cell uptake of $Me^{203}Hg^{+}$-*L*-taurine (91.9 ± 16.9) was significantly increased (P = 0.0026) at 37°C when compared to uptake of $Me^{203}Hg^{+}$-*L*-taurine at 12°C (7.8 ± 3.2). The average cytosolic concentration of $Me^{203}Hg^{+}$-*L*-taurine at 12°C and 37°C was 106.8 μM ± 3.8 and 1,179.7 μM ± 210.4 respectively, demonstrating significantly (P = 0.0022) increased cellular contents of $Me^{203}Hg^{+}$-*L*-taurine at normal physiological temperatures. The amount of $Me^{203}Hg^{+}$-*L*-taurine at 12°C and 37°C bound to the basolateral epithelium of the tubule (fmol mm^{-1}) and percentage of tubular contents are noted in Figure 30. The amount of bound $Me^{203}Hg^{+}$-*L*-taurine complex at 37°C was 15,523.2 ± 1,184.8 fmol mm^{-1} which is significantly (P = 0.0001) greater than the bound $Me^{203}Hg^{+}$-*L*-taurine at 12°C was 4,211.3 ± 565.2 fmol mm^{-1}. The percentage of bound $Me^{203}Hg^{+}$-*L*-taurine complex at 12°C compared to the percentage of $Me^{203}Hg^{+}$-*L*-taurine bound at 37°C was 97.8 % and 94 % (P = 0.008), respectively.

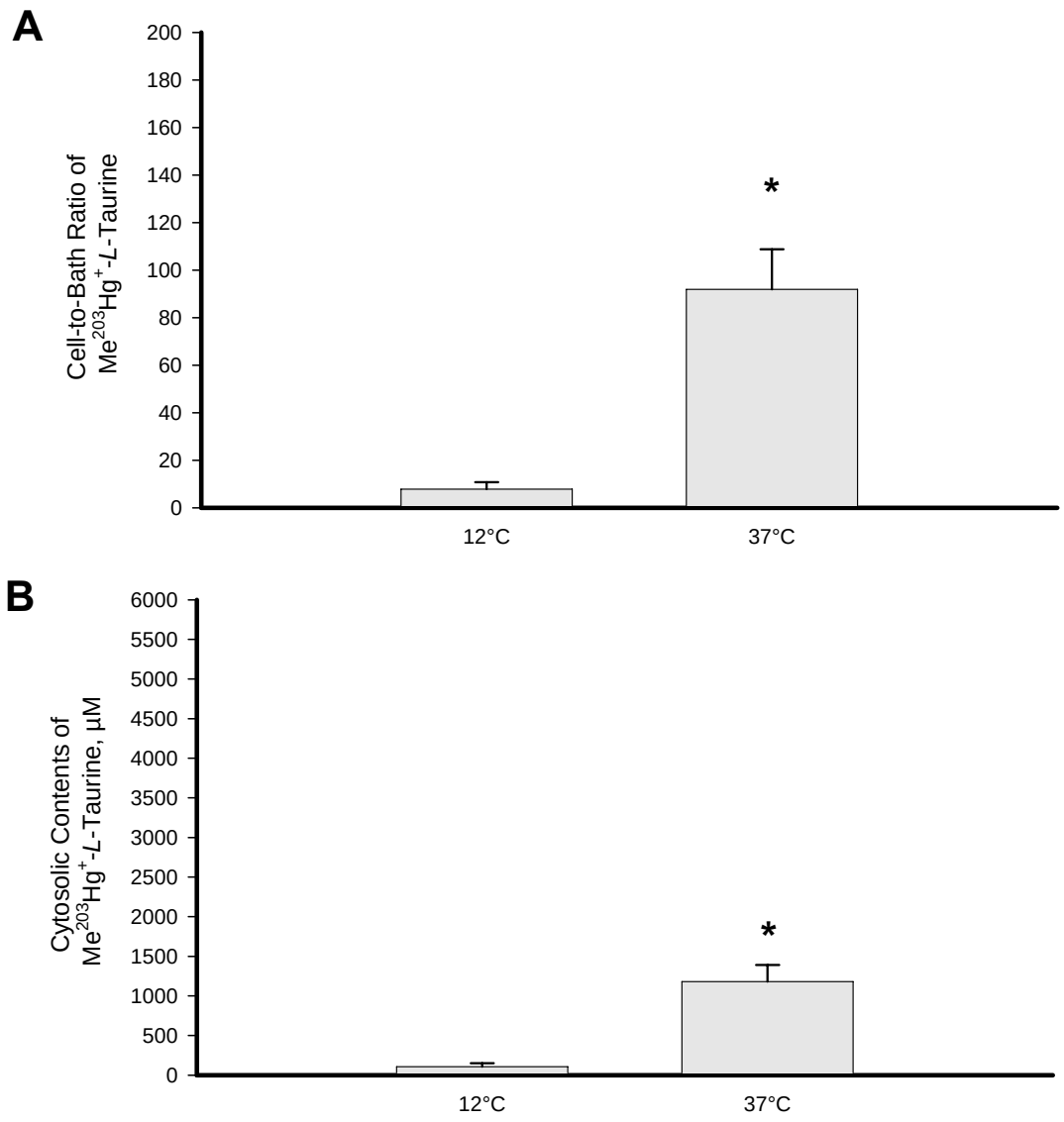

Figure 29: $Me^{203}Hg^{+}$-*L*-taurine transport in the basolateral membrane of the S_2 segments of rabbit proximal tubules (A) cell-to-bath ratio and (B) cytosolic contents, µM. Each value represents the mean ± SE with a minimum sample size of 5 tubules. The "*" indicates a significant statistical difference, $P \leq 0.05$.

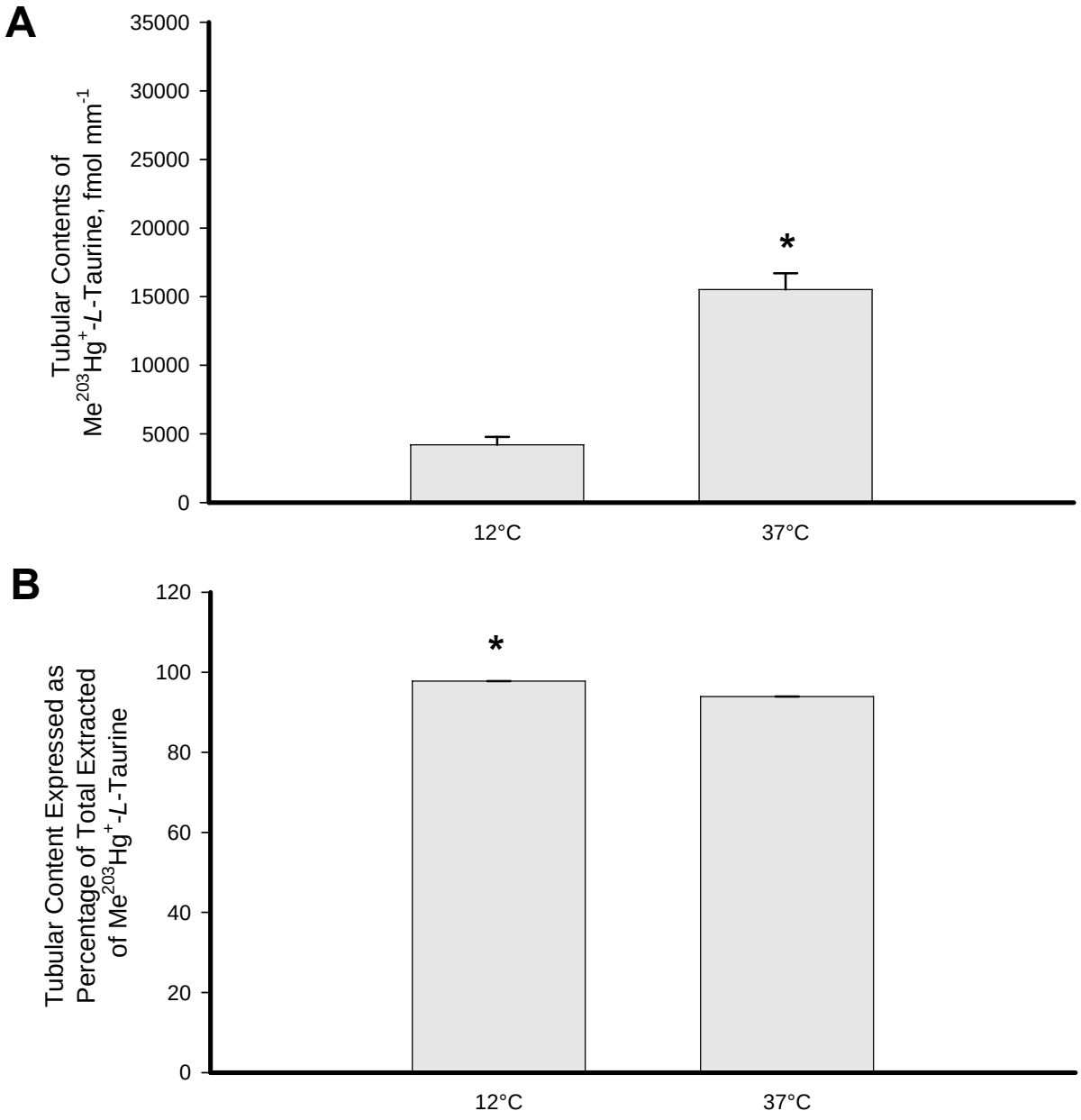

Figure 30: $Me^{203}Hg^{+}$-*L*-taurine transport in the basolateral membrane of the S_2 segments of rabbit proximal tubules (A) tubular contents and (B) tubular content expressed as percentage of total extracted. Each value represents the mean ± SE with a minimum sample size of 5 tubules. The "*" indicates a significant statistical difference, $P \leq 0.05$.

The effect of PAH on the basolateral transport of $Me^{203}Hg^{+}$-*L*-taurine, 37°C

Characterization of the effect of PAH at 37°C on the transport of $Me^{203}Hg^{+}$-*L*-taurine on the cell-to-bath ratios and the cytosolic contents is shown in Figure 31. A significant reduction in the cell-to-bath transport was noted in the presence of 200 μM PAH (A). $Me^{203}Hg^{+}$-*L*-taurine transport was reduced by 23 % (20.6 ± 2.2, P = 0.0003). The amount of $Me^{203}Hg^{+}$-*L*-taurine in the cytoplasm was also significantly reduced in the presence of PAH, 384.2 μM ± 40.5, P = 0.0009. As shown in Figure 32, the amount of bound $Me^{203}Hg^{+}$-*L*-taurine was substantially reduced as well. The tubular contents of $Me^{203}Hg^{+}$-*L*-taurine+PAH compared to $Me^{203}Hg^{+}$-*L*-taurine was -8,322.1 fmol mm^{-1} ± 847.3 versus 15,523.2 fmol mm^{-1} ± 1,184.8, P = 0.0001. The percentage of bound $Me^{203}Hg^{+}$-*L*-taurine+PAH was significantly increased (P = 0.0001).

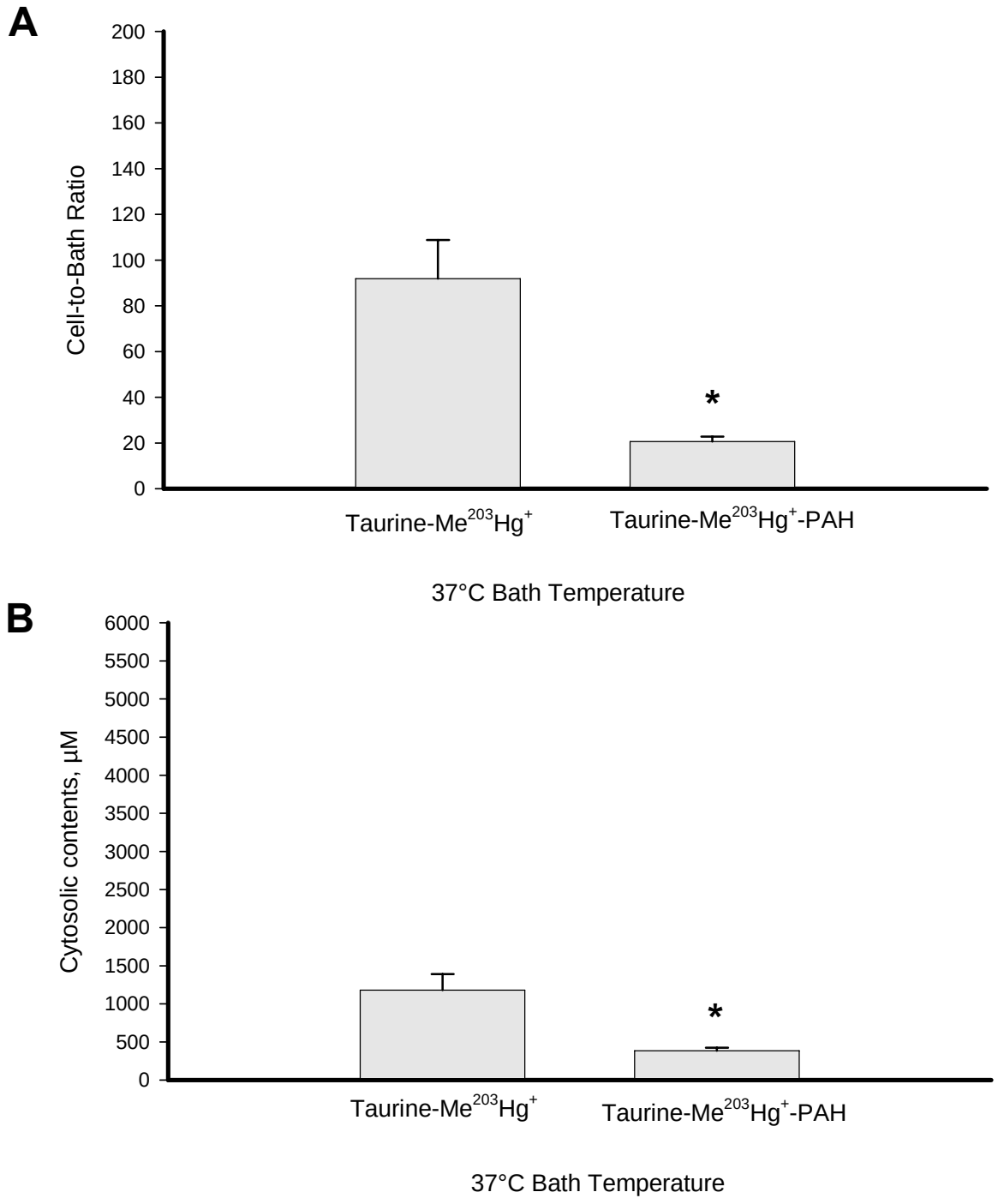

Figure 31: The effect of PAH on $Me^{203}Hg^{+}$-*L*-taurine in the basolateral membrane of the S_2 segments of rabbit proximal tubules (A) cell-to-bath ratio and (B) cytosolic contents, µM (at 37°C). Each value represents the mean ± SE with a minimum sample size of 5 tubules. The "*" indicates a significant statistical difference, $P \leq 0.05$.

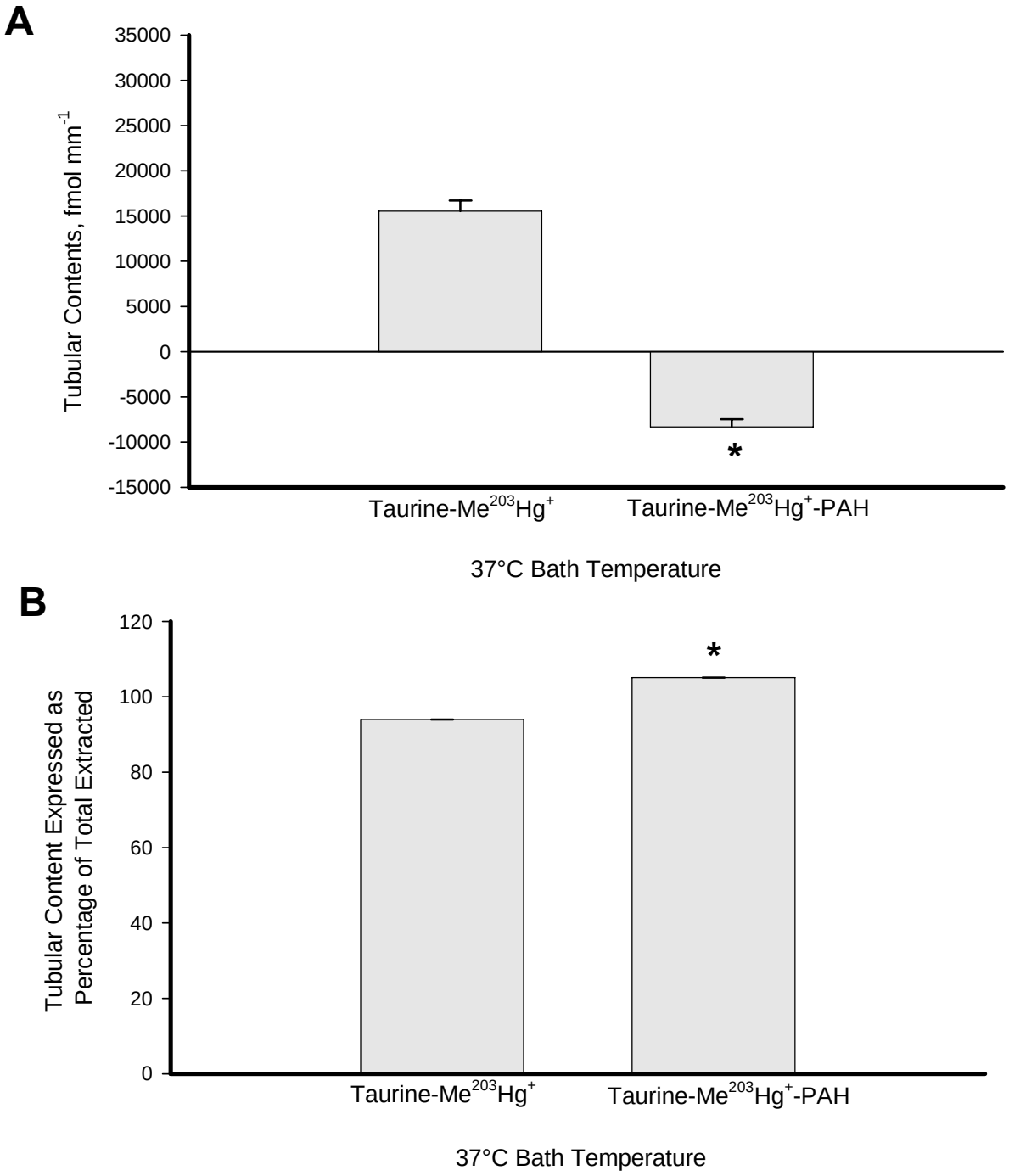

Figure 32: The effect of PAH on $Me^{203}Hg^{+}$-*L*-taurine transport in the basolateral membrane of the S_2 segments of rabbit proximal tubules (A) tubular contents and (B) tubular content expressed as percentage of total extracted (at 37°C). Each value represents the mean ± SE with a minimum sample size of 5 tubules. The "*" indicates a significant statistical difference, $P \leq 0.05$.

The effect of PAH on the basolateral transport of $Me^{203}Hg^{+}$-*L*-taurine, 12°C

When 200 μM PAH was added to the bathing solution at 12°C, no significant reduction in the cell-to-bath (12.8 ± 1.9, P = 0.2294) or cytosolic contents (224.2 μM ± 33.4, P = 0.0696) were seen as noted in Figure 33. The amount of tubular contents and the percentage of tubule contents was significantly reduced in the presence of 200 μM PAH, Figure 34. The tubular contents decreased from 4,211.3 fmol mm^{-1} ± 565.2 to -7,839.9 fmol mm^{-1} ± 1,509.4, P = 0.0001. The percentage of bound $Me^{203}Hg^{+}$-*L*-taurine+PAH at the tubular epithelium was significantly increased, 102.76 %, P = 0.0026.

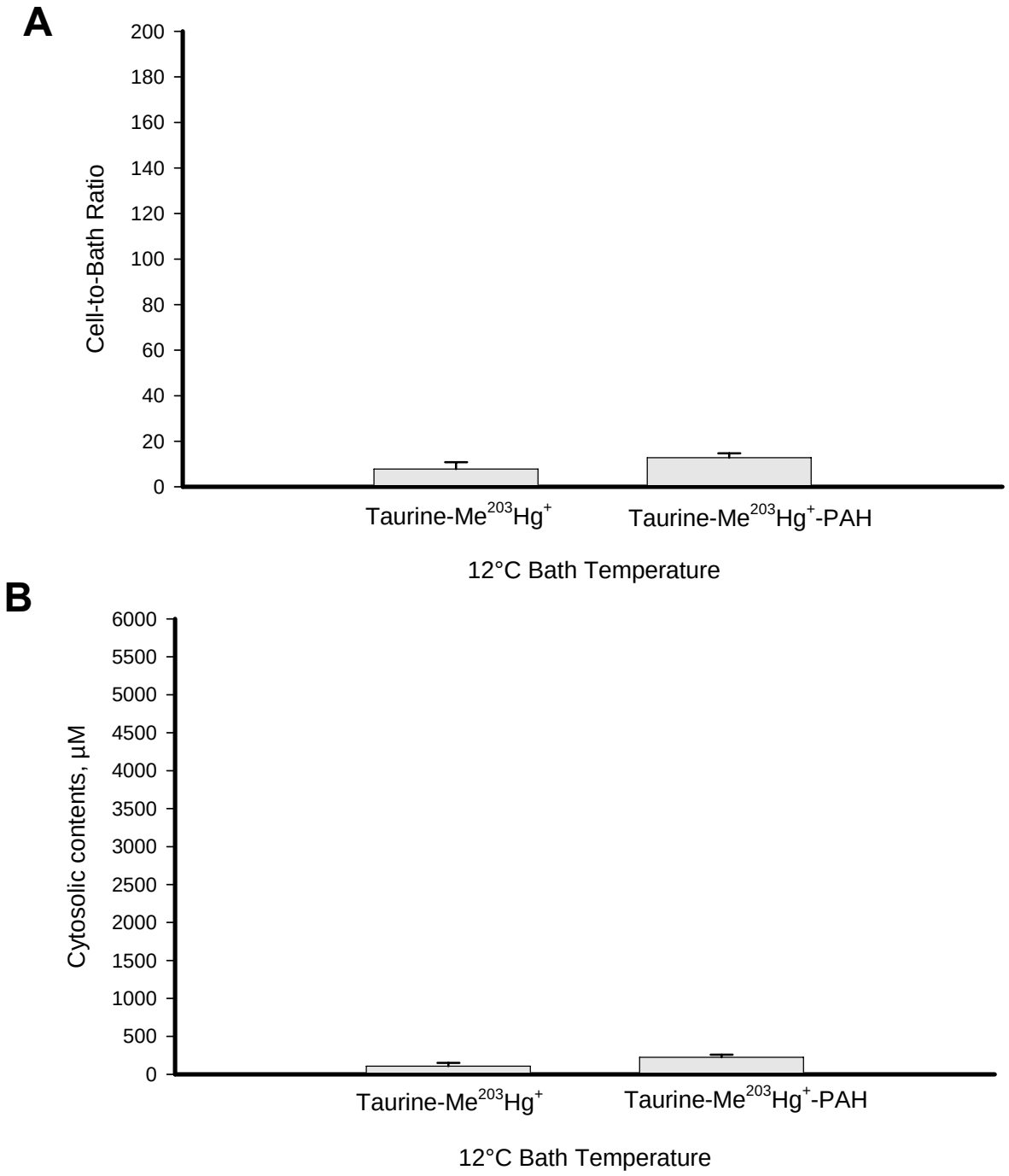

Figure 33: The effect of PAH on $Me^{203}Hg^{+}$-*L*-taurine transport in the basolateral membrane of the S_2 segments of rabbit proximal tubules (A) cell-to-bath ratio and (B) cytosolic contents, µM (at 12°C). Each value represents the mean ± SE with a minimum sample size of 5 tubules. The "*" indicates a significant statistical difference, $P \leq 0.05$.

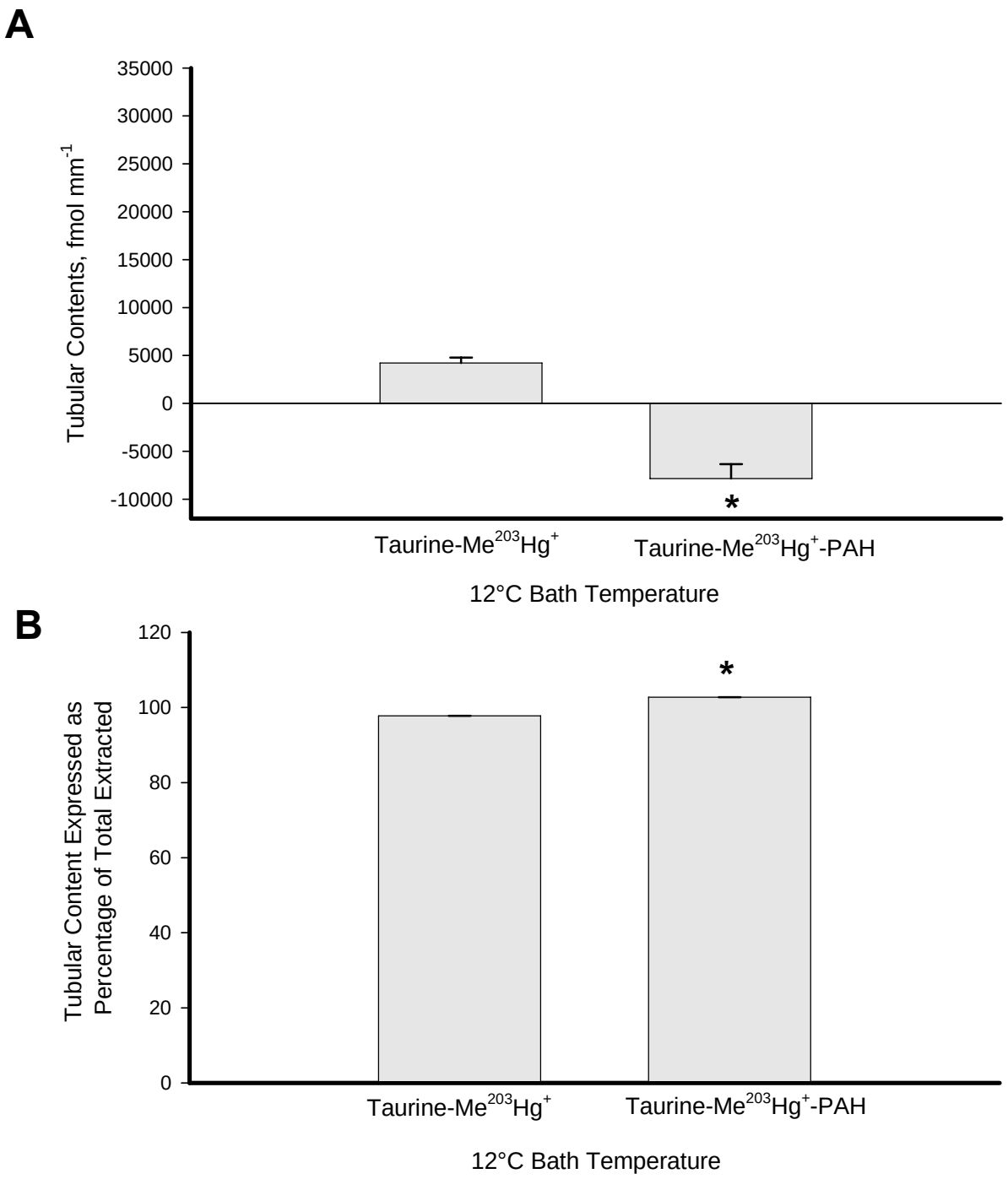

Figure 34: The effect of PAH on $Me^{203}Hg^{+}$-*L*-taurine transport in the basolateral membrane of the S_2 segments of rabbit proximal tubules (A) tubular contents and (B) tubular content expressed as percentage of total extracted (at 12°C). Each value represents the mean ± SE with a minimum sample size of 5 tubules. The "*" indicates a significant statistical difference, $P \leq 0.05$.

The effect of TEA on basolateral transport of $Me^{203}Hg^{+}$-*L*-taurine

To characterize the effect of TEA on the basolateral uptake of $Me^{203}Hg^{+}$-*L*-taurine, 20 μM $Me^{203}Hg^{+}$-*L*-taurine along with 22 μM TEA was added to the bathing solution. The average cell-to-bath ratio and cytosolic contents of $Me^{203}Hg^{+}$-*L*-taurine-TEA at 37°C are noted in Figure 35. Bath-to-cell uptake of $Me^{203}Hg^{+}$-*L*-taurine-TEA (49.1 ± 4.9) was not significantly increased (P = 0.1185) at 37°C when compared to uptake of $Me^{203}Hg^{+}$-*L*-taurine, alone (91.9 ± 16.9). The average cytosolic concentration of $Me^{203}Hg^{+}$-*L*-taurine and $Me^{203}Hg^{+}$-*L*-taurine-TEA are 1,179.7 μM ± 210.4 and 1,145.2 μM ± 113.8 (P = 0.9172), demonstrating no significant increased in the cellular contents of $Me^{203}Hg^{+}$ -*L*-taurine versus $Me^{203}Hg^{+}$-*L*-taurine -TEA at normal physiological temperatures. The amount of $Me^{203}Hg^{+}$-*L*-taurine versus $Me^{203}Hg^{+}$-*L*-taurine -TEA bound to the basolateral epithelium the tubular contents (fmol mm^{-1}) and percentage of tubular contents are noted in Figure 36. The bound $Me^{203}Hg^{+}$-*L*-taurine -TEA complex (6,988.1 ± 2,820.5 fmol mm^{-1}) was significantly less than the bound $Me^{203}Hg^{+}$-*L*-taurine (15,523.2 ± 1,184.8 fmol mm^{-1}) (P = 0.0006). The percentage of bound $Me^{203}Hg^{+}$-*L*-taurine -TEA complex compared to the percentage of $Me^{203}Hg^{+}$-*L*-taurine bound was 86.7 % and 94 % (P = 0.0005), respectively.

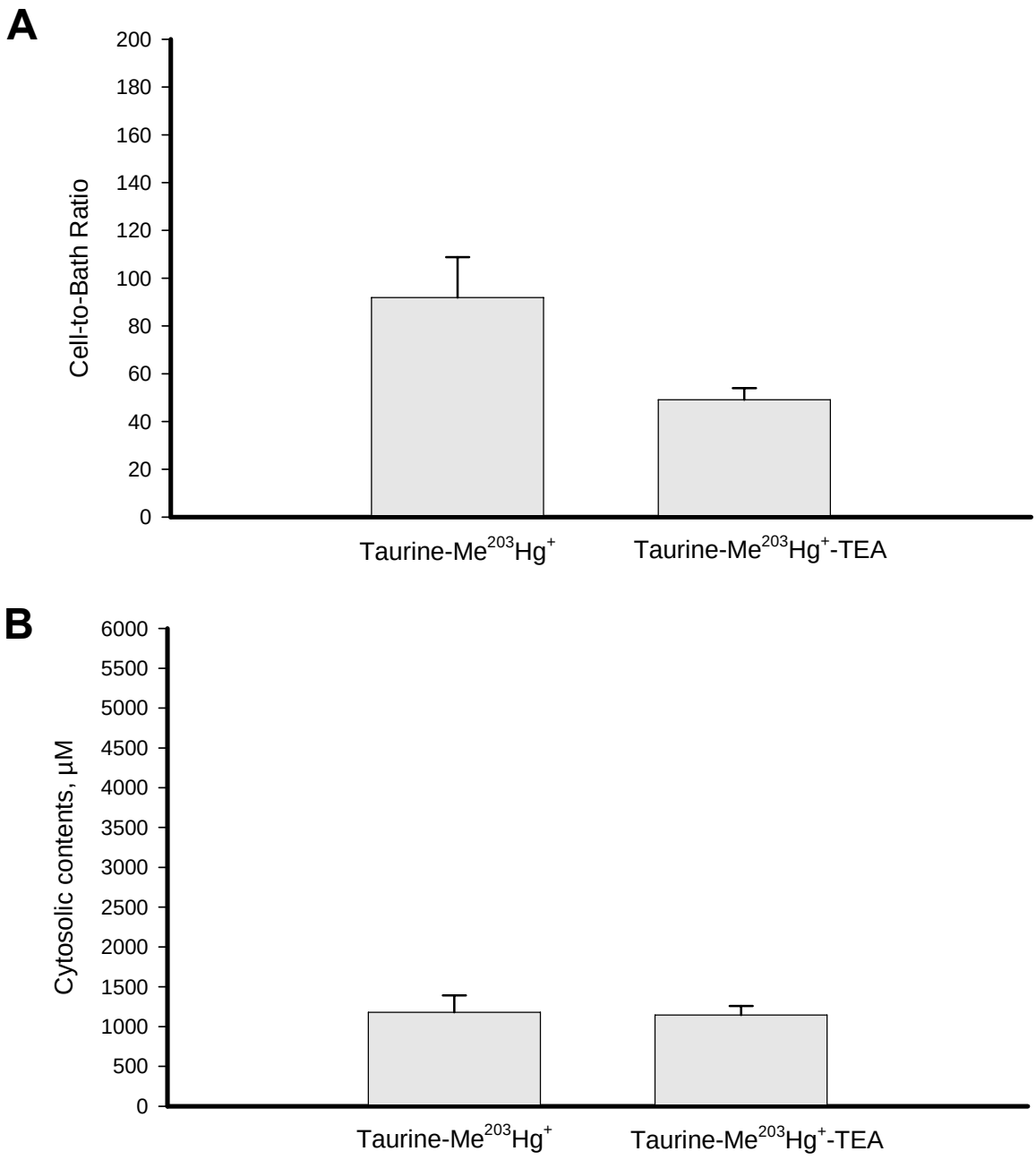

Figure 35: The effect of TEA on $Me^{203}Hg^{+}$-*L*-taurine transport in the basolateral membrane of the S_2 segments of rabbit proximal tubules (A) cell-to-bath ratio and (B) cytosolic contents, µM. Each value represents the mean ± SE with a minimum sample size of 5 tubules.

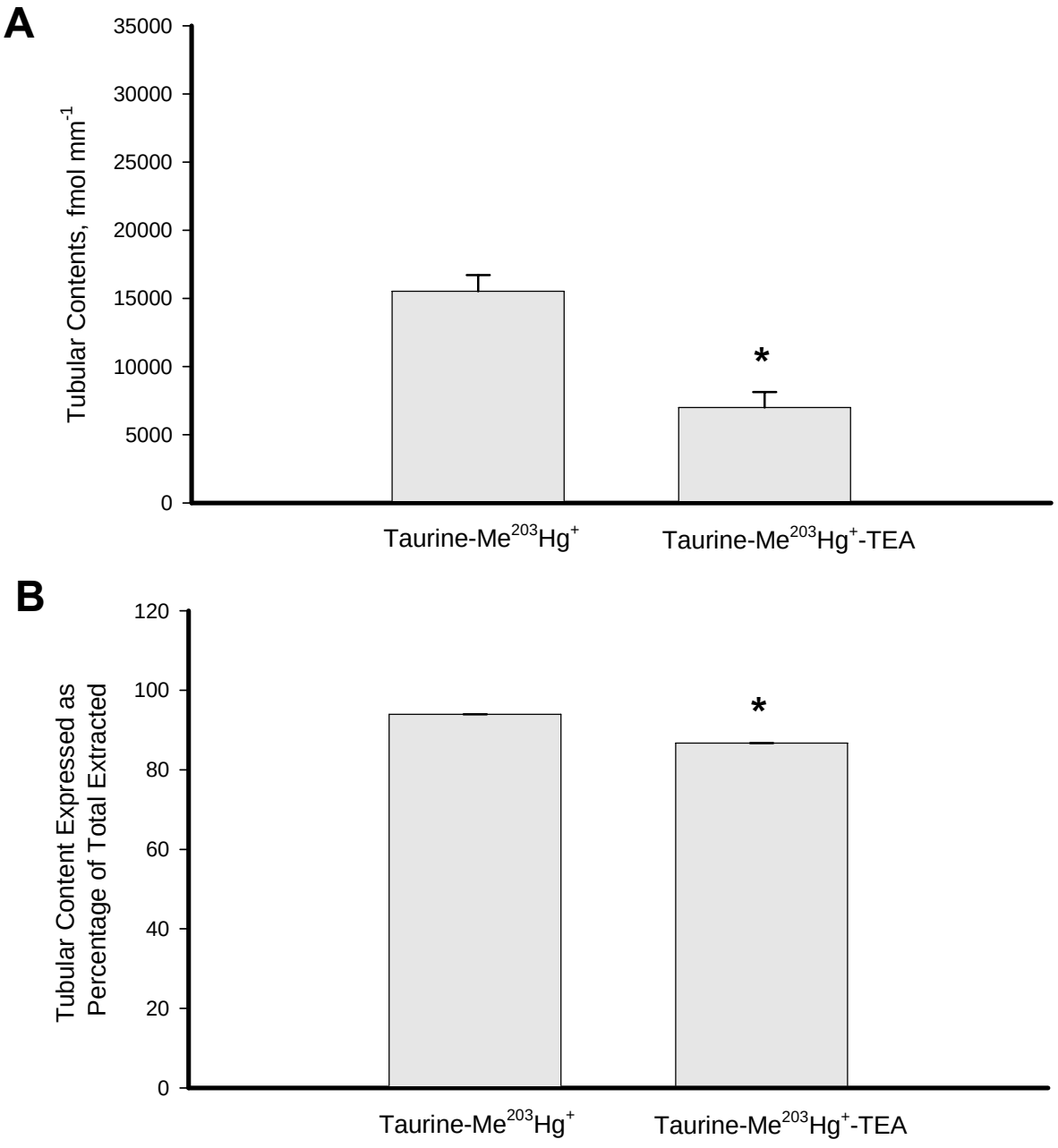

Figure 36: The effect of TEA on $Me^{203}Hg^{+}$-*L*-taurine transport in the basolateral membrane of the S_2 segments of rabbit proximal tubules (A) tubular contents and (B) tubular content expressed as percentage of total extracted. Each value represents the mean ± SE with a minimum sample size of 5 tubules.

The effect of *N*-acetylcysteine on the basolateral transport of $Me^{203}Hg^{+}$

Figure 37 shows the effect of adding 22 μM *N*-acetylcysteine to the bathing solution (12°C versus 37°C) on the cell-to-bath transport and the cytosolic contents of $Me^{203}Hg^{+}$. The cell-to-bath ratio was significantly reduced by a factor of over seven-fold at 37°C (-16.4 ± 3.1 versus -2.2 ± 0.5, P = 0.0069). The contents of the cytosol were also significantly reduced when comparing the amount of transport of $Me^{203}Hg^{+}$-*N*-acetylcysteine at 12°C versus 37°C, -28.5 μM ± 6.2 and -206.2 μM ± 37, P = 0.0051. Figure 38 shows the contents of the tubule containing $Me^{203}Hg^{+}$-*N*-acetylcysteine and the percentage of tubular contents at 12°C versus 37°C. The figure shows a significant difference between the amount of bound $Me^{203}Hg^{+}$-*N*-acetylcysteine at the tubular epithelium 12°C versus 37°C, 433.2 fmol mm^{-1} ± 279.1 and 1,207.5 fmol mm^{-1} ± 153.9, P = 0.0143. However, the percentage of tubular contents was not statistically different (P = 0.9737) between the two groups, 86.4 % and 82.3 %, respectively.

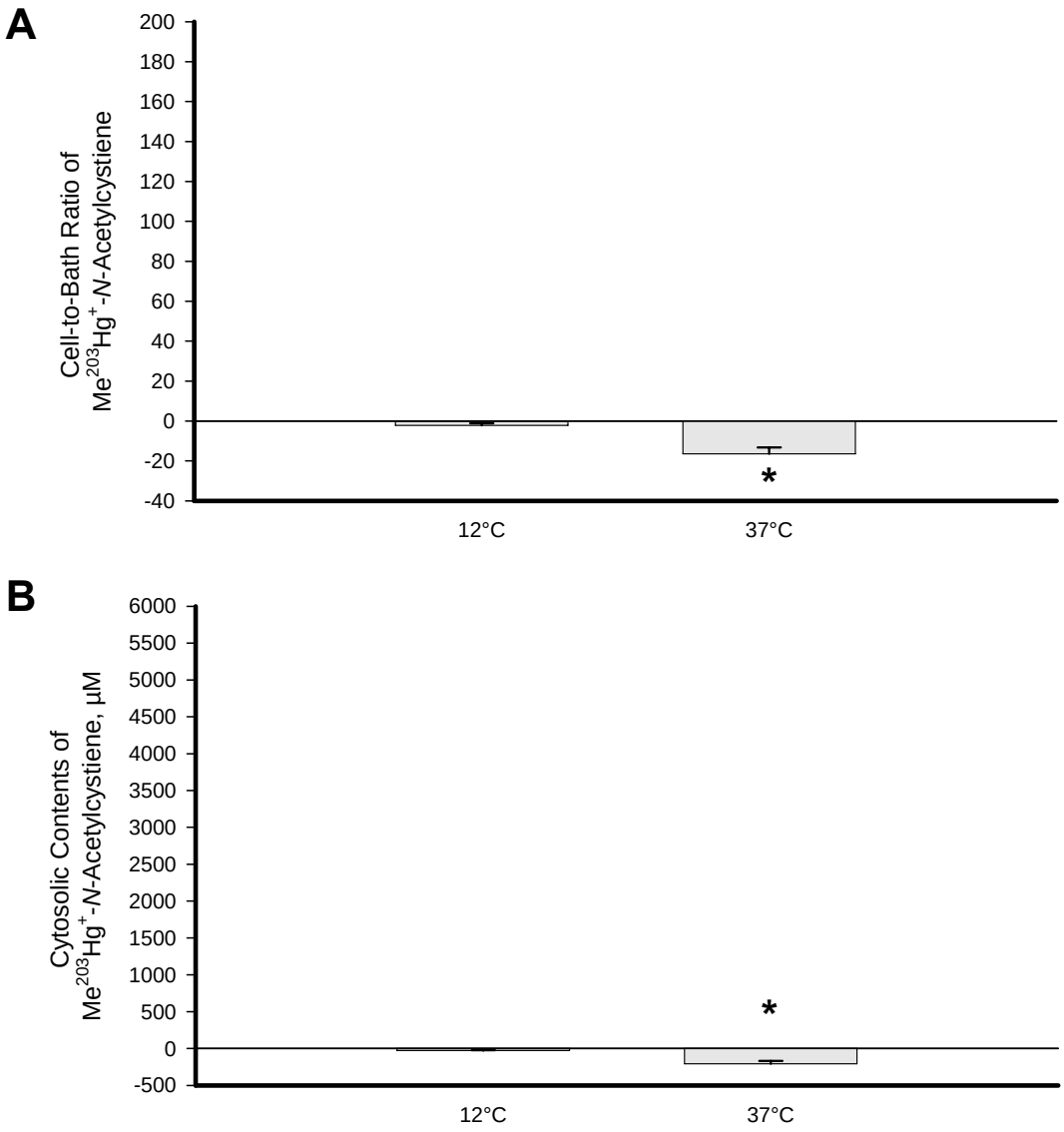

Figure 37: $Me^{203}Hg^{+}$-*N*-acetylcysteine transport in the basolateral membrane of the S_2 segments of rabbit proximal tubules (A) cell-to-bath ratio and (B) cytosolic contents, µM. Each value represents the mean ± SE with a minimum sample size of 5 tubules. The "*" indicates a significant statistical difference, $P \leq 0.05$.

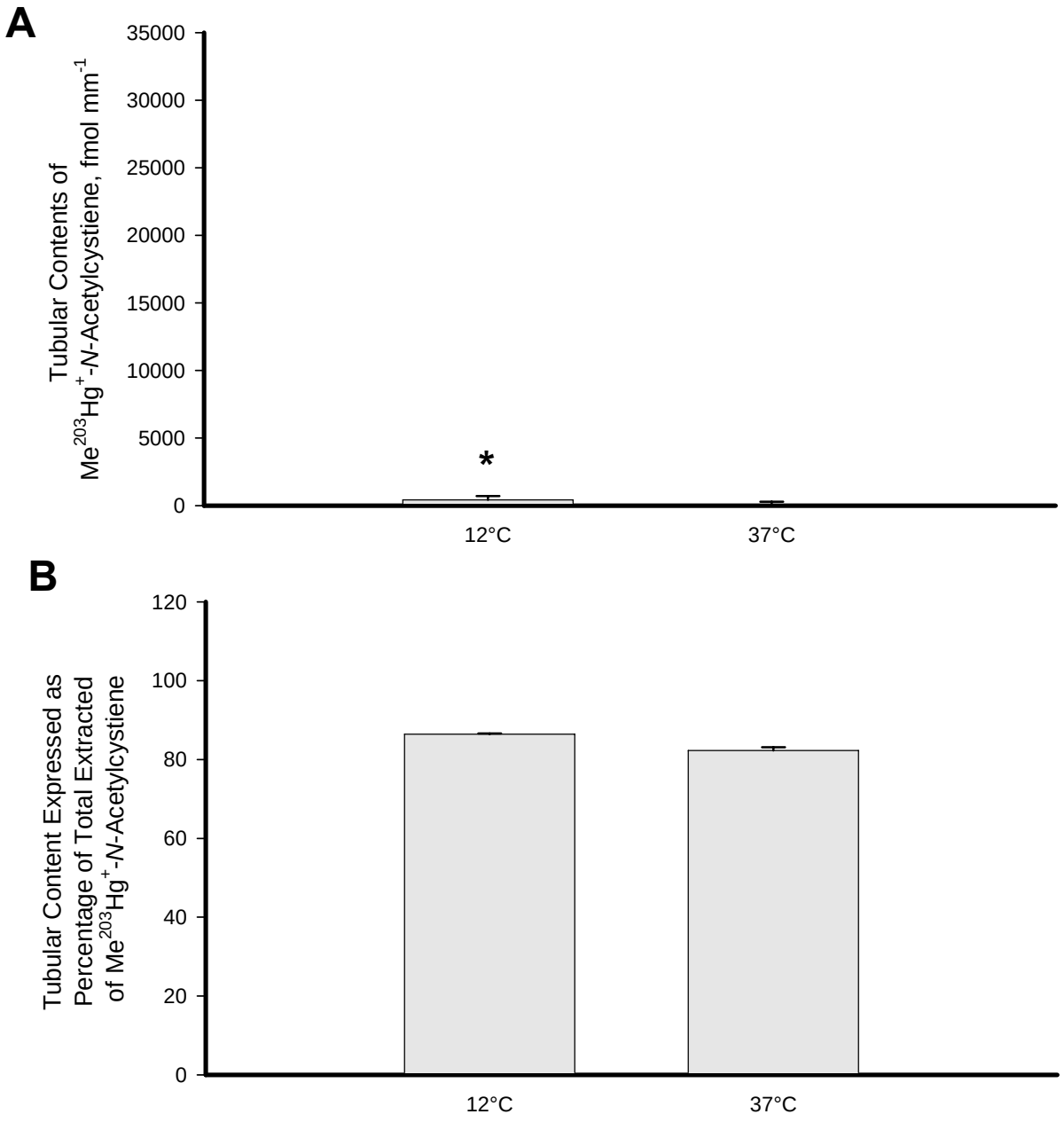

Figure 38: $Me^{203}Hg^{+}$-*N*-acetylcysteine transport in the basolateral membrane of the S_2 segments of rabbit proximal tubules (A) tubular contents and (B) tubular content expressed as percentage of total extracted. Each value represents the mean ± SE with a minimum sample size of 5 tubules. The "*" indicates a significant statistical difference, $P \leq 0.05$.

The effect of PAH on the basolateral transport of $Me^{203}Hg^{+}$-*N*-acetylcysteine, 37°C

Characterization of the effect of PAH at 37°C on the transport of $Me^{203}Hg^{+}$-*N*-acetylcysteine on the cell-to-bath ratios and the cytosolic contents is shown in Figure 39. A significant increase in the cell-to-bath ratio was noted in the presence of 200 μM PAH (A), 10.0 ± 1.2, P = 0.0001. The amount of $Me^{203}Hg^{+}$-*N*-*a*cetylcysteine in the cytoplasm was also significantly reduced in the presence of PAH, 167.7 μM ± 20.7, P = 0.0001. As noted in Figure 40, the amount of bound $Me^{203}Hg^{+}$-*N*-*a*cetylcysteine was substantially reduced as well. The tubular contents of $Me^{203}Hg^{+}$-*N*-*a*cetylcysteine+PAH compared to $Me^{203}Hg^{+}$-*N*-*a*cetylcysteine was -13,875.0 fmol mm^{-1} ± 1,518.4 versus 1,207.5 fmol mm^{-1} ± 153.9, P = 0.0001. The percentage of bound $Me^{203}Hg^{+}$ *N*-*a*cetylcysteine+PAH was not significantly changed (P = 0.8864).

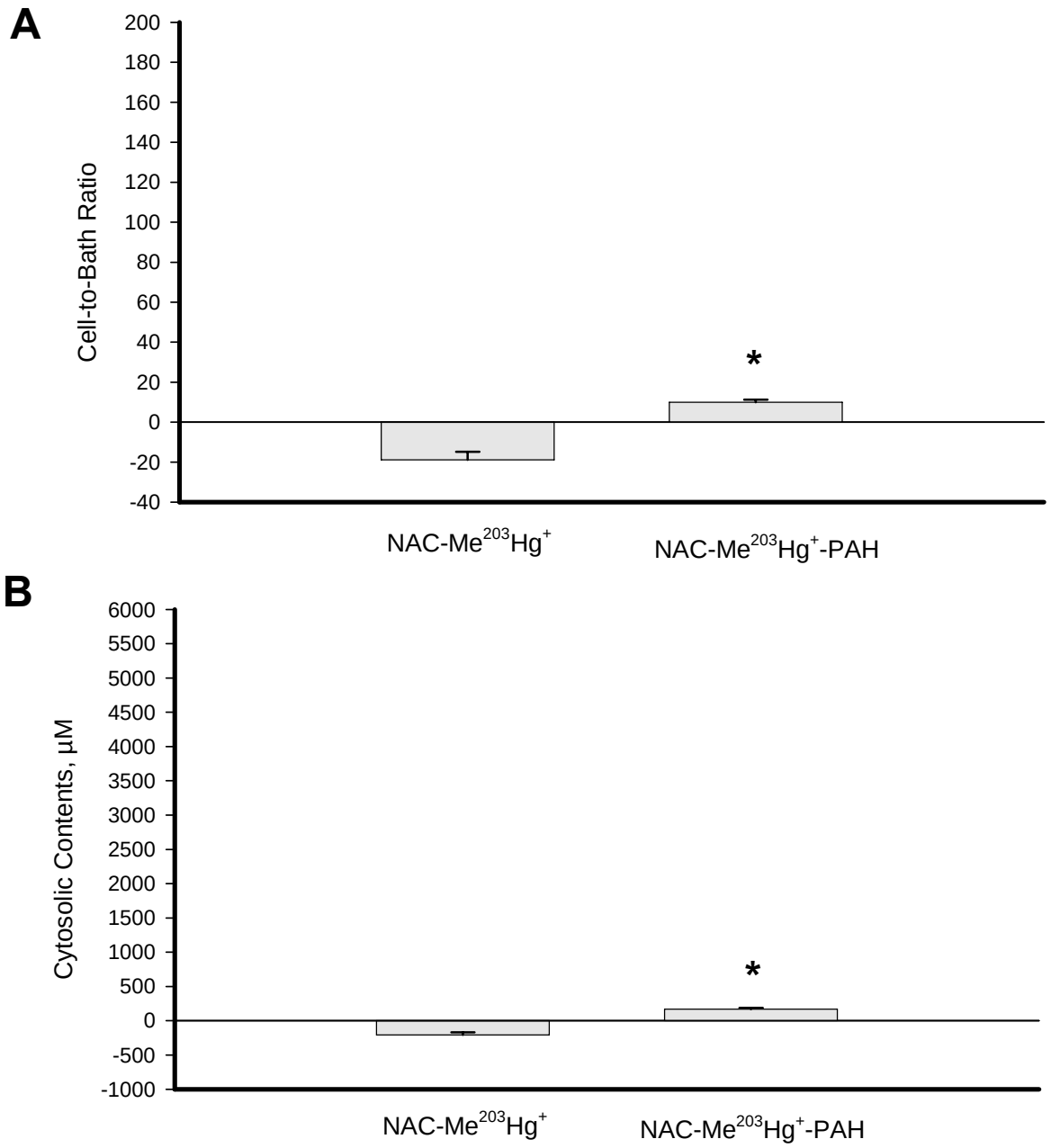

Figure 39: The effect of PAH on $Me^{203}Hg^{+}$-*N*-acetylcysteine transport in the basolateral membrane of the S_2 segments of rabbit proximal tubules (A) cell-to-bath ratio and (B) cytosolic contents, µM. Each value represents the mean ± SE with a minimum sample size of 5 tubules. The "*" indicates a significant statistical difference, $P \leq 0.05$.

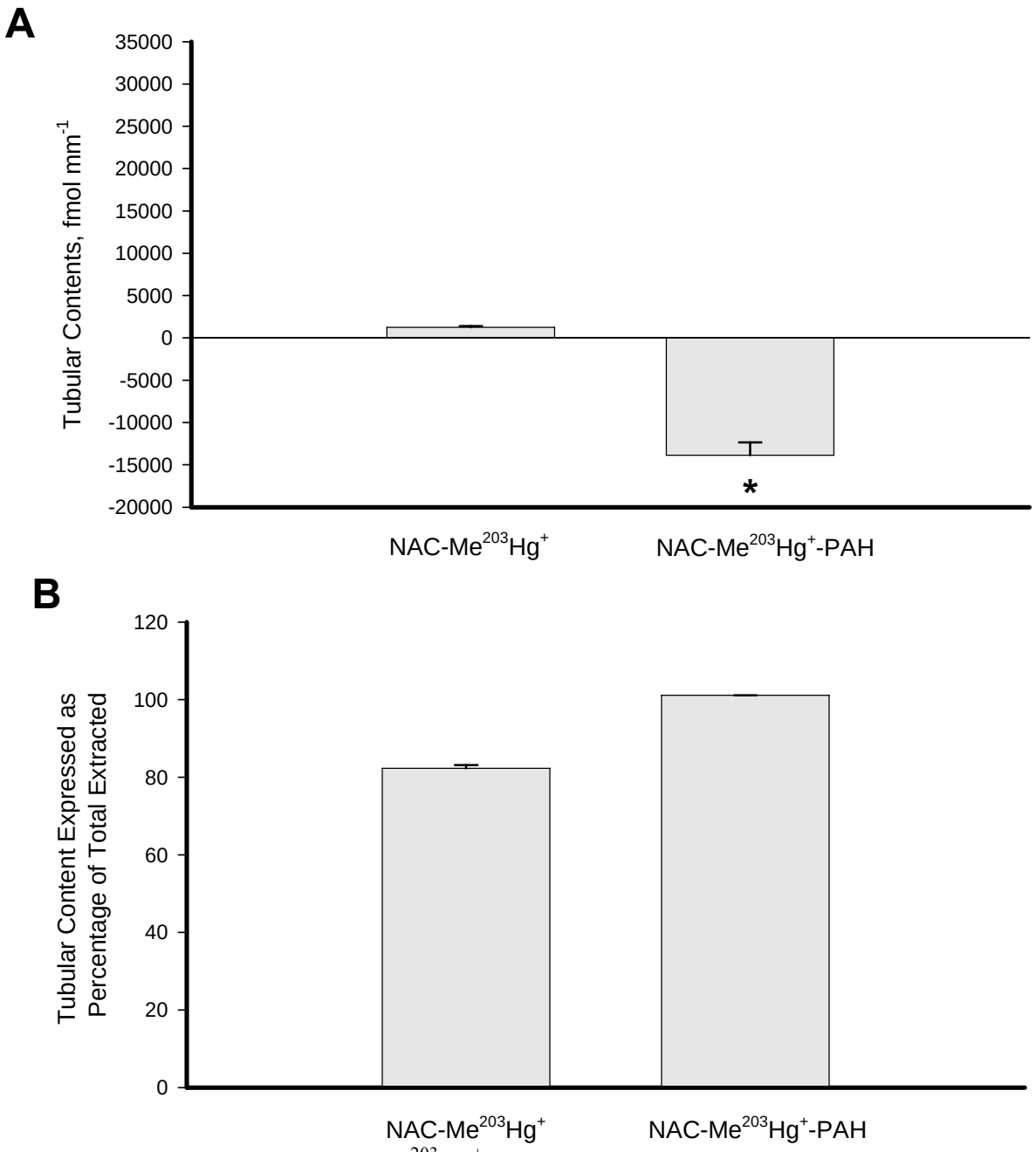

Figure 40: The effect of PAH on $Me^{203}Hg^{+}$-*N*-acetylcysteine transport in the basolateral membrane of the S_2 segments of rabbit proximal tubules (A) tubular contents and (B) tubular content expressed as percentage of total extracted. Each value represents the mean ± SE with a minimum sample size of 5 tubules. The "*" indicates a significant statistical difference, $P \leq 0.05$.

The effect of *L*-glutathione on the basolateral transport of $Me^{203}Hg^{+}$

Figure 41 shows the effect of adding 22 μM *L*-glutathione to the bathing solution containing 20 μM $Me^{203}Hg^{+}$. There was no significant increase in either the cell-to-bath (-2.9 ± 0.6 and -2.8 ± 0.3, P = 0.9655) or the cytosolic contents (-47.9 μM ± 5.0 and -58.6 μM ± 8.2, P = 0.4341), at both 12°C and 37°C respectively. The amount of $Me^{203}Hg^{+}$-*L*-glutathione bound to the tubule was significantly increased at 37°C, 1,267.8 fmol mm^{-1} ± 290.2, P = 0.0253 compare to the amount presumably bound at 12°C, 128.9 fmol mm^{-1} ± 26 [Fig. 42].

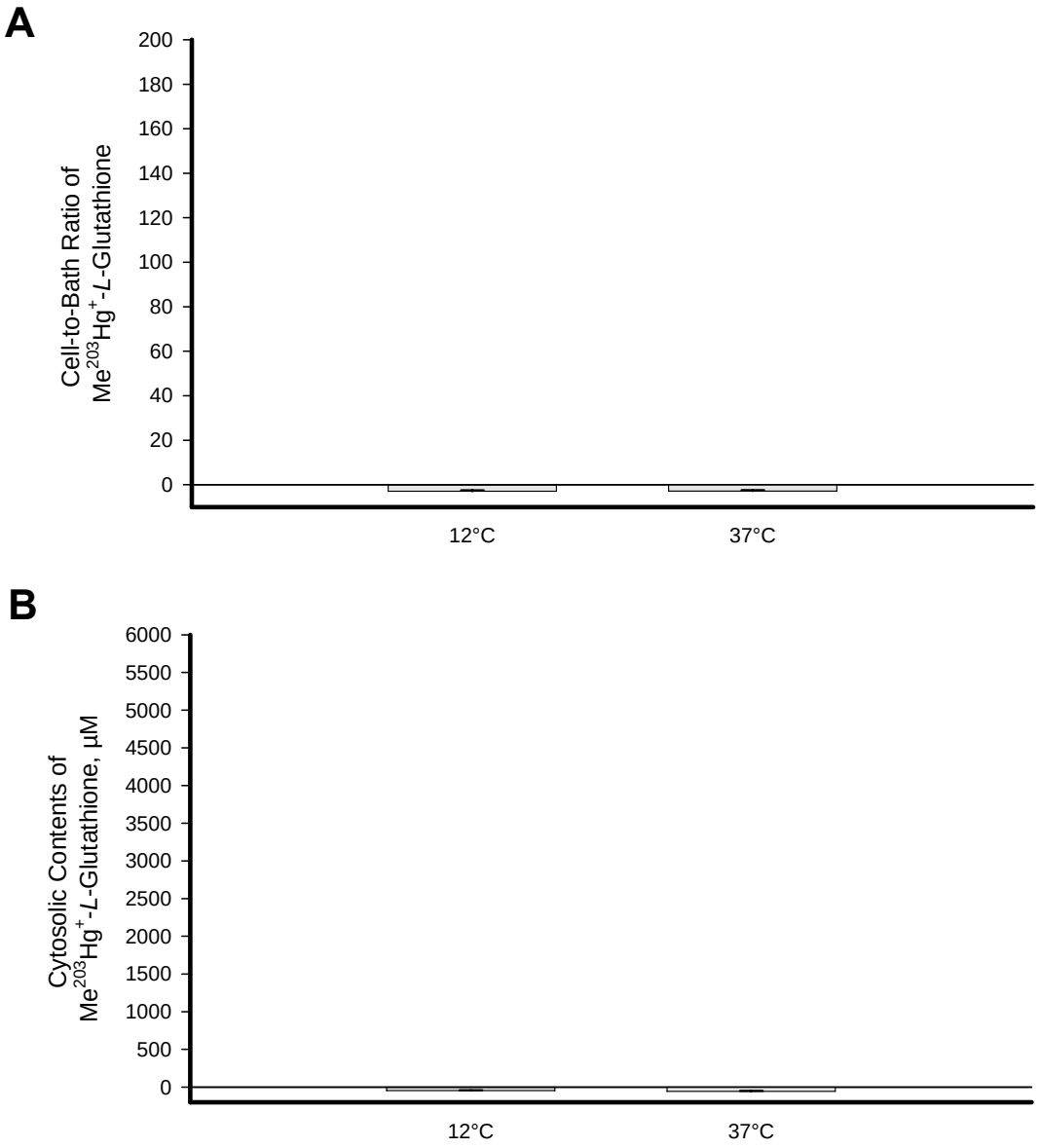

Figure 41: $Me^{203}Hg^{+}$-*L*-glutathione transport in the basolateral membrane of the S_2 segments of rabbit proximal tubules (A) cell-to-bath ratio and (B) cytosolic contents, µM. Each value represents the mean ± SE with a minimum sample size of 5 tubules.

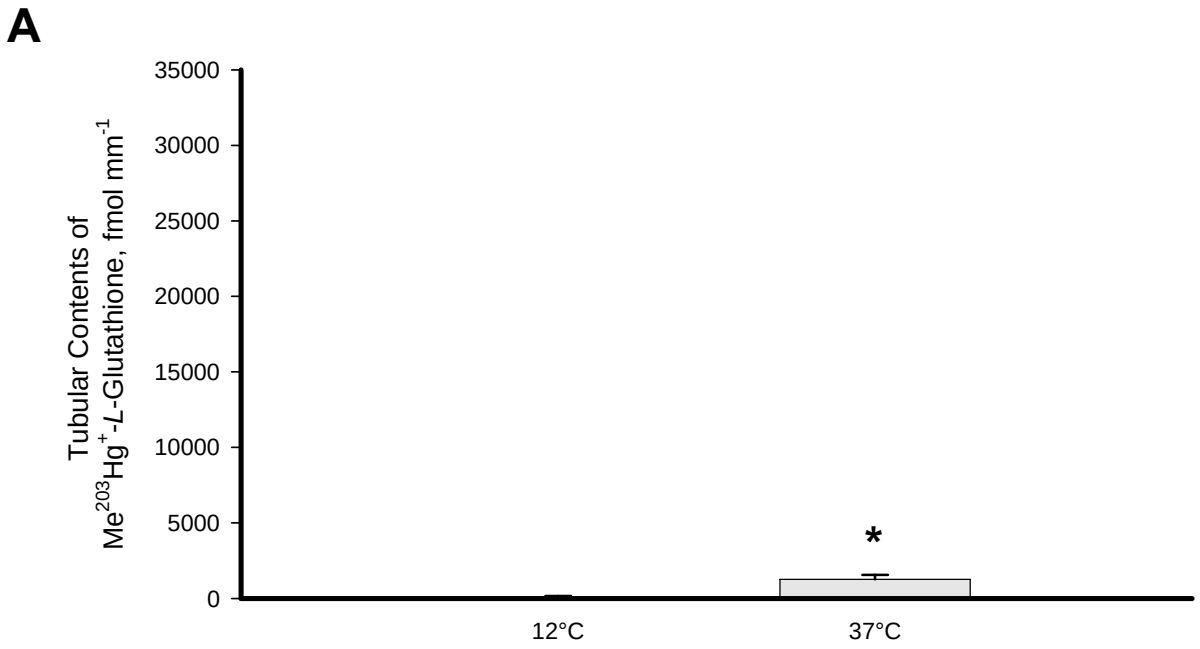

Figure 42: $Me^{203}Hg^{+}$- *L*-glutathione transport in the basolateral membrane of the S_2 segments of rabbit proximal tubules (A) tubular contents. Each value represents the mean ± SE with a minimum sample size of 5 tubules. The "*" indicates a significant statistical difference, $P \leq 0.05$.

The effect of *DL*-homocysteine on the basolateral transport of $Me^{203}Hg^{+}$

Figure 43 shows the effect of adding 22 µM *DL*-homocysteine to the bathing solution containing 20 µM $Me^{203}Hg^{+}$. A significant increase in the cell-to-bath ratio (-5.2 ± 1 and -10.9 ± 2, P = 0.0427) and the cytosolic contents (-62.6 µM ± 22.7 and -143.5 µM ± 21.5, P = 0.0201), was noted at both 12°C and 37°C respectively. The amount of $Me^{203}Hg^{+}$-*DL*-homocysteine bound to the tubule was significantly increased at 37°C, 360.1 fmol mm^{-1} ± 62.6, P = 0.0003 compare to the amount bound at 12°C, 22.9 fmol mm^{-1} ± 18.6 [Fig. 44].

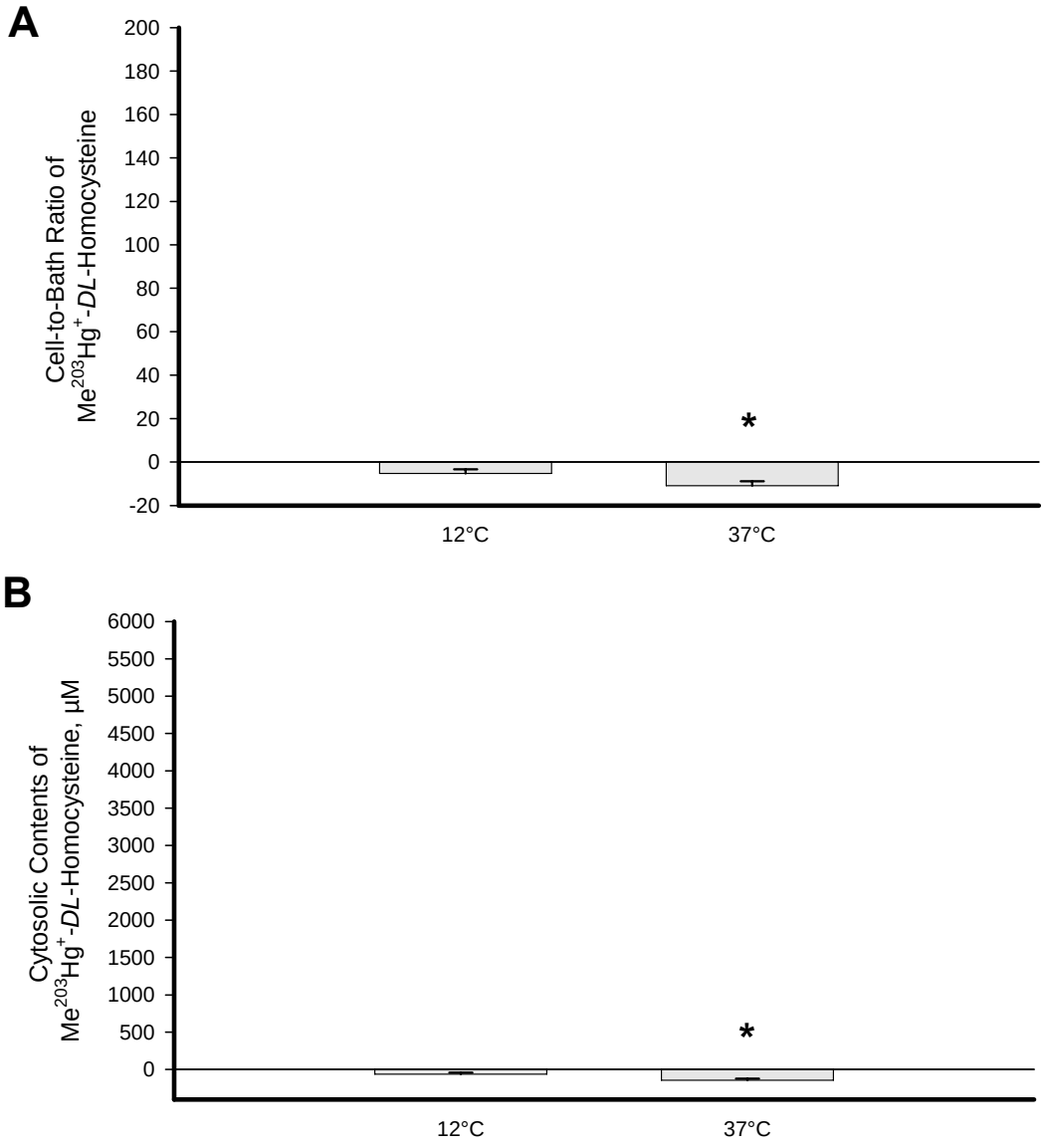

Figure 43: $Me^{203}Hg^{+}$-D*L*-homocysteine transport in the basolateral membrane of the S_2 segments of rabbit proximal tubules (A) cell-to-bath ratio and (B) cytosolic contents, µM. Each value represents the mean ± SE with a minimum sample size of 5 tubules. The "*" indicates a significant statistical difference, $P \leq 0.05$.

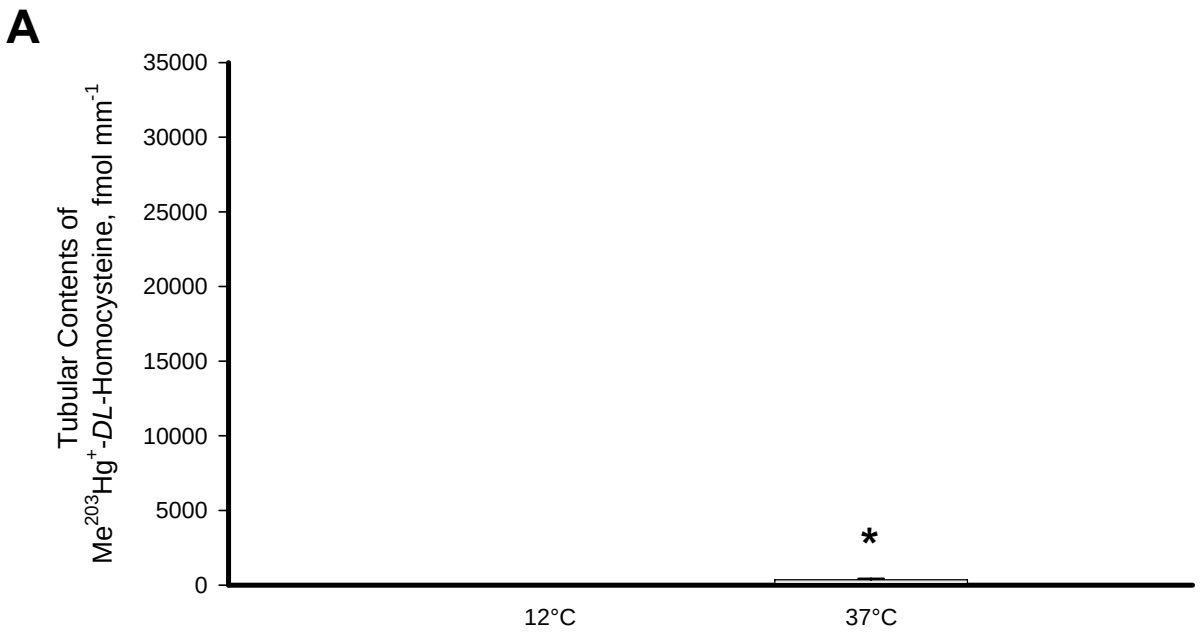

Figure 44: $Me^{203}Hg^{+}$- *DL*-homocysteine transport in the basolateral membrane of the S_2 segments of rabbit proximal tubules (A) tubular contents. Each value represents the mean ± SE with a minimum sample size of 5 tubules. The "*" indicates a significant statistical difference, $P \leq 0.05$.

Table 1 shows the outcome of $Me^{203}Hg^{+}$ mixed with rabbit whole blood and plasma. As noted in the table, the concentration of $Me^{203}Hg^{+}$ is predominantly found with the protein pellet (87% for whole blood and 98% for the plasma pellet). There is however about 1% of the $Me^{203}Hg^{+}$ that remains in the supernatant.

Table 1: Concentration of $Me^{203}Hg^{+}$ in Plasma

Whole Blood
Blood pellet 86.99 ± 0.49 %
Plasma 13.01 ± 0.49 %
Supernatant 0.72 ± 0.03 %
Protein Pellet 99.27 ± 0.02 %
Plasma
Supernatant 0.94 ± 0.08 %
Protein Pellet 98.27 ± 0.21 %

Mass spectrometry analysis of only MeHgCl showed one dominant peak at 216.9 and one small peak at 545.1 [Fig. 45]. Analysis of *L*-taurine alone also showed a dominant peak at 124 [Fig. 46] with two smaller ones at 97 and 212.1, while MeHgCl + *L*-taurine displayed a number of peaks two were distinct, one at 251 and 409.1 [Fig. 47]. Mass spectrometry analysis of *L*-cysteine also had one discrete peak at 120 [Fig. 48] and the MeHgCl + *L*-cysteine conjugate had several spikes with the predominant one at 409.2 [Fig. 49]. *L*-methionine showed one clear spike at 150.2 [Fig. 50], while MeHgCl + *L*-methionine had numerous spikes, but one well-defined 409.2 [Fig. 51]. Figure 52 shows the mass spectrometry analysis of *N*-acetylcysteine with one spike at 162 and MeHgCl + *N*-acetylcysteine has multiple spikes but four discrete peaks, with the predominant ones at 212.1 and 378 [Fig. 53]. *DL*-homocysteine has a dominant spike at 136.1 [Fig. 54] and MeHgCl + *DL*-homocysteine shows numerous peaks, although two are more distinct (113 and 212.1) in [Fig. 55]. *L*-glutathione has several smaller spikes and one dominant

one at 306.1 [Fig. 56]. Figure 57 shows MeHgCl + *L*-glutathione with many spikes, several of which are distinct (113, 172.1, 212.1 and 255.2). The mass spectrometry of plasma in a heparin solution shows numerous spikes with the most distinctive one at 213.0 [Fig. 58]. Analysis of the plasma after precipitation with a 20% TCA solution demonstrated one predominant spike at 160.9 [Fig. 59]. The addition of MeHgCl to the plasma TCA precipitate produced multiple spikes with two dominant ones at 116.9 and 160.9 [Fig. 60]. Plasma was also analyzed in a Na-Citrate solution and is shown in Figure 61-63. Figure 61 has two discrete peaks at 116.9 and 215 and the TCA precipitate of plasma in Na-Citrate also showed one predominant spike at 160.9 [Fig. 62]. The addition of MeHgCl to the plasma TCA precipitate again produced multiple peaks with two distinct ones 116.9 and 160.9 [Fig. 63].

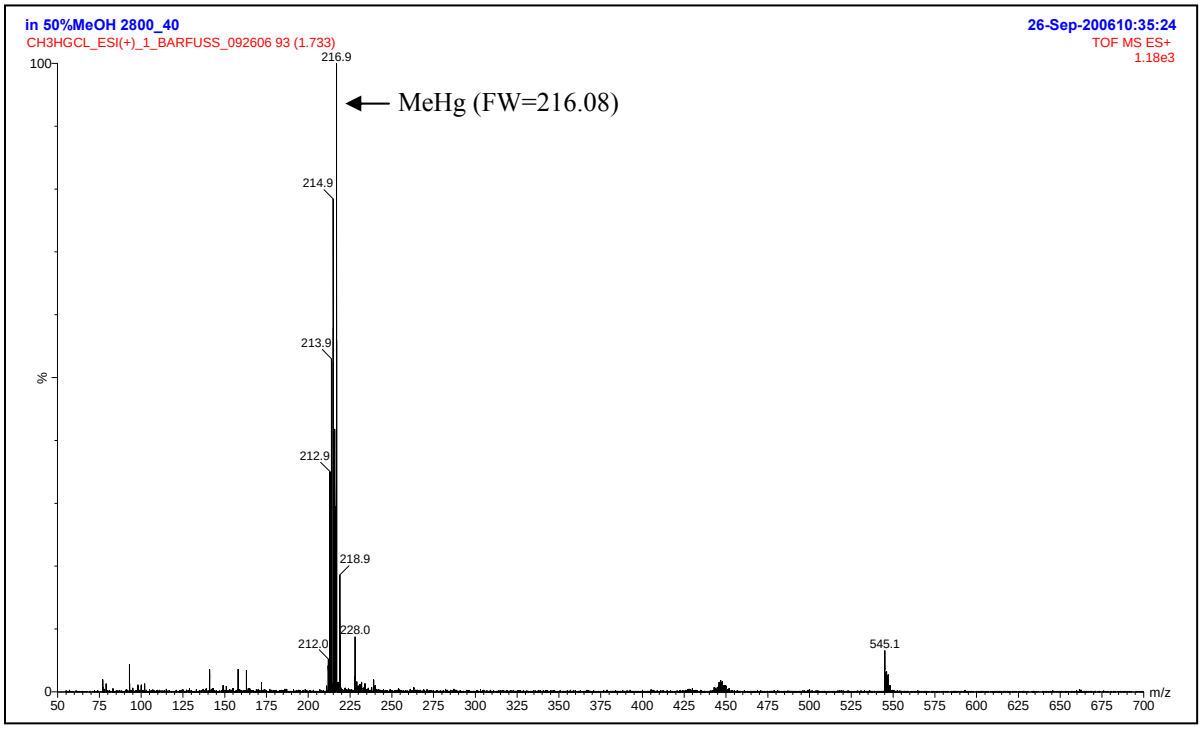

Figure 45: Molecular ion MALDI-TOF mass spectrum of 20 µM MeHgCl in Millipore water.

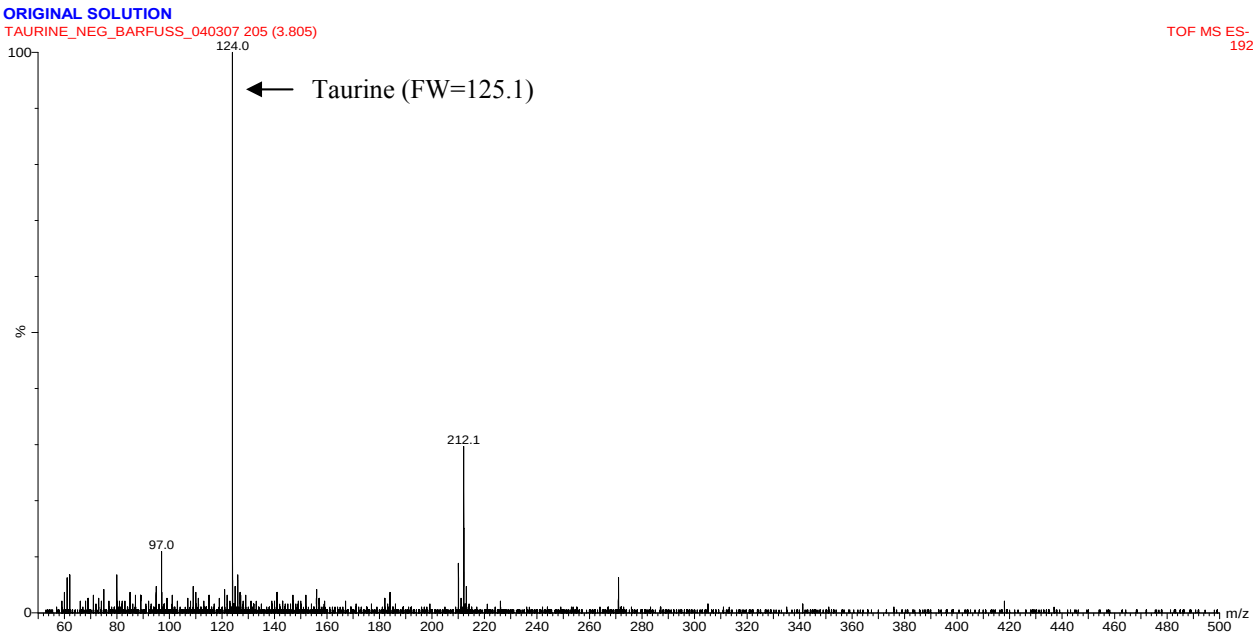

Figure 46: Molecular ion MALDI-TOF mass spectrum of 22 µM *L*-taurine in Millipore water.

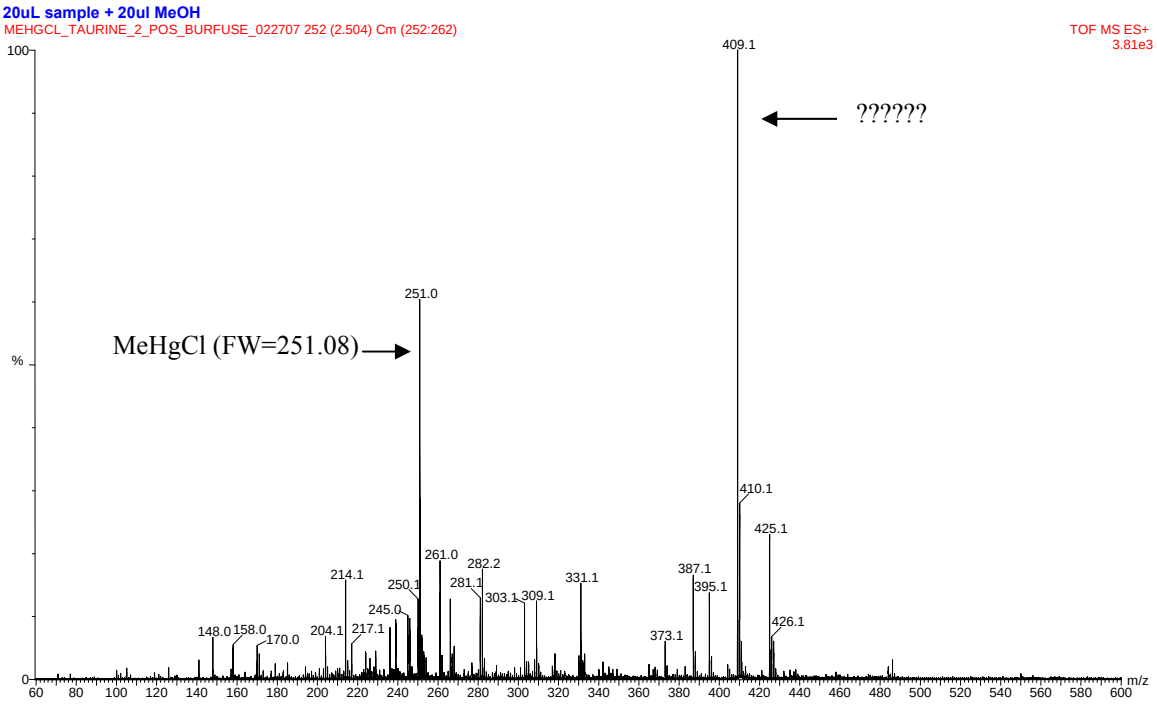

Figure 47: Molecular ion MALDI-TOF mass spectrum of 20 µM MeHgCl + 22 µM *L*-taurine in Millipore water.

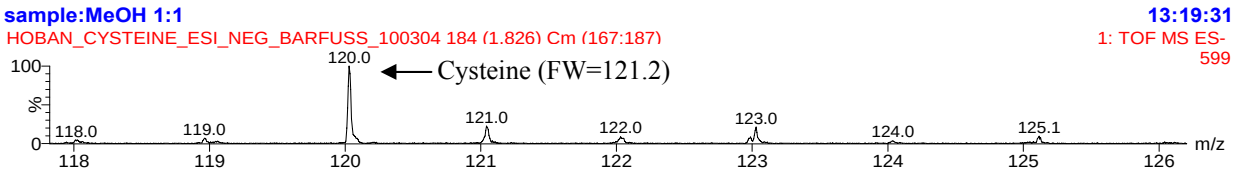

Figure 48: Molecular ion MALDI-TOF mass spectrum of 22 µM *L*-cysteine in Millipore water.

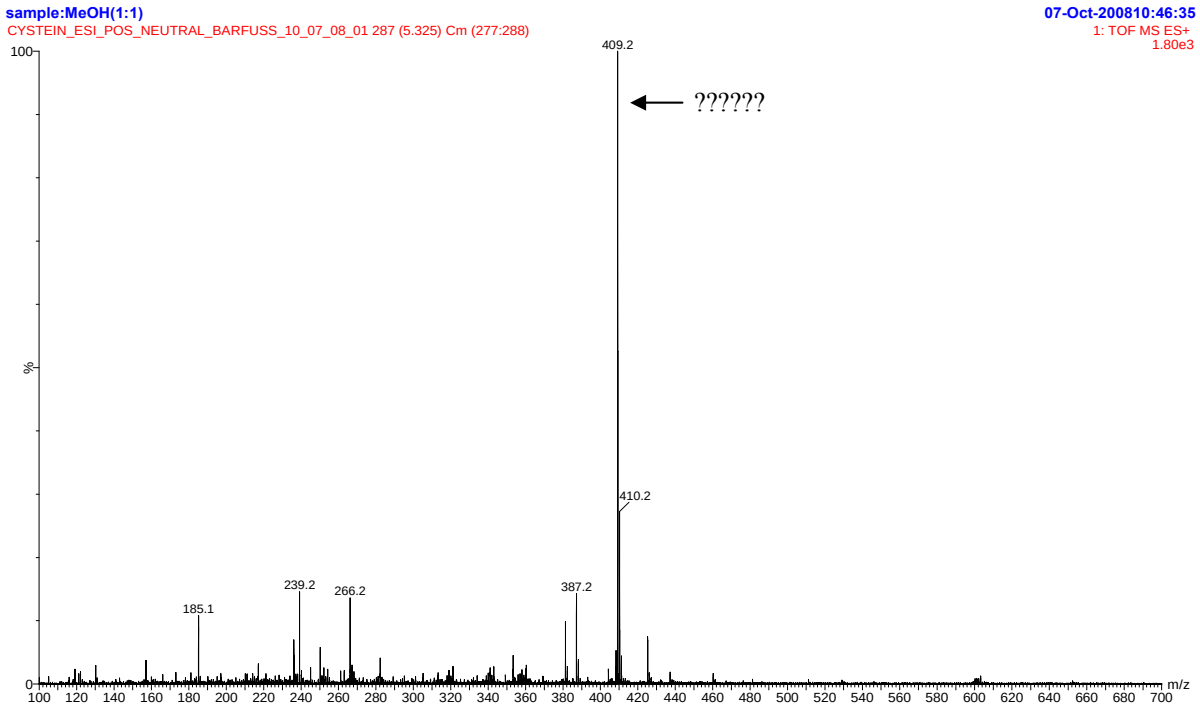

Figure 49: Molecular ion MALDI-TOF mass spectrum of 20 µM MeHgCl + 22 µM *L*-cysteine in Millipore water.

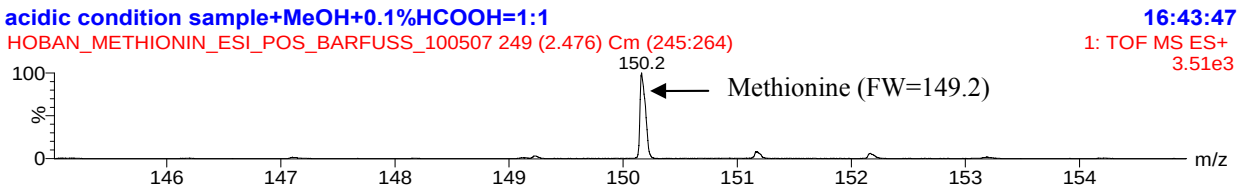

Figure 50: Molecular ion MALDI-TOF mass spectrum of 20 µM *L*-methionine in Millipore water.

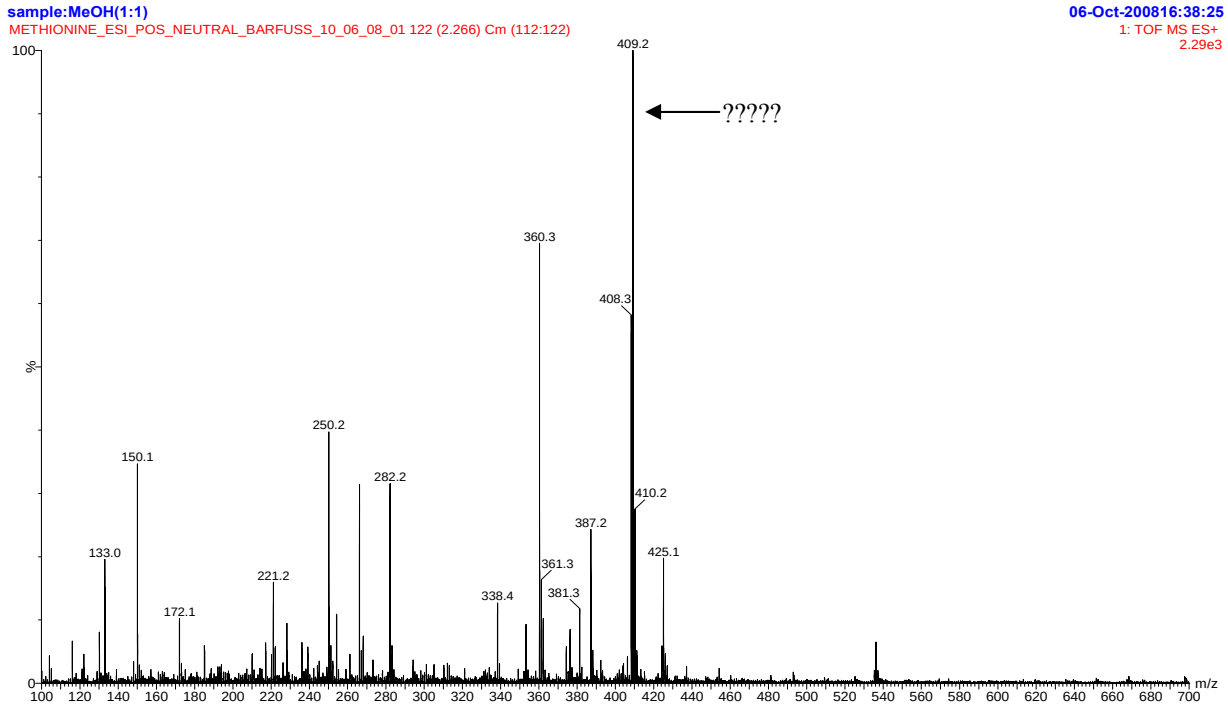

Figure 51: Molecular ion MALDI-TOF mass spectrum of 20 µM MeHgCl + 22 µM *L*-methionine in Millipore water.

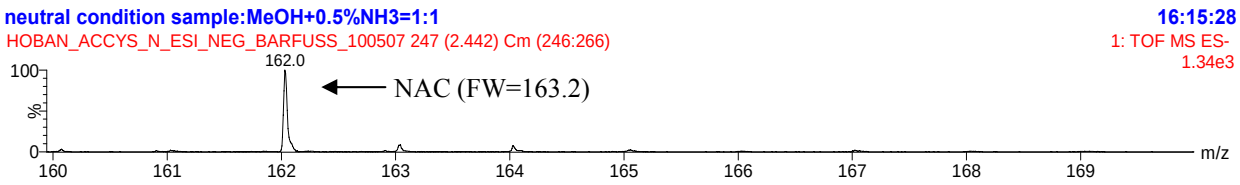

Figure 52: Molecular ion MALDI-TOF mass spectrum of 20 µM *N*-acetylcysteine in Millipore water.

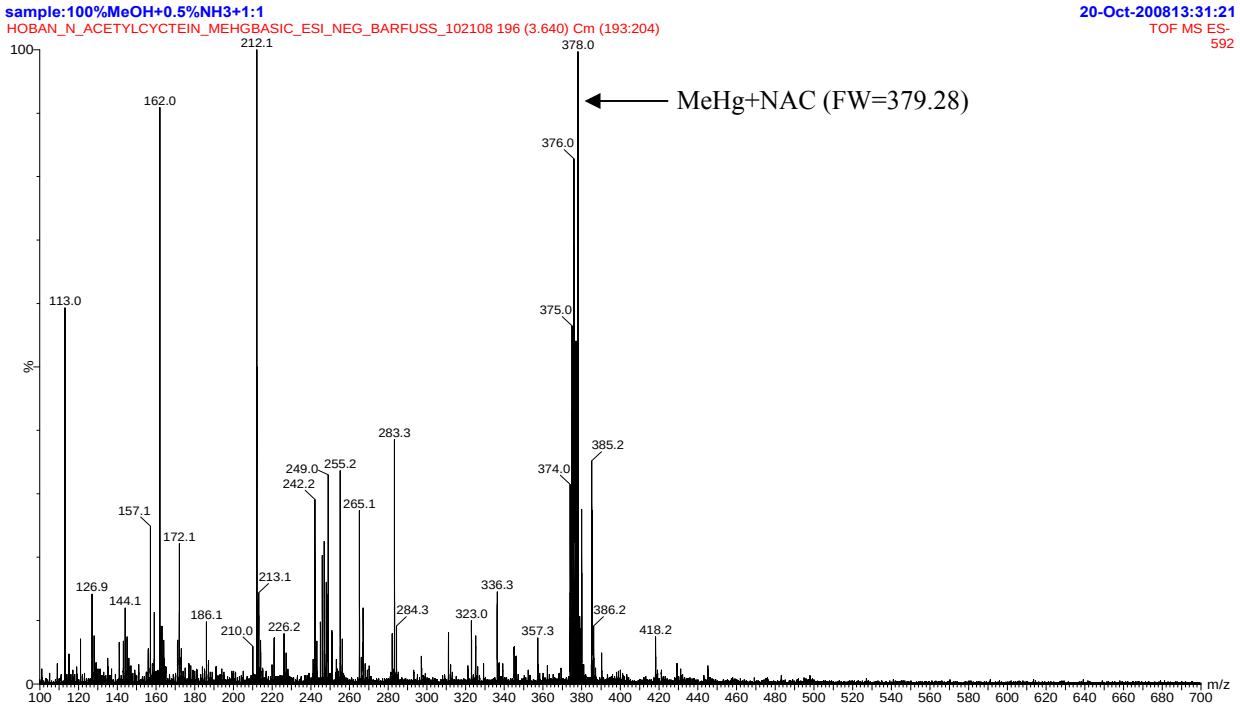

Figure 53: Molecular ion MALDI-TOF mass spectrum of 20 µM MeHgCl + 22 µM *N*-acetylcysteine in Millipore water.

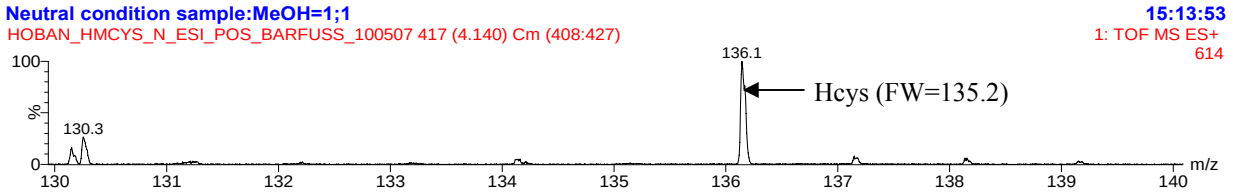

Figure 54: Molecular ion MALDI-TOF mass spectrum of 20 µM *DL*-homocysteine in Millipore water.

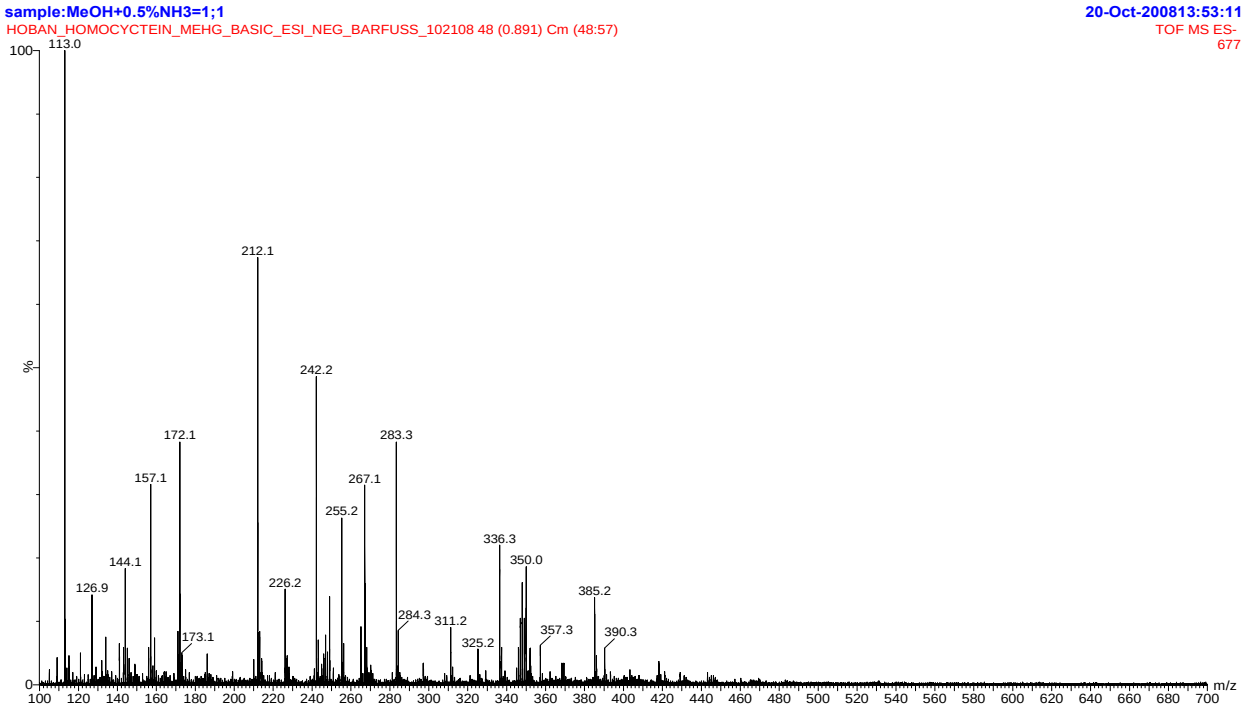

Figure 55: Molecular ion MALDI-TOF mass spectrum of 20 µM MeHgCl + 22 µM *DL*-homocysteine in Millipore water.

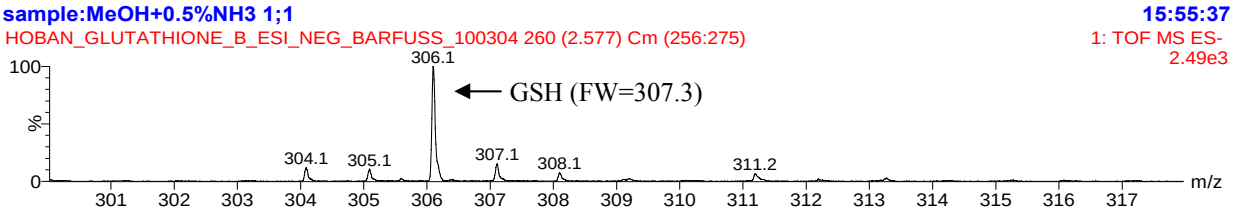

Figure 56: Molecular ion MALDI-TOF mass spectrum of 20 µM *L*-glutathione in Millipore water.

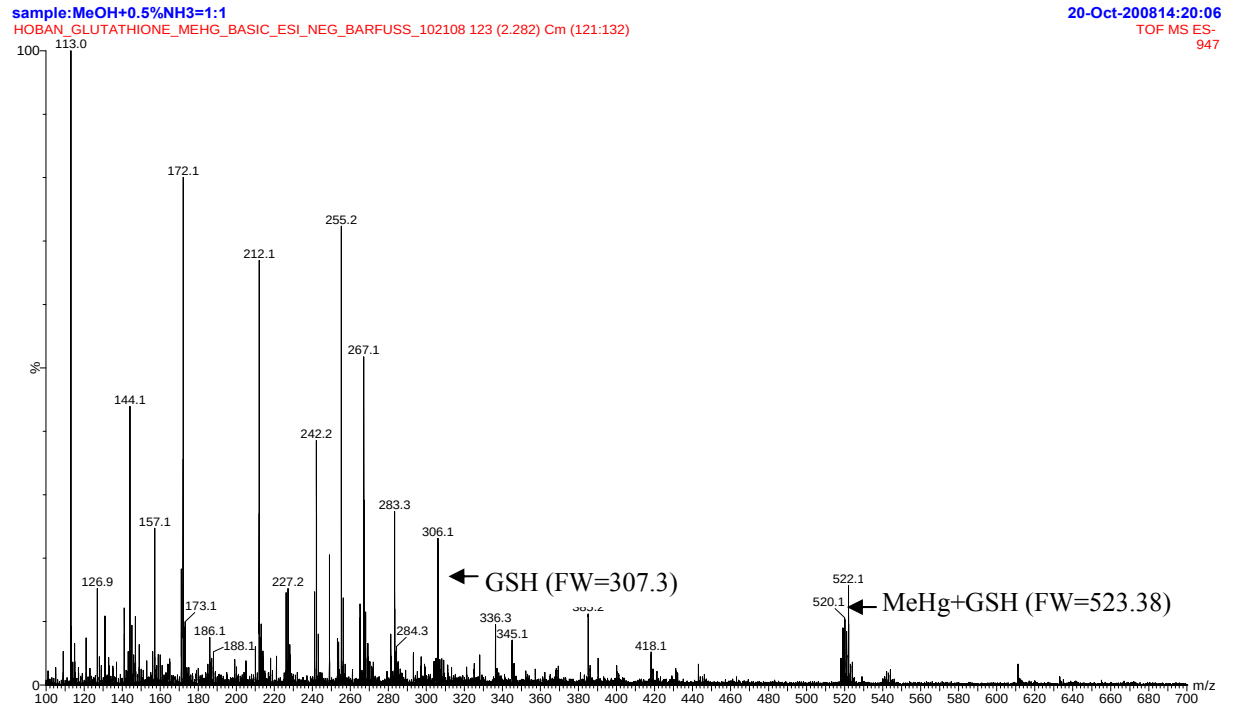

Figure 57: Molecular ion MALDI-TOF mass spectrum of 20 µM MeHgCl + 22 µM *L*-glutathione in Millipore water.

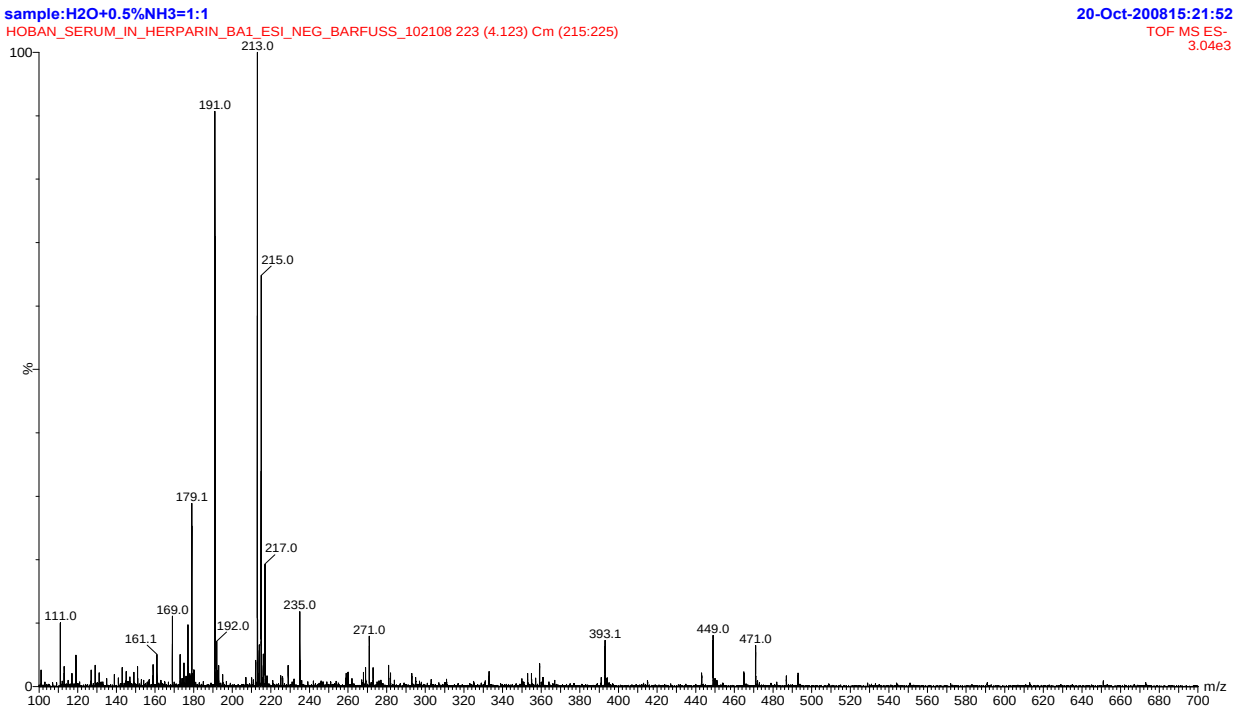

Figure 58: Molecular ion MALDI-TOF mass spectrum of heparinized plasma.

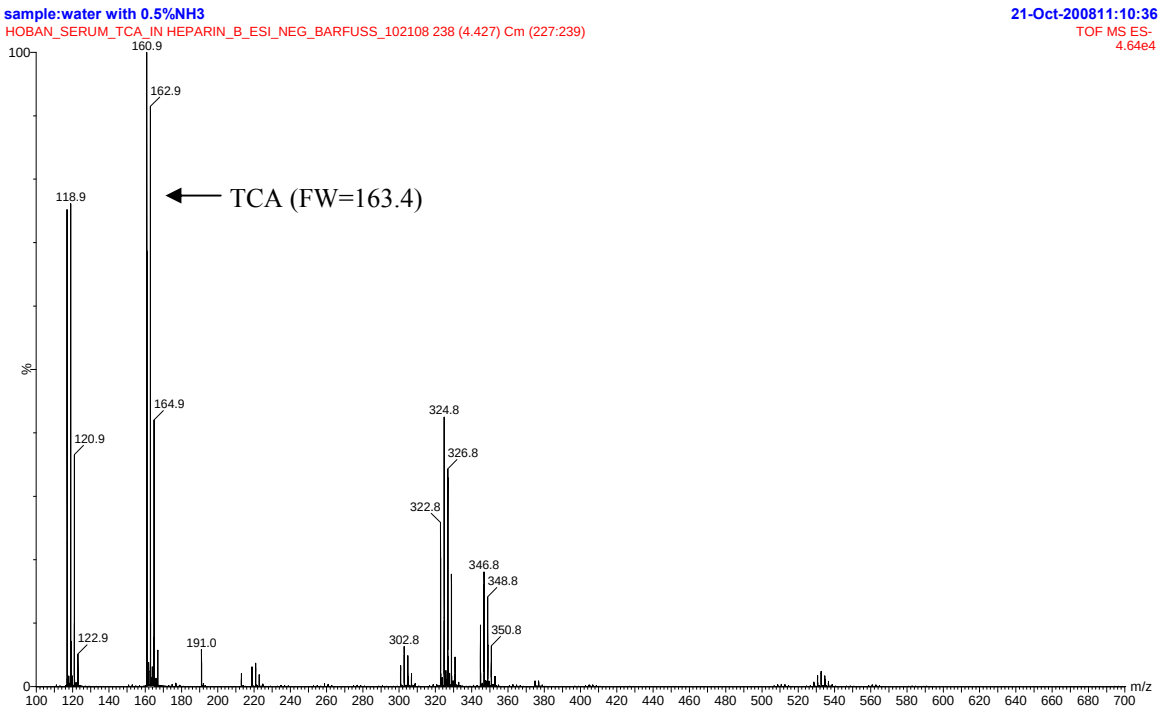

Figure 59: Molecular ion MALDI-TOF mass spectrum of heparinized plasma precipitated with TCA.

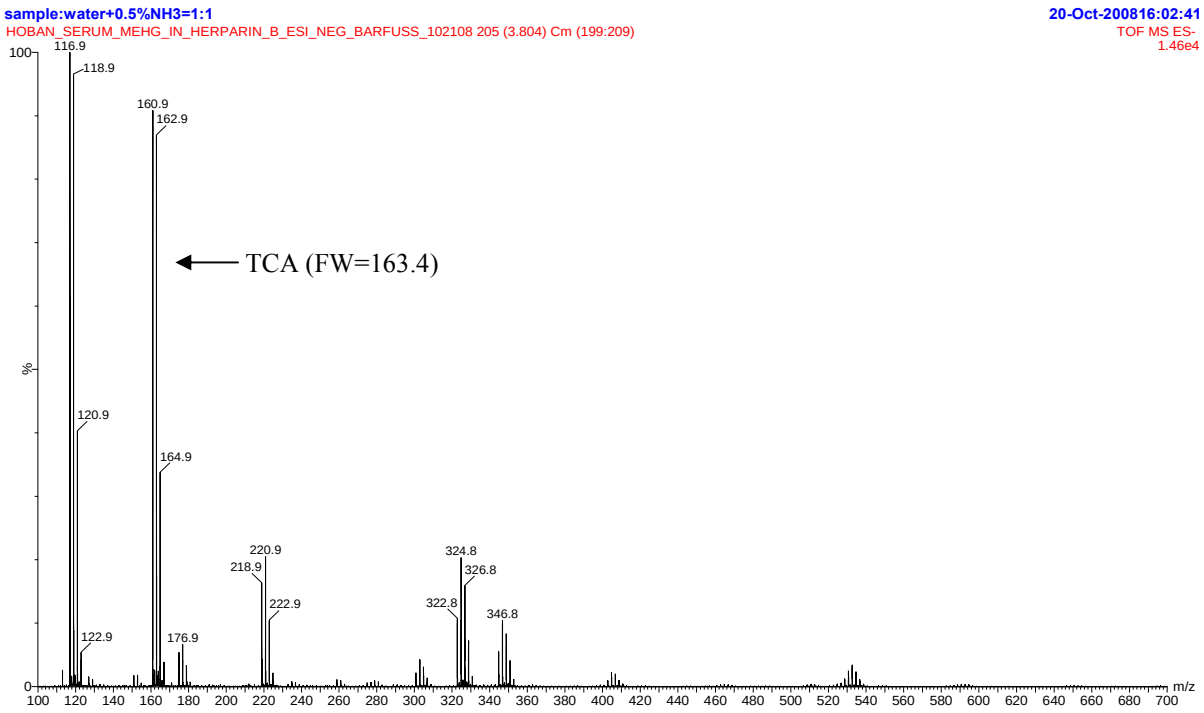

Figure 60: Molecular ion MALDI-TOF mass spectrum of MeHgCl in heparinized plasma precipitated with TCA.

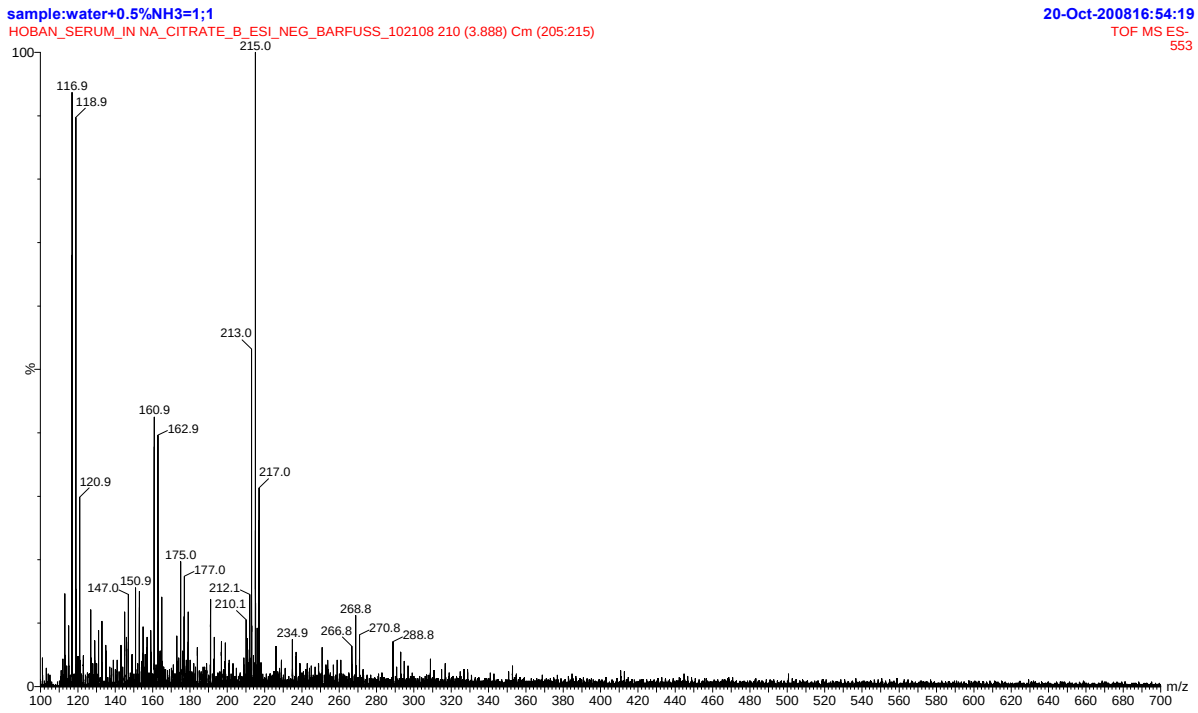

Figure 61: Molecular ion MALDI-TOF mass spectrum of sodium-citrate plasma.

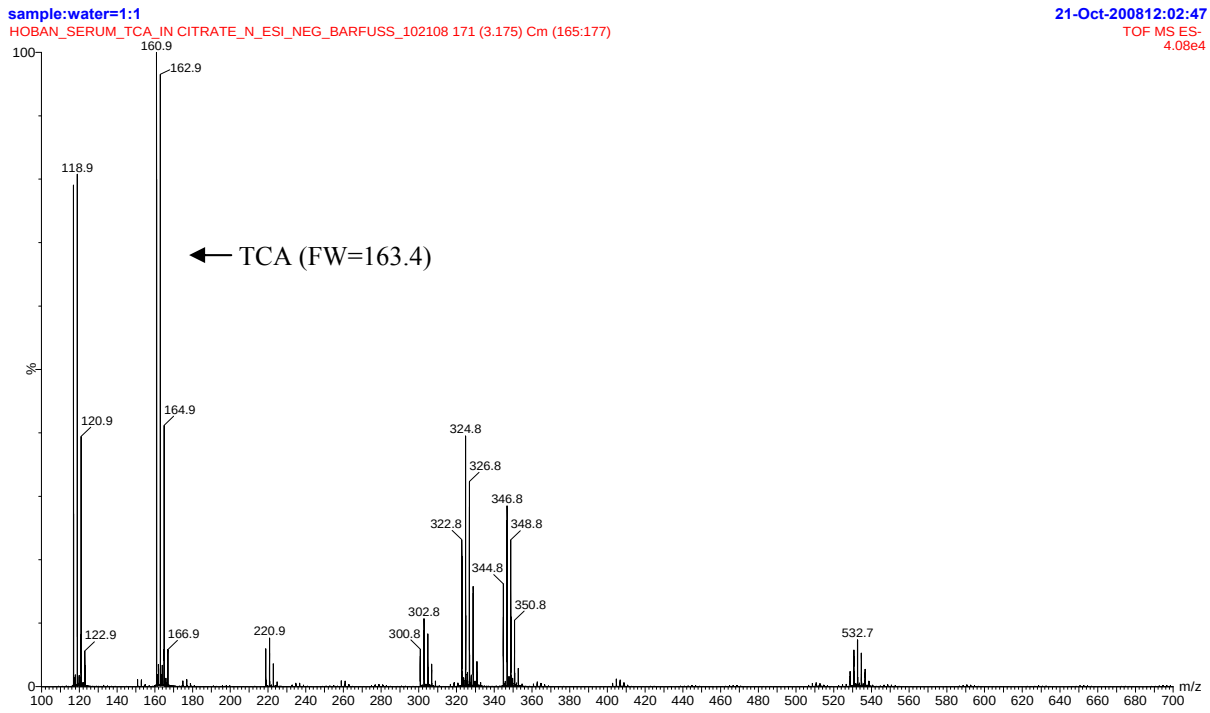

Figure 62: Molecular ion MALDI-TOF mass spectrum of sodium-citrate plasma precipitated with TCA.

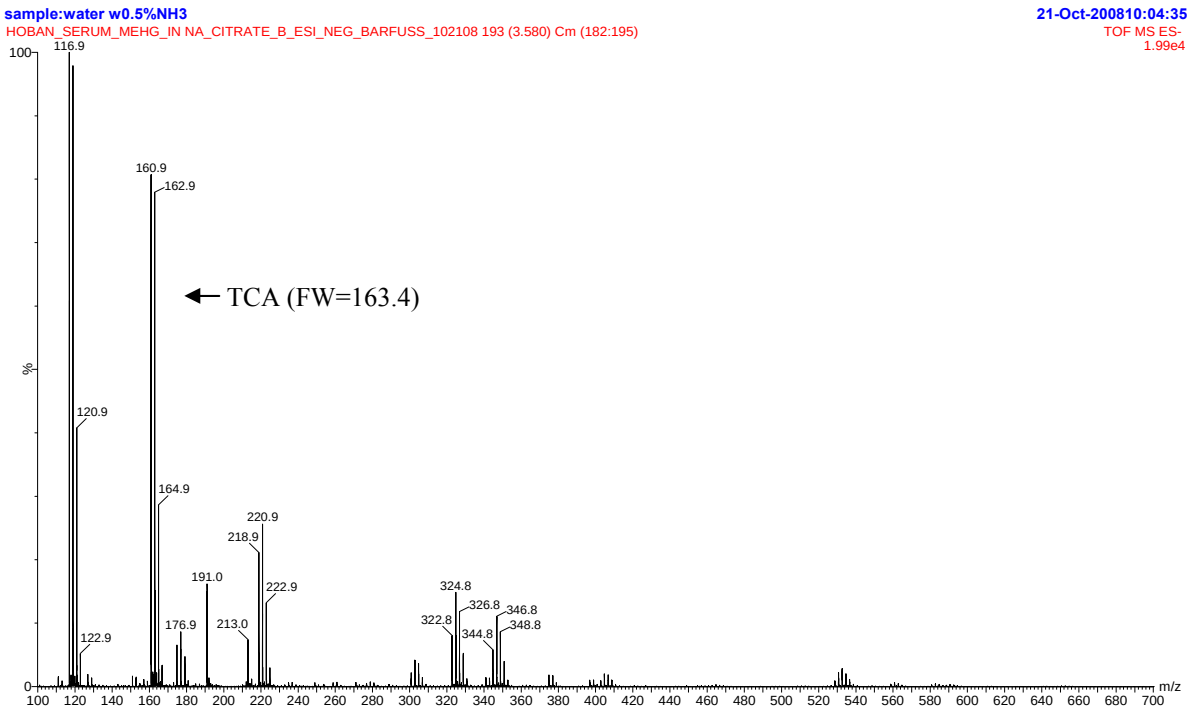

Figure 63: Molecular ion MALDI-TOF mass spectrum of MeHgCl in sodium-citrate plasma precipitated with TCA.

CHAPTER V: DISCUSSION

The purpose of the present study is to examine the characteristics of the transport systems involved in the uptake of methylmercury and methylmercury conjugates at the basolateral membrane of the rabbit renal proximal tubule.

Evidence for an active transport mechanism involved in the uptake of ionic methylmercury was demonstrated by the effects of temperature. The transport of methylmercury appears to be a temperature dependent process [Fig. 9, 10 A]. Reducing the temperature to 12°C caused a significant percent decrease in the transport of methylmercury, thereby excluding the possibility that the uptake of the heavy metal is due to diffusion through the lipid bilayer membrane. Although there still appears to be some non-specific binding to the membrane [Fig. 10 A], this can not solely account for the significant increase in the uptake of $Me^{203}Hg^{+}$ seen in the temperature dependent experiments.

Since the kidney plays an important role in clearing endogenous organic cations (OCs) like acetylcholine, creatinine, dopamine and certain drugs such as, cimetidine, morphine, and quinidine from the blood with the proximal tubule being the main site of OC secretion and containing two organic cation transporters (OCT1 and OCT2), we investigated the possibility of methylmercury being taken up at the basolateral membrane via an organic cation transporter using tetraethylammonium which is considered to be a representative compound for transport by the organic cation system. The addition of 22 μM TEA to the bathing solution did not significantly decrease the uptake of methylmercury [Fig, 11, 12] thereby excluding transport of methylmercury via an organic cation transporter.

Methylmercury readily forms conjugates with thiol compounds *in vivo* because methylmercury has a high affinity for sulfhydryl groups; therefore, metabolism and transport of these derivatives are important determinants of tissue distribution and the elimination of methylmercury from the body. In the present study, the bath-to-cell transport of methylmercury-*L*-cysteine conjugate (MeHg-S-Cys), methylmercury-*L*-methionine conjugate (MeHg-S-Met), methylmercury-*L*-taurine conjugate (MeHg-S-Tau), methylmercury-*N*-acetylcysteine conjugate (MeHg-S-NAC), methylmercury-*L*-glutathione conjugate (MeHg-S-GSH), and methylmercury-*DL*-homocysteine conjugate (MeHg-S-Hcys) were investigated as each of these compounds contain either a thiol group or a sulfur atom [Fig. 64].

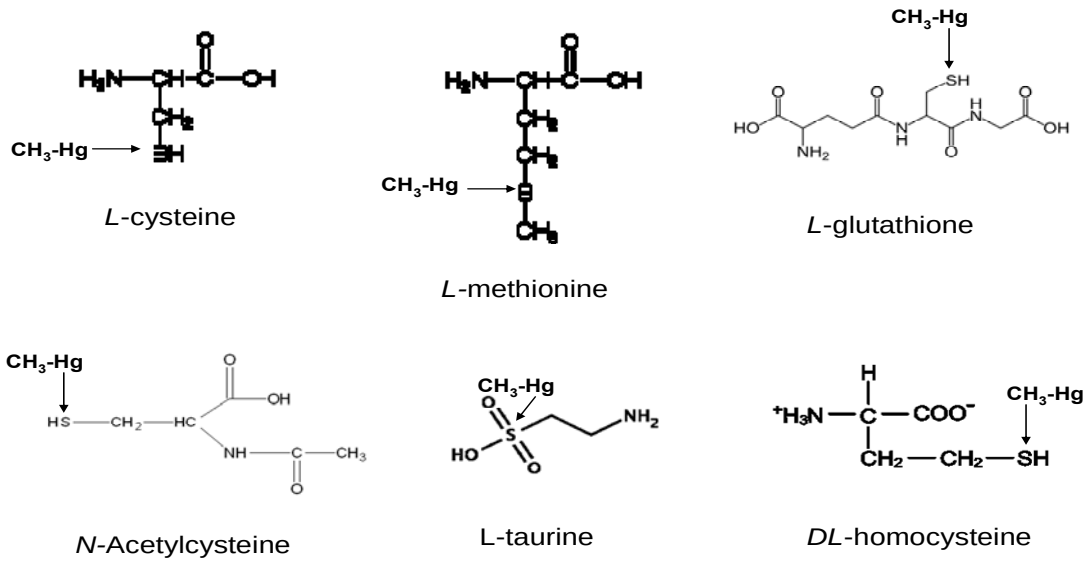

Figure 64: Thiol-containing amino acids and amino acid derivatives.

The molecular homology of these conjugates is very similar to the amino acid *L*-cystine (Cys-S-S-Cys) suggesting that due to the structural similarity, the methylmercury-sulfhydryl conjugates may in fact mimic *L*-cystine and compete for transport via the *L*-cystine transport mechanism possibly through one of the basolateral amino acid transport systems (*A* or *ASC*). The data from the current study support this hypothesis for the transport of the methylmercury-*L*-cysteine conjugate, the methylmercury-*L*-methionine conjugate, and the conjugate of methylmercury-*L*-taurine.

In the basolateral membrane of the proximal tubule, several organic anion transport mechanisms (OAT1, OAT2, OAT3) have been located. The organic anion transporters represent the renal secretory mechanism for organic anions all of which are expressed in the kidney, while some are also expressed in other tissues, such as the liver, brain and placenta. The organic anion transporters are classified based upon their energy requirements, either Na^+-independent exchangers, primary active transporters requiring ATP hydrolysis, or Na^+-dependent organic anion transporters (Sekine et al, 2000). The Na^+-independent exchangers and primary active transporters have broad substrate selectivity, while the Na^+-dependent transporter portrays a relatively narrow substrate specificity (Sekine et al, 2000). OAT1 is a sodium-independent transporter of PAH predominantly expressed in the basolateral membrane of the S_2 segment of the proximal tubule in the kidney. The organic anion transporter 2 (OAT2) is a Na^+-independent exchangers predominantly expressed in the liver and only mildly expressed in the kidney. OAT3 is expressed in a number of tissues, including the basolateral membrane of the proximal tubule in the kidney, liver, brain and eye and shows the same diversity for substrates as OAT1.

Previous studies have demonstrated that inorganic mercury is taken up at the basolateral membrane via OAT1 (Zalups and Ahmad, 2004) leading to the hypothesis that a methylmercury

conjugate may also be transported in the basolateral via OAT1 as well. Uptake of $Me^{203}Hg^{+}$-*L*-cysteine was significantly decreased in the presence of PAH, a specific competitive substrate for the renal organic anion transporters [Fig. 15] suggesting that the mercuric conjugate is indeed being transported by the OAT system. Interestingly, the tubular contents of $Me^{203}Hg^{+}$-*L*-cysteine conjugate were significantly increased in the presence of PAH [Fig. 16]. The addition of 200 μM probenicid, another competitive substrate and inhibitor of the organic anion transporters, to the bathing solution decreased the amount of uptake in the basolateral membrane of the proximal tubule, although the results were not statistically significant [Fig. 17]. However, the amount of tubular contents bound to the membrane was significantly increased in the presence of probenicid [Fig. 18]. These findings suggest that the primary mechanism of basolateral uptake of organic mercury complexed to *L*-cysteine is indeed occurring through an organic anion transport system.

There is current evidence suggesting that the organic anion transport systems are driven by an organic anion/dicarboxylate acid exchange (Pritchard and Miller 1993). During normal metabolic processes α-ketoglutarate is generated which contributes to an intracellular gradient favoring the movement of this dicarboxylate out of the cell. As the amount of α-ketoglutarate increases, it may be transported out of the cell in exchange for an organic anion at the organic anion transporter. It has been implicated that the dicarboxylates that exit the proximal tubule cell at the organic anion transporter may re-enter at the basolateral membrane via a Na^{+} or sodium ion dicarboxylic acid cotransporter driven by the Na^{+} gradient generated from the Na^{+}, K^{+} ATPase system (Pritchard and Miller 1993). Previous studies have shown that the basolateral transport of inorganic mercury was inhibited by pretreatment with small aliphatic dicarboxylates, such as glutarate or adepate (Zalups, 2000) suggesting that these dicarboxylates may create

competition for the sodium-dependent entry of α-ketoglutarate. This would result in a decrease in the uptake of any organic anions transported at the site of the organic anion exchanger and if the organic form of mercury conjugated to *L*-cysteine is also being transported by this system, a net decrease in the basolateral uptake of the mercuric conjugate would also be noted. Therefore we postulated that the basolateral uptake of the organic form of the metal may also be inhibited by these same dicarboxylates. The data demonstrated that both adepate and glutarate did indeed create competition by decreasing the amount of glutamine (which is a source of α-ketoglutarate) being transported at the dicarboxlyate exchanger thereby reducing the transport of the $Me^{203}Hg^{+}$-*L*-cysteine conjugate at the site of the organic anion transporter and significantly decreasing the rate of uptake at the basolateral membrane [Fig. 19, 20, 21, 22].

Further classification of the transport of $Me^{203}Hg^{+}$ conjugated to sulfhydryl containing amino acids was examined using *L*-taurine. Taurine is a non-essential amino acid, which means that it is manufactured from other amino acids in the liver, and is found in high concentrations in the white blood cells, skeletal muscles, central nervous system and the heart muscles. Although *L*-taurine does not contain a sulfhydryl group it does have a sulfur atom making it a potential candidate for conjugating to $Me^{203}Hg^{+}$ *in vivo*. The data shows evidence for the active basolateral transport of the $Me^{203}Hg^{+}$-*L*-taurine conjugate as demonstrated by a significant increase in the transport indicated by the cell-to-bath ratio of $Me^{203}Hg^{+}$-*L*-taurine [Fig. 29] at 37°C compared to the uptake of the conjugate at 12°C. Furthermore, the total tubule contents of $Me^{203}Hg^{+}$ were also significantly increased in the presence of *L*-taurine [Fig. 30] at normal physiological temperatures suggesting some protein on the plasma membrane has a higher affinity for the mercuric conjugate than just the organic metal by itself.

Since *L*-taurine stimulated a significant increase in the basolateral uptake of $Me^{203}Hg^{+}$ we also investigated the effect of PAH on the transport of this conjugate at both 37°C and 12°C. At 37°C, the addition of PAH significantly decreased the cell-to-bath ratio, cytosolic concentration and the tubular contents [Fig. 31, 32] suggesting that not only is the $Me^{203}Hg^{+}$-*L*-taurine conjugate likely being transported by the organic anion system, it is an active process and not simply diffusing through the plasma membrane. When the bathing solution was cooled to 12°C to eliminate any active transport processes, no further significant decreases in bath-to-cell transport or the cytosolic concentration were seen [Fig. 33]. However, a significant reduction in the amount of bound $Me^{203}Hg^{+}$-*L*-taurine conjugate was demonstrated [Fig. 34A] suggesting that PAH interfered with the $Me^{203}Hg^{+}$-*L*-taurine conjugate from binding to the plasma membrane.

The amino acid, *L*-taurine, when bound to $Me^{203}Hg^{+}$ may be positively charged thereby allowing uptake of the conjugate through one of the organic cation transport systems. To investigate this possibility, 200 μM TEA was added to the bathing solution containing the $Me^{203}Hg^{+}$-*L*-taurine conjugate. The data did not show a significant change in the cell-to-bath or cytosolic concentration of this mercuric conjugate in the presence of TEA [Fig. 35] indicating that the conjugate is probably not gaining entry in the basolateral via the organic cation transport systems. A significant reduction in the bound $Me^{203}Hg^{+}$-*L*-taurine conjugate was seen [Fig. 36] suggesting that the TEA molecule is in some way interfering with the binding of the mercuric conjugate to the plasma membrane.

Another potential conjugate of $Me^{203}Hg^{+}$ for transport at the basolateral membrane is *N*-acetylcysteine. Previous studies have demonstrated an increased uptake of inorganic mercury when co-administered with *N*-acetylcysteine and the addition of PAH inhibited this uptake (Zalups and Barfuss, 1998) suggesting the organic form when conjugated to NAC may also

demonstrate amplified uptake. The data from this study however did not show any increase in the basolateral transport of $Me^{203}Hg$-*N*-acetylcysteine conjugate [Fig. 37, 38], nor did the addition of PAH to the bathing solution inhibit [Fig. 39, 40]. The finding that NAC was not transported by the basolateral membrane of the proximal tubule is in direct correlation with research demonstrating the chelating effect of NAC on methylmercury poisoning (Ballatori et al, 1998). In that study, NAC was shown to increase the urinary excretion of methylmercury and decrease the tissue mercury levels. Therefore, we would not expect to see $Me^{203}Hg$-NAC conjugate being transported at the basolateral membrane of the proximal tubule.

The remaining potential conjugates of $Me^{203}Hg^{+}$ for transport at the basolateral membrane that were examined are *L*-glutathione and *DL*-homocysteine. Glutathione being the most abundant organic molecule in the cell and containing a free thiol group was hypothesized to have a substantial effect on the transport of $Me^{203}Hg^{+}$. As the data clearly shows, virtually no transport was seen with the addition of GSH to the bathing solution [Fig. 40, 41]. This same phenomenon was also demonstrated when Hcys was conjugated to $Me^{203}Hg^{+}$ [Fig. 42, 43]. Therefore, it appears that these two conjugates of methylmercury are not involved in the basolateral transport of methylmercury, but like NAC could add to excretion by increasing the filtered load. A summary of the transport findings from this study is represented in Figure 65.

Analysis of $Me^{203}Hg^{+}$ in plasma obtained from rabbits showed nearly 99% of the compound bound to some protein within the blood [Table 1]. However, approximately 1% of $Me^{203}Hg^{+}$ in plasma is bound to some compound(s) within the supernatant which has yet to be identified. Further examination of the supernatant was performed via molecular ion mass spectrometry to isolate this unknown compound. Initial studies by mass spectrometry analysis

were to confirm that the MeHg compound was combining with the amino acids studied in the non-perfused tubule experiments.

Mass spectrometry of MeHgCl confirmed that the chloride ion is cleaved off when the compound is in solution as the dominant peak was shown at 216.9 and the molecular weight of $MeHg^{+}$ is 251.08 with subtraction of the chloride ion leaving a formula weight of 216.08 [Fig. 45]. *L*-taurine has a molecular weight of 125.14 and the mass spectrometry output showed a clear distinct peak at 124 indicating that *L*-taurine was being identified in solution [Fig. 46]. When MeHgCl was combined with *L*-taurine numerous peaks were identified [Fig. 47] with spikes at 251 and 409.1, the latter being the more distinctive peak. The peak at 251 is indicative of excess MeHgCl compound in solution. If MeHgCl (with the chloride ion being removed) is combining with *L*-taurine we would have expected at spike at 341.22 which was not shown. This means that some of the *L*-taurine is combining with MeHg, but not the entire intact compound is forming a conjugate. *L*-taurine has a sulfur group bonded to two oxygen atoms and a hydroxyl group [Fig. 64] along with two carbons and an amine group. Sulfur can form anywhere from 1-6 bonds and the affinity of sulfur for mercuric compounds is on the order of $10^{15} – 10^{20}$ which is quite high suggesting the mercuric atom should displace either the hydroxyl group or one or both oxygen. However, this combination does not coincide with mass spectrometry peak of 409.1. Therefore, some form of two *L*-taurine compounds must be combining with MeHg to form a conjugate as evidenced by the increase in transport of $Me^{203}Hg^{+}$-*L*-taurine conjugate demonstrated in the non-perfused tubule studies described above.

L-cysteine has a molecular weight of 121.2 and the mass spectrometry output showed a clear discrete spike at 120 indicating that *L*-cysteine was being identified in solution [Fig. 48]. When MeHgCl was combined with *L*-cysteine numerous smaller peaks were identified [Fig. 49]

with the spike at 409.2 clearly standing out as distinctive spike. The MeHgCl + *L*-cysteine conjugate should show a peak at 337.28 with the removal of the chloride ion. This again shows that some form of *L*-cysteine is being conjugated with MeHg, but either the entire compound is not binding or some form of multiple *L*-cysteine compounds are binding to MeHg possibly forming a coordinate covalent bond as *L*-cystine does with the inorganic form of mercury (Cys-Hg-Cys).

Figure 50 shows the mass spectrometry analysis of *L*-methionine which has a discrete peak of 150.2 which is in direct correlation with the molecular weight of 149.2. When *L*-methionine is combined with MeHgCl the mass spectrometry output shows several spikes, but again the most discrete peak is at 409.2 [Fig. 51]. A one-to-one conjugation of *L*-methionine + MeHg would yield a spike at 365.28, again assuming the chloride ion is removed, which is not shown in the output. Therefore, some form of *L*-methionine must be combining with MeHg for transport across the basolateral membrane of the renal proximal tubule cells as evidenced by the non-perfused studies described above.

The three conjugates (*L*-cysteine, *L*-methionine and *L*-taurine) that demonstrated transport within the basolateral membrane of the proximal tubule all produced distinctive peaks at 409, none of which corresponded to a one-to-one conjugation with MeHg. Since each of these amino acids contains a different combination of elements, it was postulated that something must be occurring which is common to all three structures. The only possible construct which would coincide with the mass spectrum is if all three amino acids are combining with MeHg as $^{-}$HOOC -CH-CH_2-S-Hg-S-CH_2-CH-COOH^{-} which would have a molecular weight of 408. This compound would be in direct alignment with the results from the mass spectrum, but does indicate that MeHg is being transported across the basolateral membrane with a negative charge

as the inorganic form of mercury. The proposed negatively charged compound may explain why MeHg appears to be transported by OAT and not OCT.

Mass spectrometry analysis of *N*-acetylcysteine produced one distinct peak at 162 which is again in direct alignment with the molecular weight of 163.2 [Fig. 52]. The combination of MeHgCl and *N*-acetylcysteine would be expected to produce a spike at 379.28 and Figure 53 demonstrates that this conjugate is forming as the most distinctive spike is occurring at 378. In addition, MeHg has numerous naturally occurring isotopic forms which is confirmed in the mass spectrometry as the peak at 378 shows various molecular weights of 376, 375 and 374 [Fig. 53]. This result confirms what is known in the literature that NAC has been effectively used as a chelating agent in methylmercury poisoning, thereby confirming that NAC must be forming a conjugate with MeHg.

Figure 54 shows the mass spectrometry analysis of *DL*-homocysteine with a discrete spike at 136.1 which is complementary to the molecular weight of 135.2. When *DL*-homocysteine is combined with MeHgCl many spikes were produced, none of which correspond to the expected formula weight of 351.28 if the combination was producing a 1:1 conjugate [Fig. 55]. Analysis of *L*-glutathione clearly showed the compound as the spike at 306.1 corresponds to the formula weight of 307.3 [Fig. 56]. Figure 57 demonstrates that *L*-glutathione is conjugating with MeHg as the mass spectrometry produced a 522.1 and the combined formula weight would be expected at 523.38. It is not surprising that MeHg is conjugating with GSH due to its high abundance in cells.

Figures 58 and 61 show plasma in either a heparin or Na-Citrate solution which produced many peaks most likely corresponding to the various compounds found in blood. When the plasma samples were then precipitated with TCA (molecular weight of 163.4) and analyzed

many of the previous spikes were removed [Fig. 59 and 62]. However, both analyses showed the TCA with a peak at 160.9. The addition of MeHgCl to both of the plasma TCA precipitates in heparin [Fig. 60] and sodium-citrate [Fig. 63] were inconclusive. There was no clear spike corresponding to the methylmercury conjugates (*L*-cysteine, *L*-methionine and *L*-taurine) that demonstrated active transport at the basolateral membrane of the proximal tubule in the non-perfused tubule experiments described above. Further characterization of methylmercury transport, in particular, what form of methylmercury is being excreted in the urine will need to be examined to fully elucidate the conjugate being formed *in vivo*.

In conclusion, the current study clearly demonstrated that methylmercury could be transported at the basolateral membrane of the S_2 segment of the proximal tubule by multiple mechanisms, depending on the form in which it is presented to the membrane. Figure 65 shows that methylmercury may enter the renal epithelial cells from the basolateral membrane via either the OAT system when conjugated to *L*-cysteine, *L*-taurine, or *L*-methionine or via the amino acid transporter when conjugated to *L*-cysteine. This knowledge is the first step in understanding how methylmercury gains access to the renal epithelial cells of the proximal tubule on the basolateral membrane and will assist in the development of treatment strategies to prevent methylmercury from gaining access and inducing toxicity.

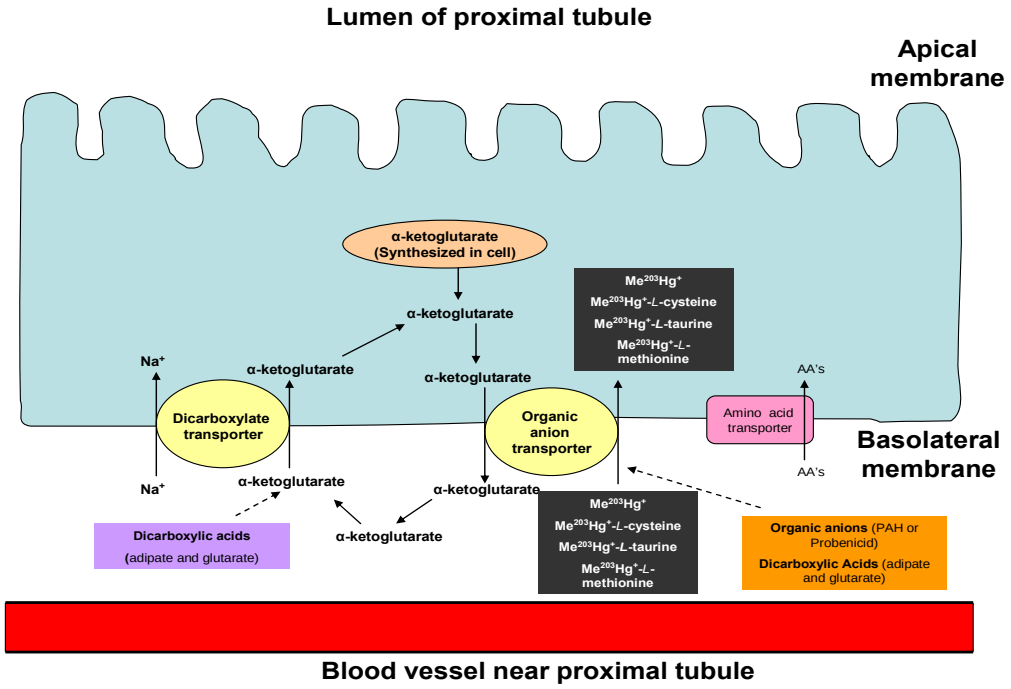

Figure 65: Diagram outlining the roles of the organic anion, dicarboxylate acids, and amino acid transport systems in the basolateral uptake of methylmercury along the proximal tubule. Intracellular generation of α-ketoglutarate (from normal metabolic processes) generates a gradient which favors the movement out of the cell. If these gradients are high enough, α-ketoglutarate will exit the cell in exchange for an organic anion. Once out of the cell α-ketoglutarate may re-enter via exchange with sodium. The driving force behind this exchange mechanism is the Na^+, K^+-ATPase located in the basolateral membrane of the proximal tubule. As the diagram shows, methylmercury enters the proximal tubule cell conjugated to *L*-cysteine, *L*-taurine, or *L*-methionine via the organic anion transport system in exchange for intracellular α-ketoglutarate. The diagram also depicts adepate and glutarate compete with α-ketoglutarate at the site of the dicarboxylic acid transporter.

REFERENCES

Agency, E. P. (1997). "Mercury Study Report to Congress." 1.

Aschner, M. and T. Syversen (2005). "Methylmercury: Recent advances in the understanding of its neurotoxicity." Ther Drug Monit 27: 278-283.

Ballatori, N., Lieberman, Michael W., and Wang, Wei (1998). "N-Acetylcysteine as an Antidote in Methylmercury Poisoning." Environmental Health Perspectives 106(5): 267-271.

Barbier, O. (2005). "Effect of heavy metals on, and handling by, the kidney." Nephron Physiology 99: 105-110.

Barfuss, Delon W., Mays, JoAnn M., and Schafer, James A. (1980). "Peritubular uptake and transepithelial transport of glycine in isolated proximal tubules." Am J Physiol Renal Physiol 238(7): F324-F333.

Bridges, Christy C. and Rudolfs K. Zalups (2006). "System $B^{0,+}$ and the Transport of Thiol-*S*-Conjugates of Methylmercury." J. Pharmacol and Exp Therap 319:948-956.

Bronstein, A. C., Spyker, Daniel A., Cantilena Jr, Louis R., Green, Jody, Rumack, Barry H. and Heard, Stuart E. (2007). "2006 Annual Report of the American Association of Poison Control Centers' National Poison Data System (NPDS)." Clinical Toxicology 45(8): 815-917.

Cannon, Vernon T. (2000). "Molecular homology and the luminal transport of Hg2+ in the renal proximal tubule cell." J Am Soc Nephrol 11: 394-402.

Cannon, Vernon T. (2001). "Amino acid transporters involved in luminal transport of mercuric conjugates of cysteine in rabbit proximal tubule." J. Pharmacol and Exp Therap 298: 780-789.

Choi, Ben H., Yee, Simon and Mario Robles (1996). "The Effects of Glutathione Glycoside in Methyl Mercury Poisoning." Toxicology and Applied Pharmacol 141: 357-364.

Clarkson, Thomas W. (2002). "The Three Modern Faces of Mercury." Environmental Health Perspectives 110(Supplement 1).

Dantzler, William H. (2002). "Renal organic anion transport: a comparative and cellular perspective." Biochimica et Biophysica Acta 1566: 169-181.

Diner, Barry (2004). "Toxicity, Mercury."

Gonska, T., J. R. Hirsch and E. Schlatter (2000). "Amino acid transport in the renal proximal tubule." Amino acids 19: 395-07.

Hernando, N., Wagner, Carsten A., Gisler, Serge M., Biber, Jürg, and Murer, Heini (2004). "PDZ proteins and proximal ion transport." Curr Opin Nephrol Hypertens 13: 569-574.

Hoffmeyer, Ruth E., Singh, Satya P., Doonan, Christian J., Ross, Andrew R. S., Hughes, Richard J., Pickering, Ingrid J., and George, Graham N. (2006). "Molecular Mimicry in Mercury Toxicology." Chem Res Toxicol 19: 753-759.

Huber, Kimberly (1997). "Mercury Use: Wastewater Treatment Plants." 602-29.

Jasinski, Stephen M. (1994). "The Materials Flow of Mercury in the United States." Bureau of Mines, Information Circular 9412.

Kajiwara, Y., Yasutake, A., Adachi, T. and Hirayama, K. (1996). "Methylmercury transport across the placenta via neutral amino acid carrier." Arch Toxicol 70: 310314.

Kanai, Yoshikatsu and Hitoshi Endou (2003). "Functional Properties of Multispecific Amino Acid Transporters and Their Implications to Transporter-Mediated Toxicity." The Journal of Toxicological Sciences 28(1): 1-17.

Kershaw, T. G., Dhahir, Patricia H, and Clarkson, Thomas W (1980). "The Relationship between Blood Levels and Dose of Methylmercury in Man." Archives of Environmental Health 35(1): 28-36.

Kluger, Jeffrey (2006). "Mercury Rising." Time 168(11): 66-68.

Koh, A. S. (2002). "Identification of a mechanism by which the methylmercury antidotes N-Acetylcysteine and Dimercaptopropanesulfonate enhance urinary metal excretion: Transport by the Renal Organic Anion Transporter-1." Mol Pharmacol 62: 921-926.

Northeast States for Coordinated Air Use Management (2003). "Mercury emissions from coal-fired power plants."

Ozuah, Philip O. (2000). "Mercury Poisoning." Curr Probl Pediatr 30: 91-9.

Palacín, Manuel, Estévez, Raúl, Bertran, Joan, and Zorzano, Antonio (1998). "Molecular Biology of Mammalian Plasma Membrane Amino Acid Transporters." Physiol Rev 78(4): 969-1038.

Patrick, L. (2002). "Mercury toxicity and antioxidants: Part I: Role of glutathione and alpha-Lipoic acid in the treatment of mercury toxicity." Alt Med Rev 7: 456-471.

Pritchard, JB and Miller, DS (1993). "Mechanisms mediating renal secretion of organic anions and cations." Physiol Rev 73: 765-788.

Quig, David (1998). "Cysteine Metabolism and Metal Toxicity." Alt Med Rev 3(4): 262-270.

Rahman, G. M. Mizanur, Kingston, H. M. Skip, Bhandari, Sandeep (2003). "Synthesis and characterization of isotopically enriched methylmercury ($CH_3{}^{201}Hg+$)." Appl Organometal Chem 17: 913-20.

Rouleau, Claude and Block, Mats (1997). "Fast and High-yield Synthesis of Radioactive $CH_3{}^{203}Hg(II)$." Appl Organometal Chem 11: 751-53.

Rubino, Federico Maria, Verduci, Cinzia, Giampiccolo, Salvatore Pulvirenti, Brambilla, Gabri, and Colombi, Antonio (2004). "Molecular Characterization of Homo- and Heterodimeric Mercury(II)-*bis*-Thiolates of Some Biologically Relevant Thiols by Electrospray Ionization and Triple Quadrupole Tandem Mass Spectrometry." J Am Soc Mass Spectrum 15: 288-300.

Sekine, Takashi, Ho Cha, Seok, and Endou, Hitoshi (2000). "The multispecific organic anion transporter (OAT) family." Eur J Physiol 440: 337-350.

Smith, John C and Fred F Farris (1996). "Methyl Mercury Pharmacokinetics in Man: A Reevaluation." Toxicology and Applied Pharmacol 137: 245-252.

Watson, W. A. (2003). "2003 Annual Report of the American Association of Poison Control Centers Toxic Exposure Surveillance System." American Association of Poison Control Centers.

Wright, SH and Dantzler, WH (2004). "Molecular and Cellular Physiology of Renal Organic Cation and Anion Transport." Physiol Rev 84: 987-1049.

Wright, Steven H., Evans, Kristen K, Zhang, Xiaohong, Cherrington, Nathan J, Sitar, Daniel S and Dantzler, William H (2004). "Functional map of TEA transport activity in isolated rabbit renal proximal tubules." Am J Physiol Renal Physiol 287: F442-F451.

Wu, Guang (1996). "Effect of probenicid on the transport of methyl mercury in erythrocytes by the organic anion transport system." Arch Toxicol 71: 218-222.

Zalups, R. K. and D. W. Barfuss (1993). "Transport and toxicity of methylmercury along the proximal tubule of the rabbit." Toxicology and Applied Pharmacol 121: 176-185.

Zalups, R. K. (2000). "Molecular interactions with mercury in the kidney." Pharmacol Reviews 52: 113-144.

Zalups, R. K. and D. W. Barfuss (2002). "Simultaneous coexposure to inorganic mercury and cadmium: A study of the renal and hepatic disposition of mercury and cadmium." J. Toxicology and Env Health 65: 1471-1490.

Zalups, R. K. (2004). "Human organic anion transporter 1 mediates cellular uptake of cysteine-S conjugates of inorganic mercury." Kidney Int 66: 251-261.

Zalups, R. K. and A., Sarfaraz (2004). "Homocysteine and the Renal Epithelial Transport and Toxicity of Inorganic Mercury: Role of Basolateral Transporter Organic Anion Transporter 1." J Am Soc Nephrol 15: 2023-2031.

Zalups, R. K. and A., Sarfaraz (2005). "Transport of *N*-Acetylcysteine *S*-Conjugates of Methylmercury in MDCK Cells Transfected Stably with hOAT1." Journal of Pharmacology and Experimental Therapeutics 314: 1158-1168.

Zhang, X., Groves, CE, Bahn, A, Barendt, WM, Prado, MD, Rödiger, M, Chatsudthipong, V, Burckhardt, G, and Wright, SH (2004). "Relative Contribution of OAT and OCT Transporters to Organic Electrolyte Transport in Rabbit Proximal Tubule." Am J Physiol Renal Physiol 287(5): F999-1010.